UNIVERSIDAD CARLOS III DE MADRID
Escuela Politécnica Superior
Departamento de Ingeniería Térmica y de Fluidos

"TWO DIMENSIONAL FLUIDIZED BED DYNAMICS"

Thesis for the degree of Doctor of Philosophy

Autor:
Sergio Sánchez Delgado
Ingeniero Industrial

Director de Tesis:
Domingo Santana Santana
Licenciado en Matemáticas
Doctor en Ingeniería Industrial

Leganés, Madrid, Febrero de 2010

Tesis Doctoral

"TWO DIMENSIONAL FLUIDIZED BED DYNAMICS"

Autor: Sergio Sánchez Delgado
Director de Tesis: Domingo Santana Santana

El tribunal, nombrado por el Magfco. y Excmo. Sr. Rector de la Universidad Carlos III de Madrid,

Presidente D. Jorge Xiberta Bernat, Universidad de Oviedo

Vocal D. Pedro Ollero de Castro, Universidad de Sevilla

Vocal D. Juan José Hernández Adrover, Universidad de Castilla la Mancha

Vocal D. David Pallarès Tella, Chalmers University of Technology

Secretario D. Javier Villa Briongos, Universidad Carlos III de Madrid

Suplente Dña. Mercedes de Vega Blázquez, Universidad Carlos III de Madrid

Suplente D. Jose Antonio Almendros Ibáñez, Universidad Carlos III de Madrid

acuerda la calificación de: _____

El presidente El secretario

Los vocales

Leganés, Madrid, Febrero de 2010

A mis padres, a Sandra y a Laura

Always start by trying the simplest model and then only add complexity to the extent needed.
Levenspiel O.

Si tu intención es describir la verdad hazlo con sencillez y la elegancia déjasela al sastre.
Einstein A.

Contents

List of Figures

List of Tables

Agradecimientos

Muchas son las personas a las que les debo agradecer su ayuda en la realización de ésta tesis doctoral: A Domingo Santana por su esfuerzo, atención, sinceridad y buenas ideas a lo largo de todos estos años, sin duda su apoyo y dirección han sido fundamentales durante el desarrollo de ésta tesis. A los miembros del grupo de investigación de Ingeniería de Sistemas Energéticos (ISE), especialmente a Mercedes y a Ulpiano por su apoyo y ánimo desde el primer día que llegué al grupo, no me puedo olvidar de Néstor, Antonio Acosta, Javier Villa y Antonio Soria por su paciencia y ayuda siempre que la he necesitado, y desde luego a Jose y a Celia por todos los momentos que hemos pasado juntos compartiendo mucho más que ciencia. A Alberto, Fernando, Luismi y Javier Sánchez, aunque nos conozcamos de menos tiempo, desde luego que es un placer trabajar con vosotros. A los técnicos, Manolo, Carlos, Isra y David, por su ayuda y buenas ideas.

A los estudiantes de doctorado del área por los buenos momentos que hemos compartido juntos. Especialmente a Rafa Salgado por su buen humor y a Mat por tantos momentos de música compartida.

Al grupo de Mecánica de Fluidos por su apoyo y ayuda desinteresada en la realización de esta tesis. Gracias por la cámara de alta velocidad y por el ánimo y la predisposición que os caracteriza. A Pablo, Wil, Dani y Jorge todo su buen hacer y buen humor a lo largo de estos años y como no a Carol por su paciencia lingüística.

No puedo olvidarme de Carlos Y Pepe, con los que empezé esta aventura hace cuatro años y con los que he compartido momentos maravillosos dentro y fuera de la universidad.

A Carmen y a Isabel, por contribuir directamente en mi desarrollo académico y personal.

A mis padres y a mi hermana, a ellos les dedico esta tesis, fruto de tanto esfuerzo y dedicación, que desde luego ha sido mucho más llevadero gracias a su apoyo, entrega y cariño. Gracias.

Por último quiero agradecerle a Laura toda su paciencia, comprensión y apoyo mostrado durante todos estos años, gracias por estar cerca.

Acknowledgment

During the last four years, the ISE research group have received the pleasant visits of several researchers during different conferences related with the main research lines of our group. I would like to thank for their visits to all of them, which have been a great source of ideas for this thesis.

- Naoko Ellis, *University of British Columbia*
- Filip Johnsson, *Chalmers University of Technology*
- Alberto Gómez Barea, *University of Seville*
- Bo Leckner, *Chalmers University of Technology*
- Mikko Hupa, *Åbo Akademi University*
- Joachim Werther, *Hamburg University of Technology*
- Piero Salatino, *Universit'a degli Studi di Napoli Federico II*

I would like to thank for the personnel of the Inorganic Chemistry research group of the Åbo Akademi University. Especially to Mikko Hupa, Patrik Yrjas and Peter Backman for their help and ideas during my stay in 2007.

Dori, Pati and Kemo, I would also like to thank you for your support and the good moments we spent together.

Resumen

Actualmente existen multitud de procesos en las que se pueden encontrar reacciones sólido-gas. Los reactores de lecho fluidizado se muestran como uno de los sistemas más adecuados para este tipo de reacciones debido a su alta capacidad de mezcla por unidad de volumen. Precisamente ésta característica hace que en los lechos fluidos presenten diferentes longuitudes de escalas haciendo muy compleja su modelización, de ahí la importancia de los estudios fundamentales sobre lechos fluidos a la hora de ayudar en el modelado y diseño de este tipo de reactores.

De entre los diferentes campos de investigación en los lechos fluidos, esta tesis se centra en el estudio experimental de la dinámica de un lechos fluido bidimensional mediante el uso de sondas de presión así como de técnicas no intrusivas de medida basadas en la Velocimetría por Imágenes de Partículas (PIV) y en Análisis Digital de Imágenes (DIA), para diferentes condiciones de operación. En concreto, se ha utilizado la técnica DIA para el tratamiento digital de las imágenes capturadas mediante una cámara de alta velocidad , pudiendo así hacer una clara separación entre la fase densa y la fase burbuja, caracterizando las burbujas mediante su diámetro equivalente, posición de centro de masas y velocidad. La técnica DIA permite además observar de manera detallada los fenómenos de formación, crecimiento y coalescencia de las burbujas a lo largo del lecho. Además, para caracterizar la influencia de la burbuja sobre la fase densa, se ha utilizado la técnica de PIV para medir la velocidad de ésta.

Esta tesis aporta resultados relevantes con el objetivo de ayudar a entender mejor la interacción entre ambas fases del lecho para diferentes condiciones de operación, tipos de distribuidor, altura de lecho fijo, tamaño de partícula y espesor del lecho.

Como resultado novedoso se ha calculado el tiempo de recirculación medio de las partículas del lecho, pudiendo así definir el grado de mezcla del reactor. Este trabajo también estudia la influencia del tamaño del espesor del lecho en la velocidad de mínima fluidización, ya que éste valor es uno de los parámetros de diseño más importantes.

También se ha calculado la región de influencia que una burbuja provoca a su paso en la fase densa, identificando y midiendo el movimiento de los sólidos alrededor de la burbuja.

Se ha establecido una relación entre el tamaño y velocidad de la burbuja con la disipación de energía cinética en la fase densa, esta relación está directamente relacionada con los procesos de degradación de la materia. Este fenómeno es de gran importancia ya que la degradación de la fase densa genera partículas de menor tamaño y esto influye directamente en el comportamiento general del lecho.

En esta tesis también se ha investigado la influencia de la distribución de orificios a lo largo del distribuidor. Se ha comprobado que dos distribuidores multi-orificio homogéneamente distribuidos, con la misma perdida de carga pero diferente disposición de orificios, generan, bajo las mismas condiciones de operación, la misma respuesta dinámica del lecho. Podemos entonces concluir que para las condiciones de operación de este trabajo y una distribución de gas uniforme, el comportamiento global del lecho fluido no depende de la disposición de orificios a lo largo del distribuidor.

Abstract

There are different equipments where solid-gas reactions can take place. One of the most used equipments for these processes, are the fluidized beds due to their high reaction rate per unit reactor volume. This complex gas-solid flow is often difficult to model because of the very different length scales that are present, so that additional fundamental investigations are needed before reliable models can be developed for the performance of fluidized beds.

Among the different aspects in need of additional research, this PhD thesis focuses on the experimental investigation of the fluid dynamics of the fluidized bed by use of pressure probes as well as nonintrusive measurements, based on Particle Image Velocimetry (PIV) and Digital Image Analysis (DIA) techniques, to characterize the flow in a two-dimensional experimental facility. In particular, the DIA technique is employed for the interpretation of images taken with a high-speed camera for different operating conditions. A clear difference between the dense phase and the bubble phase is established, thereby enabling different bubble parameters such as equivalent diameter, bubble mass center and bubble velocity to be quantified. In addition, the selected DIA technique allows us to detect and characterize dynamical bubble phenomena including bubble formation, growth and coalescence. In addition, to characterize the influence of the bubbles on the dense phase, the dense phase velocity has been measured with use made of the PIV technique.

This PhD thesis reports relevant results with the aim to a better understanding of the dense and bubble phases interaction for different operation conditions, distributor design, fixed bed height, particle size and bed thickness.

As a novel result, the circulation time was obtained, yielding an order-of-magnitude estimate for the mixing degree within the reactor. The present work also analyzes the effect of the bed thickness in the minimum fluidization velocity, since this value is one of the most important parameters for reactor-design purposes.

The influence regions promoted by the bubbles in the dense phase have been calculated, identifying and measuring the upwards and downwards solid movement regions around the bubble.

The bubble size and the bubble velocity have been correlated with the volumetric dissipation of kinetic energy in the dense phase, providing information about the attrition phenomena responsible of the mechanical stress which leads to the gradual degradation of the individual bed particles, which in turn affects the fluidized bed behavior.

Also, the influence of the grid configuration has been investigated. It has been proved that two uniform multi-orifice distributors, having the same pressure drop but different grid configurations yield the same dynamical bubble pattern and global bed behavior when the beds are operated at the same fluidization conditions. Consequently for the fluidization conditions covered, the overall bed dynamics for uniform gas distribution, do not depend on the grid configuration.

Chapter 1

Introduction

Fluidized-bed technology has received a growing interest and it use has increased almost exponentially over the past few decades, in commercial applications such as chemical industry in the fluidized catalytic cracking of petroleum feedstock among other applications, also the development of the synthetic fuels industry, fluidized reactor systems are being considered and are employed for coal and more recently biomass gasification and pyrolysis.Other current operations include combustion, drying and coating technology.

Despite its wide use in industry, the state-of-the-art design technology for fluidized-bed reactors is not complete. One of the main drawbacks is the scale-up to commercial operations. Typically high cost pilots units of different sizes must be built and tested. Nevertheless, even often these pilots tests are run and even if non-dimensional analysis have also been proposed (Glicksman , 1984; Glicksman et al., 1993), in many cases final designs do not always meet expectations. The reasons for this shortcoming are that the flow behavior of a fluidized bed of solids is complex and much of the design criteria are specific to the system size its geometry and the limited operating conditions of the give application. That is the reason why detailed experimental studies of the dense and freeboard region provide understanding and a basis for developing more generalized design approaches.(Cheremisinoff, 1986)

With the aim to help in the design of the fluidized beds, Computational Fluid Dynamics (CFD) is used to simulate the fluid mechanism of the fluidized bed. Traditionally CFD has been very successful in solving single-phase flows, and, due to the advances in the computational capabilities has also becomes a powerful tool in solving multi-phase flows. However in multi-phase flows different approaches can be taken to describe the behavior of the different phases. Firstly, one can describe both phases as interpenetrating continua (Eulerian-Eulerian model). A second approach can be described as a discrete method based on molecular dynamics (Lagrangian model). Currently the two most common discrete techniques are Discrete Bubble Model (DBM)

and Discrete Element Method (DEM).

Discrete Bubble Model

The DBM is an EulerLagrange type of model, where the dynamics of the continuous emulsion phase is modelled with the continuity and volume-averaged NavierStokes equations and solved on an Eulerian grid, while the bubbles are tracked individually by integrating the equations of motion. A collision model is needed to account for the bubblewall and bubble-bubble interactions (coalescence effect). Constitutive relations are required for the drag force exerted on the bubbles, which are derived from empirical correlations for the terminal rise velocity of a single bubble in fluidized beds, and for the virtual mass force. The emulsion phase density and viscosity are assumed constant (and known from experiments).

Discrete Element Method

The DEM defines each particle as an individual element of which its velocity and trajectory are calculated. The Newtonian equations of motion are solved with inclusion of the effects of particle collisions and forces acting on the particles by the gas. Due to the high computational cost the model is limited to include only a relatively small numbers of particles.

To validate the previously mentioned simulation techniques they need to be compared with experimental results acquired from two-dimensional and three-dimensional fluidized beds. For this purpose, different experimental methods exist and will be outlined in the following section.

1.1 Experimental methods for measuring in fluidized beds

In fluidized beds, it is of high importance the distribution of particles since for certain processes the performance is strongly affected by the variation of this distribution. Therefore the scientific community has paid special attention to this subject and there are many efforts to obtain quantitative measurements of the particles distribution and void fraction. Despite all the efforts, there is not a technique that is significantly more accurate than the others, due to the varying distribution of particles and void fraction in time and space. The most common techniques are briefly discussed herein.

In 2-D fluidized beds a very popular technique is direct visualization that allows measuring the particles distribution very accurately. Applying further processes to the images obtained, particle velocities can also be calculated. As a relevant results of this technique, the 2-D fluidized bed allowed the characterization of the through-flow

within bubbles. However this technique cannot be used in 3-D fluidized beds.

Void-fraction distribution can be obtained by tomography: either electric capacitance or nuclear tomography. The former is faster but has limited spatial resolution, whereas the latter has a higher spatial resolution but the time resolution is still limited.

To measure the void fraction in a fluidized bed optical probes are frequently used. They can determine the temporal variation of voidage distribution in a small measurement volume by the degree of reflection or transmission of a light bundle.

Another interesting technique to determine the voidage as a function of time is measuring the dielectric permittivity in a measurement volume with capacitance probes.

Finally, time-averaged pressure measurements are used to determine the average bed density and bed height. By increasing the frequency of these measurements quantitative information about the hydrodynamic behavior of the fluidized beds can also be obtained.(van Ommen and Mudde, 2008)

1.2 Scope of the thesis

The key objectives of this thesis are:

- The application and combination of different non-intrusive techniques in a two-dimensional fluidized bed in order to obtain the necessary information to understand the global behavior of the fluidized bed.
- Characterize the influence of the fluidized bed thickness, particle size and bed height in the determination of the minimum fluidization velocity.
- Study the region of influence and the velocity fluctuation of the dense phase promoted by a bubble, and characterize the volumetric dissipation of kinetic energy in the dense phase
- Study the effect of different distributors in the bubble generation mechanism, and the influence on the global behavior of the fluidized bed

For all the experiments a 2-D freely bubbling fluidized bed has been used. The bed has been filled with Geldart B particles fluidized with atmospheric air. A high speed video camera has been used to capture the bubble and particle motion. The images have been analyzed to obtain the results presented in this thesis. These results are not directly exportable to a 3-D geometry, but they provide very useful information to understand the behavior of fluidized beds. (Ramos et al., 2002; Briongos and Guardiola, 2005)

1.3 Experimental techniques

Mainly, two non-intrusive experimental techniques have been used in this thesis, the Digital Image Analysis (DIA) and the Particle Image Velocimetry (PIV), summarized as follows:

Digital Image Analysis

Once the images were acquired with the high speed camera, the DIA technique was applied on the images with two mains objectives:

- A clear identification of the two phases of the fluidized bed: the bubble phase free of particles where porosity ε is equal to 1, and the dense phase free of bubbles considered under minimum fluidization conditions $\varepsilon = \varepsilon_{mf}$.
- The complete characterization of the bubbles based in equivalent diameter, mass center position and bubble velocity.

The images have been acquired in a gray scale with values from 0 to 255, a threshold transformation has been necessary for the identification of the two phases explained above, the original image has been transformed into a black and white image where the pixels with values equal to 0 represent the bubble phase and the pixels of the dense phase take the value equal to 1 (Otsu, 1979). Now, the bubble properties can be calculated. Fig. 1.1 shows an example of the scale transformation, and some bubble velocities where the origin of the vector is the mass center position for the bubble.

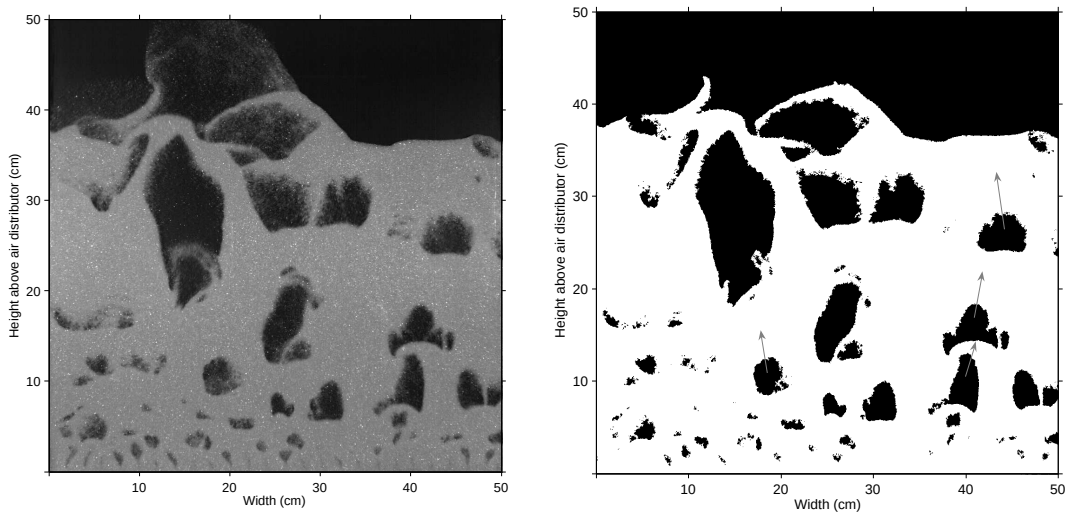

(a) (b)

Figure 1.1: Threshold transformation.

Particle image velocimetry

The PIV technique has been used to characterize the dense phase velocity (Sveen, 2004). PIV uses the cross-correlation as the basic calculation algorithm. The domain (images in this case) is divided in smaller sections called interrogation windows, which size decreases for consecutive steps. The cross-correlation calculates the displacement vector for each window. In this work the window size varies from 64 pixels to 16 pixels, with an overlap of 0.5. The velocity can be calculated dividing the displacement by the lapse of time between two images, therefore the velocity vectors were obtained each 8 pixels.

Fig. 1.2 represents an example of the normalized cross-correlation, R, for two consecutive images in a selected region.

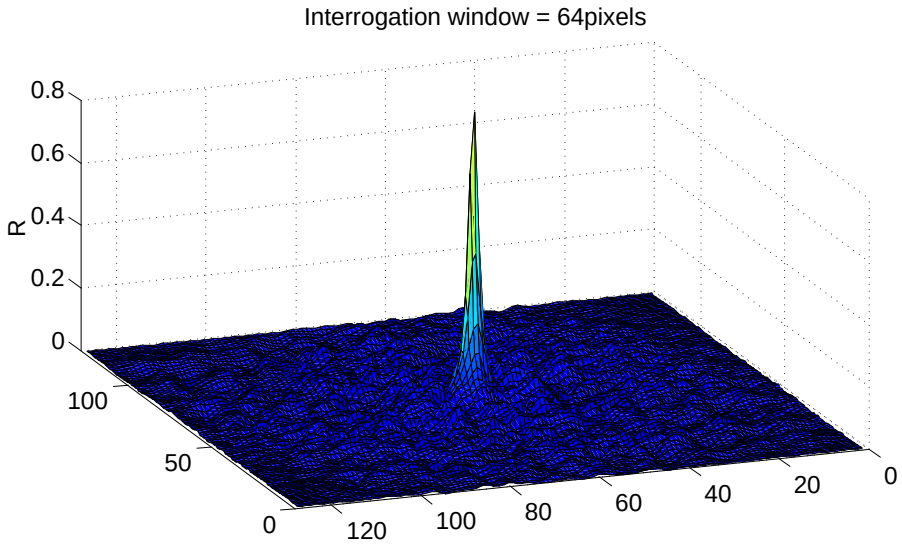

Figure 1.2: Normalized cross correlation value

Chapter 2

Fluid-Dynamic structures in a 2-D fluidized bed by DIA-PIV analysis

Contents

2.1 Abstract

This work presents an experimental study to characterize the time-averaged behavior of the dense and bubble phase in a 2-D fluidized bed by means of: digital image analysis (DIA) and particle image velocimetry (PIV). Three different processes, based on the digital analysis of the images obtained with a high speed camera, have been developed and applied. First, the bubble paths were characterized with time-averaged bubble phase maps, representing the fraction of time that a point is occupied by a

bubble. Second, bubble velocities were obtained using a tracking algorithm over the mass centers of the bubbles. Finally, a PIV technique was used to characterize the time-average dense phase velocity field. In addition, the time-averaged global behavior of the dense phase was described using information from the time-averaged maps.
The PIV measurements provide information about the location of the time-averaged recirculation regions and bed mixing. This procedure was repeated for different bed aspect ratios and different superficial gas velocities, analyzing the influence of these variables on the bed behavior and on the bubble path.

The results report qualitative information about solids transport, showing the most probably location where the particles leave the bubble path and where the particles are ingested again into the bubble path. Besides, with the combination of PIV-DIA results, this work presents the results of the averaged particle circulating time as a function of the bed aspect ratio and the flow rate.

2.2 Introduction

Fluidized beds are widely used in many industrial processes due to their high solid mixing capacity. In a gas-solid system, an increase in the flow rate beyond minimum fluidization can change the internal structure of the bed: the fluid-dynamic structures change, the coalescence phenomenon is more significant, and bubble shape, size, and velocity change within the bed (Goldsmith and Rowe, 1975). Therefore, the particle transport phenomena are more relevant and recirculation regions change their size and position.

There have been several studies on bubble spatial distribution in fluidized beds. Tzeng et al. (1993) studied the macroscopic flow structures of gas-liquid and gas-liquid-solid fluidization systems with flow visualization techniques, examining the effect of particle size, inlet liquid velocity and gas flow distribution in a two-dimensional column. Another technique, based on tracking a phosphorescent tracer particle using a video recorder and digital image analysis, was developed by Pallarès and Johnsson (2006). Lim et al. (2007) used a gas solid fluidized bed to observe the bubbling phase directly, using real time vision instrumentation. They obtained a contour plot of time-averaged spatial bubble residency depicting the bubble spatial distribution in a planar fluidized bed at steady state. Recently, Busciglio et al. (2007) presented a digital image analysis technique to study the fluidization dynamics in a lab-scale two-dimensional bubbling fluidized bed, they obtained simultaneous the bubble properties i.e. bubble size, bubble velocity distribution, etc. The results were compared with relevant literature correlation and resulted in sound agreement.

Rowe (1973) reported an expression to calculate the averaged particle circulation time with the aim to compare it with the reaction rate to test, in cases where the particle composition is changing, whether the bed can be assumed perfectly mixed (Rowe, 1964)(Kunii and Levenspiel, 1969).

The two main objectives of this paper are the following: First, to develop a methodology, combining the information provided by DIA and PIV, to characterize the general bed behaviour: bubble phase; size, position and velocity of the bubbles, dense phase velocity, proportion of time that a point is occupied by bubble, solid path, recirculation regions, etc Then, it is possible to study the fluid-dynamic and the structures over 2-D fluidized bed. Second, once the experimental techniques were adapted, improved and optimized for our experiments, the bed aspect ratio and the superficial gas velocity were varied with the aim of understanding the effect of these variations over the fluid-dynamic of the bed and detecting changes in its internal structure that dominates the mixing in fluidized beds.

For future works, DIA and PIV techniques have been applied over 2-D fluidized bed to characterize the solid mixing mechanism (Wei et al., 2006),(van Demeter, 1967),(Grasa and Abanades, 2002),(Wei et al., 1998)

2.3 Data collection and proccesing

Figure 2.1 shows the image acquisition system and the experimental fluidized bed. The experiments were carried out in a 2-D cold fluidized bed of dimensions $10 \times 60 \times 0.5\, cm$. A detailed description of the facility can be found in Almendros-Ibáñez et al. (2006). The air distributor consisted of 9 holes ($1\, mm$ diameter) with a $1\, cm$ gap between them. The front and the rear walls were made of glass and the back glass of the bed was covered by a black card to get a higher contrast in the images Almendros-Ibañez et al. (2009). The bed was filled with Geldart-B glass particles,Geldart (1973), $2500\, kg/m^3$ density ρ_p, and $300 - 400\, \mu m$ diameter d_p.

Two operational variables were varied during the experiments: the ratio between fixed bed height, h, and the bed width, w (0.5 and 1) and the ratio between the superficial gas velocity, U, and the minimum fluidization velocity, U_{mf} 1.2, 1.4, 1.6. Table 2.1 shows the six different cases tested.

Two 650 watts spotlights were used to get a uniform illumination of the bed. A high speed video camera, Redlake Motion pro X3, with 4 Gb memory was used to take 3271 images at 125 frames per second. The number of pixels in the picture was different for each bed aspect ratio: $789 \times 1098\, pixels$ for $h/w = 0.5$ and $554 \times 1277\, pixels$ for $h/w = 1$ From these data, two image groups (for each case) were defined. The first

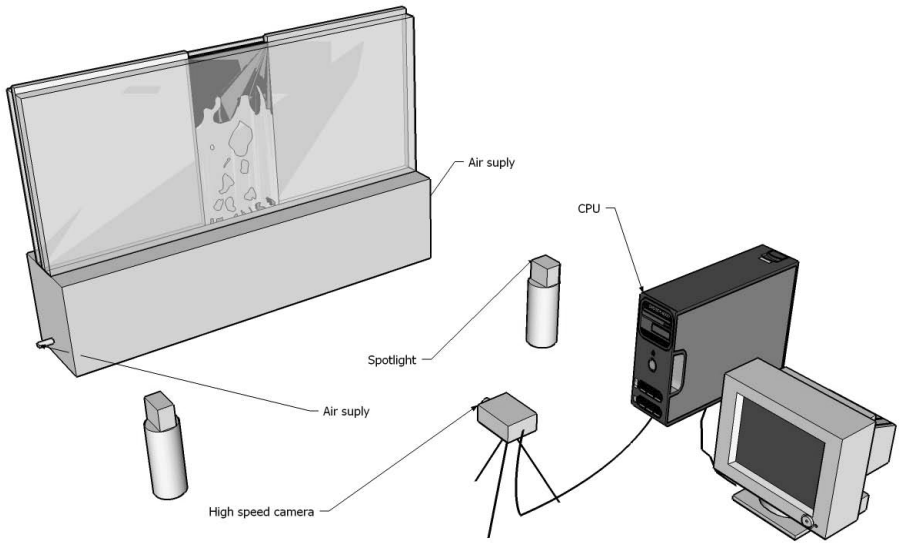

Figure 2.1: Scheme of the experimental facilities.

Case	h/w	U/U_{mf}
1	0.5	1.2
2	0.5	1.4
3	0.5	1.6
4	1	1.2
5	1	1.4
6	1	1.6

Table 2.1: Measurement cases for different variables values (h,U)

group was composed of 100 randomized samples, and the second was formed by the 100 images successive to the first group. Second group is necessary to characterize bubble velocity and dense phase velocity. Time averaging bubble and dense phases. Bubble and dense phase velocity analysis The modeling of gas-fluidized bed can be based on two distinct phases (Davidson and Harrison (1963),Kunii and Levenspiel (1969),Grace J.R. (1971)) a bubble phase consisting of large rising voids essentially free of particles, and a dense phase consisting of solid particles and interstitial gas. Therefore, for our experiments, each pixel of each image is identified as bubble phase (B) or dense phase (D) Grace and Clift (1974). For this two-phase model, and under the assumption that ε (dense phase voidage) is constant everywhere in the dense phase Grace and Clift (1974), group 1 images were processed, and calculating a threshold level (Otsu, 1979) for each one, to distinguish between dense phase $level = 0$ and bubbles $level = 1$. The images of group 1 were summed and rescaled, producing a time-average bubble phase map as follows:

$$\overline{B_{i,j}} = \frac{1}{N}\sum_{k=1}^{N} B_{i,j,k} \tag{2.1}$$

where $\overline{B_{i,j}}$ is the proportion of time that the point (i,j) is occupied by the bubbles. A similar analysis was performed by Lim et al. (2007). Therefore, the fraction of time that the dense phase occupies the point (i,j) can be expressed as follows:

$$\overline{D_{i,j}} = 1 - \overline{B_{i,j}} \tag{2.2}$$

Figure 2.2(a) shows a typical picture of the bubbling bed captured by the high speed camera, where three big bubbles are clearly observed, while other small bubbles are present in the bed in the region close to the distributor. Figure 2.2(b) shows the result of applying a threshold algorithm (Otsu, 1979) to the picture showed in figure 2.2(a). As stated above, in figure 2.2(b), a pixel value equal to 1 is assigned to the points occupied by the bubbles, whereas a pixel value equal to 0 is assigned to the point occupied by dense phase.

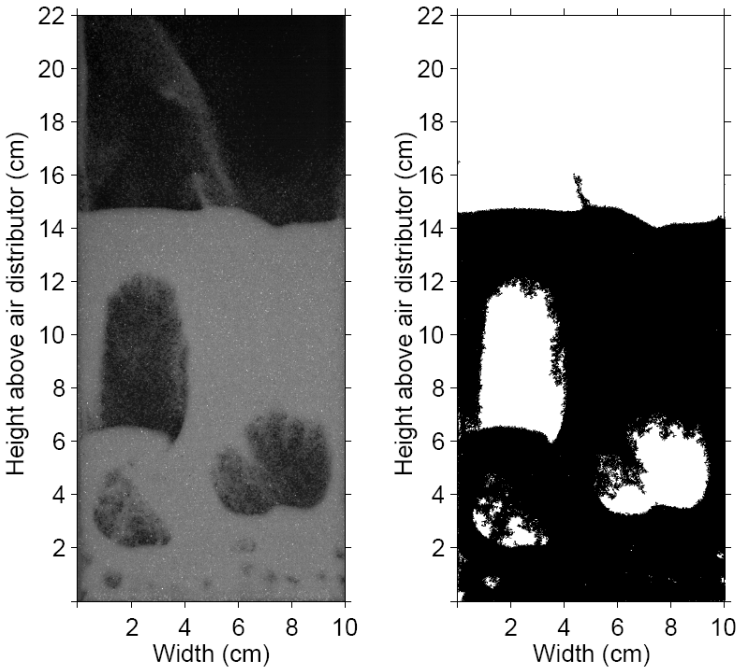

(a) (b)

Figure 2.2: Threshold transformation, and identification of bubble phase and dense phase, in an image of the fluidized bed.

For the time-averaged analysis, is not necessary to analyze all the images. As stated above, two groups of 100 randomized images, each one, were selected to be analyzed. For all time averaged measurements, the standard deviation of the measure was calculated in different point of the fluidized bed, it has been experimentally tested that for N = 100 the standard deviation keeps constant, figure 2.3 shows the results obtained in the center of fluidized bed for case 4. Therefore, $N = 100$ was the size of

the two groups generated with randomized images.

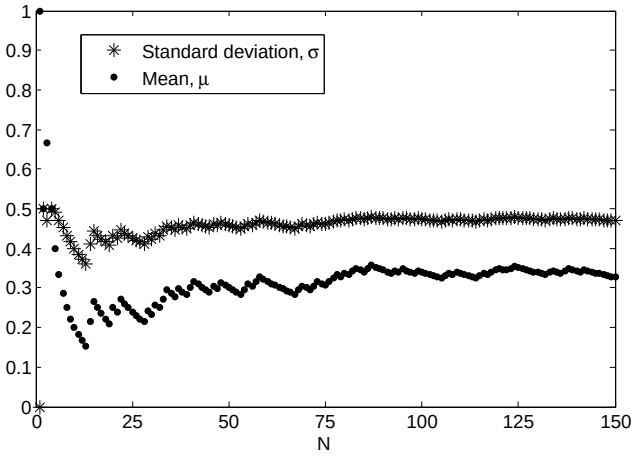

Figure 2.3: Mean value of B and standard deviation in a fixed point in the center of the fluidized bed, case 4

The two groups defined above were used for all the following analysis. First, a digital image analysis was carried out to characterize $\overline{B_{i,j}}$ and $\overline{D_{i,j}}$. Second, the bubble mass centers and their velocities were obtained using the information from both groups. The bubble mass centers in each image were identified using a computer code based on contour analysis. A max-min criterion was established to reject outliers, as the highest area in each image was the freeboard, and the lower areas were very likely to be shadow regions appearing close to the walls.

Then, to identify the mass center displacement of each bubble in each image, a method similar to the one described in Rodriguez-Rodriguez et al. (2003) was used. The bubbles on each image of the first group were transformed into a circle of radius $\lambda\ R_{eq}$, where the equivalent radio was calculated based on the bubble area. Then, the bubble mass centers on each image in the second group were compared with the information from the correlated images from the first group. The centers that lay inside of these circles were identified. The parameter λ was set equal to 0.8. In this way, the probability of finding the bubble mass center becomes higher than 0.95. When several points were inside a circle; the bubble with the most similar area was selected. As a result of this procedure, pairs of centers of consecutive images were obtained. Using the bubble displacement and time delay between frames, the bubble velocity was computed.

Finally, using a PIV technique similar to Müller et al. (2007), the dense phase velocity field of each image was calculated. F = 16 pixel square windows were selected as the smallest interrogation regions, with a 0.5 overlapping factor in the multigrid PIV freeware code Sveen (2004). The summation of the 100 PIV images yields to the time- average dense phase velocity field, Laverman J. et al. (2008).

The dense phase velocity vector is represented by $\overrightarrow{U}_{i,j,k}$ and the time-averaged dense phase velocity is calculated as follows:

$$\overline{\overrightarrow{U}_{i,j}} = \frac{1}{N}\sum_{k=1}^{N}\overrightarrow{U}_{i,j,k} \tag{2.3}$$

Note that the velocity vectors provided by the PIV method occupy a sub grid comprising a fraction of the total number of pixel position of the images. Therefore the resolution of the velocity vector maps are lower that the concentration maps.

For a sufficiently large number of ensembles, N,$\overline{D_{i,j}}$ and $\overline{\overrightarrow{U}_{i,j}}$ represent the fraction of time that a point is occupied by the dense phase and the temporal mean of dense phase velocity at point i, j, respectively. In the PIV measurement, bubbles were masked, as they were considered region free of particles, Laverman J. et al. (2008).

2.4 Results and discussion

2.4.1 Bubble pattern

The results obtained for all the cases of table 2.1 are represented in figure 2.4. This figure shows the fraction of time that a point is occupied by solids, $\overline{D_{i,j}}$. In cases 1 and 4, figure 2.4(a) and *figure* 2.4 (d), a non uniform distribution of air in the fluidized bed is observed. This maldistribution along the fluidized bed could be attributed to a small gas pressure drop through the bed distributor, compared with the bed pressure drop Johnsson F. et al. (2000), Sasic S. et al. (2005) The distributor is continuously supplying air along the width, but the bubble air flow is only visualized at the bottom right of the bed. Both cases correspond to a low excess gas velocity. A higher value of excess gas velocity gives a more uniform bubble distribution within the fluidized bed, due to the increase in the gas pressure drop through the bed distributor. In those cases the value of h/w influences the internal structure of the bed. figure 2.4(b) and figure 2.4(c) (cases 2 and 3) show higher solid concentrations in the walls and in the center of the bed, and two independent bubble paths with no coalescence effect between them. In cases 5 and 6 $h/w = 1$, figure 2.4(d) and figure 2.4(e) respectively, the two bubble paths becomes in only one before the bubbles reach the bed surface. This effect generates only one air channel in the center of the bed, displacing the particles to the walls. Therefore, higher values of h/w change the preferential paths of bubbles in fluidized beds even if excess gas velocity remains constant. This is in agreement with the well-known model of Werther J. and Molerus O. (1973), schematized in figure 2.5.

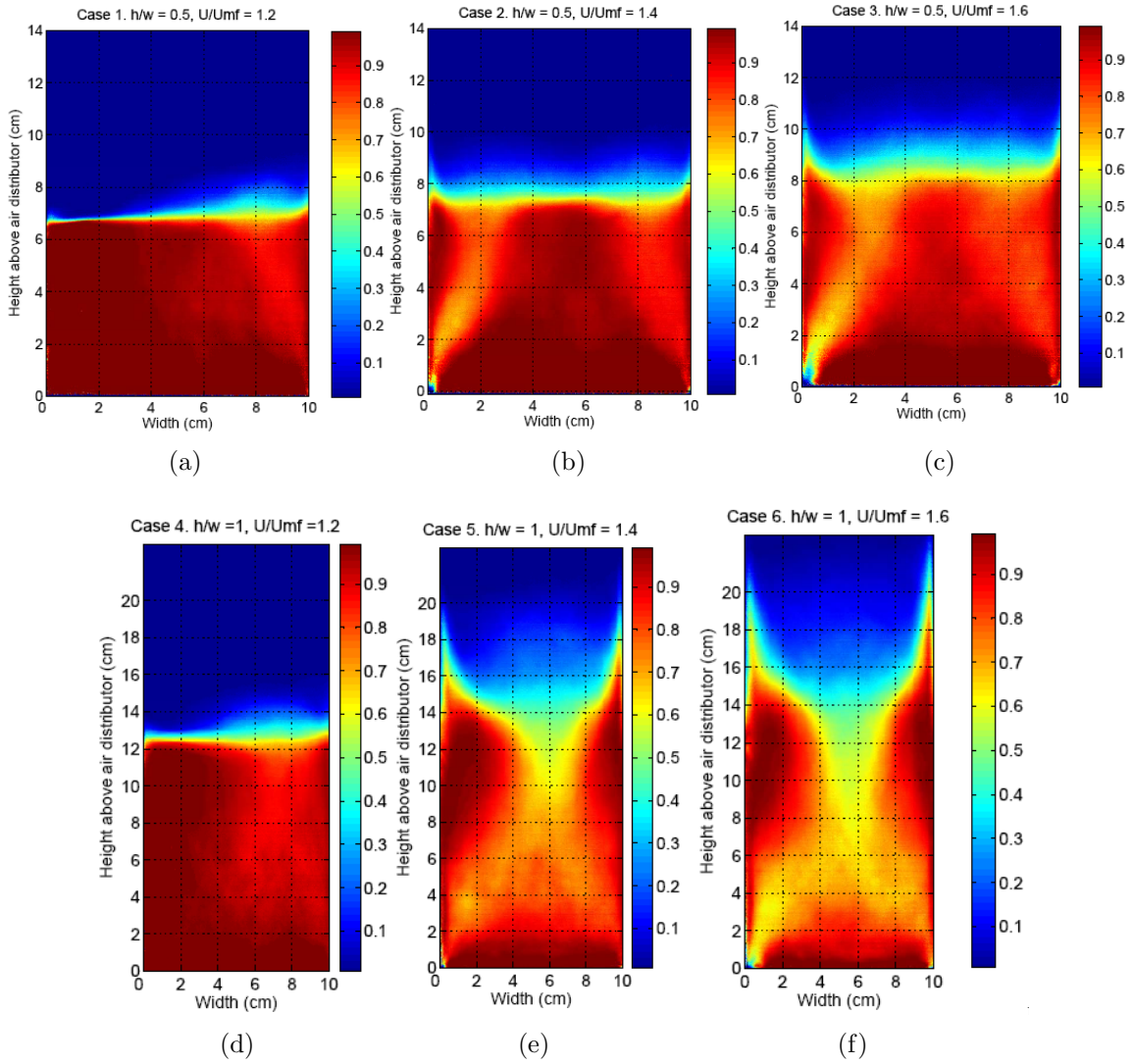

Figure 2.4: Fraction of time that a point is occupied by solids for the six cases of summed images

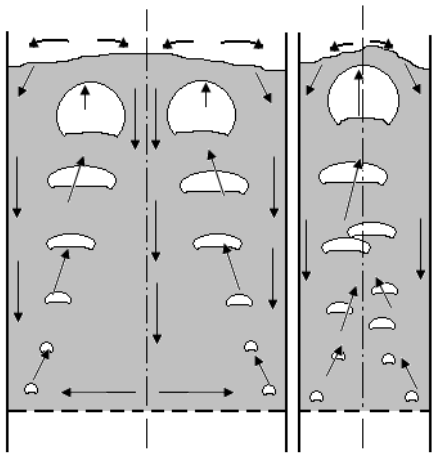

Figure 2.5: Molerus and Werther proposed model

2.4.2 Bubble mass center and bubble velocity

When images were analyzed, the mass center coordinates of identified bubbles in each image of both samples were stored. With this information and the criterion explained in the previous section, the velocity vectors of the bubbles were calculated. Figure 2.6 shows the velocity map corresponding to the motion of the mass center of the bubbles for the six cases of table 2.1.

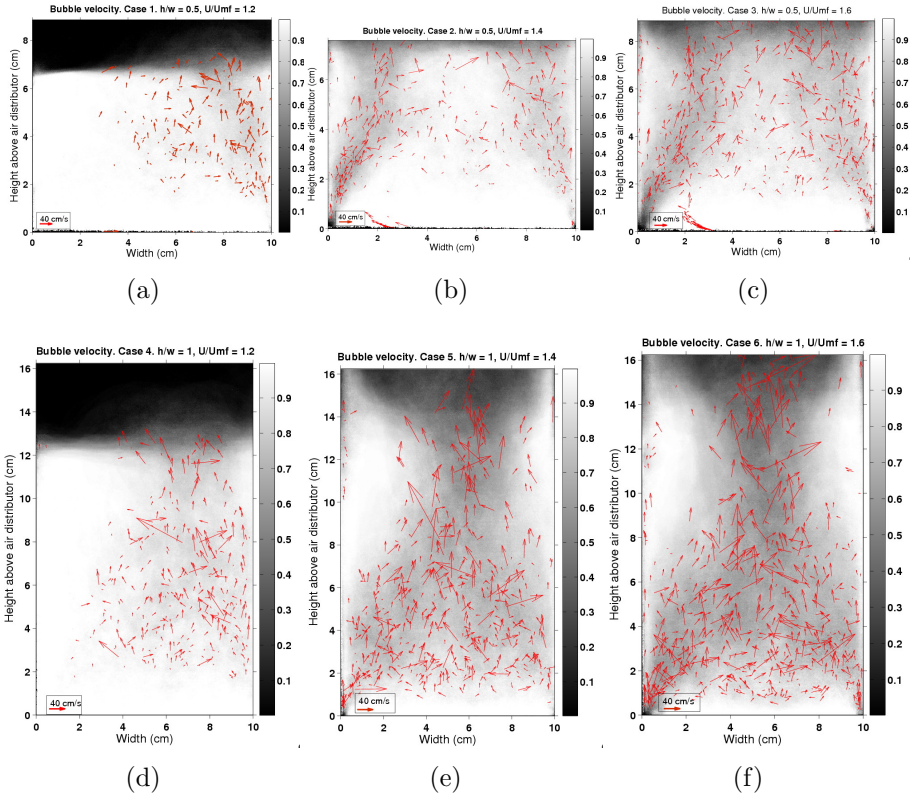

Figure 2.6: Bubble path distribution and bubble velocity vectors. The graph are superimposed on the time averaged dense phase results.

In all cases, the mass center of the bubbles is situated in the dark areas of each picture. In addition, Figure 2.6 shows that bubble velocity increases with the height above the distributor. This is a consequence of the bubble growth along the bed, since, up to a certain height, the bubble velocity is proportional to the square root of its size, Shen et al. (2004). In order to quantify this effect, a detailed analysis of the number, size and velocity of bubbles along the bed is presented in figure 2.7.

In figure 2.7 the coalescence effect for both aspect ratios tested is quantified. The cumulative decreasing along the bed height of the bubble number variation, represents the coalescence effect, i.e. which is the result of a low pressure region in the wake of a leader bubble, that affects the bubble path of a trailing bubble. As a consequence, the number of bubbles decreases from the bottom to the top of the bed, increasing the size

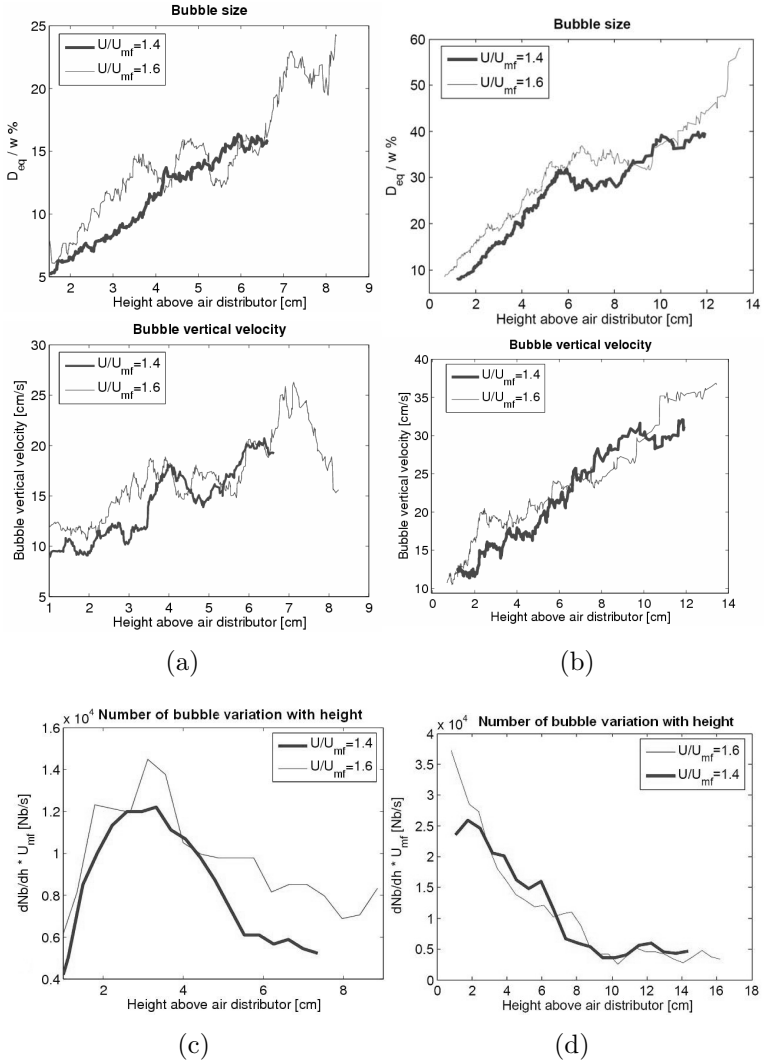

Figure 2.7: Size and velocity of bubble along the fluidized bed. a) Cases 2 and 3 (h/w = 0.5). b) Cases 5 and 6 (h/w = 1).c) and d) number of bubble variation along fluidized bed, cases 2-3 and 5-6 respectively

and velocity of the resulting bubbles after coalescence. The analysis provides enough information to relate averaged bubble speed to averaged bubble diameter and height, next figures, figure 2.8 (a) and figure 2.8 (b) represent the results obtained for both configuration $h/w = 0.5$ and 1 respectively.

The points represent the experimental averaged results for bubble diameter and bubble velocity at different bed height. In both figures, a theoretical correlation between bubble velocity and bubble diameter, Shen et al. (2004), is presented:

$$U_b = \phi(gD_b)^{0.5} \tag{2.4}$$

Shen et al. (2004) proposed a value of $\phi = 0.8 - 1$ for measurements in 2-D fluidized bed. Both bed aspect ratios configurations, i.e. $h/w = 0.5$ and 1, are in reasonable

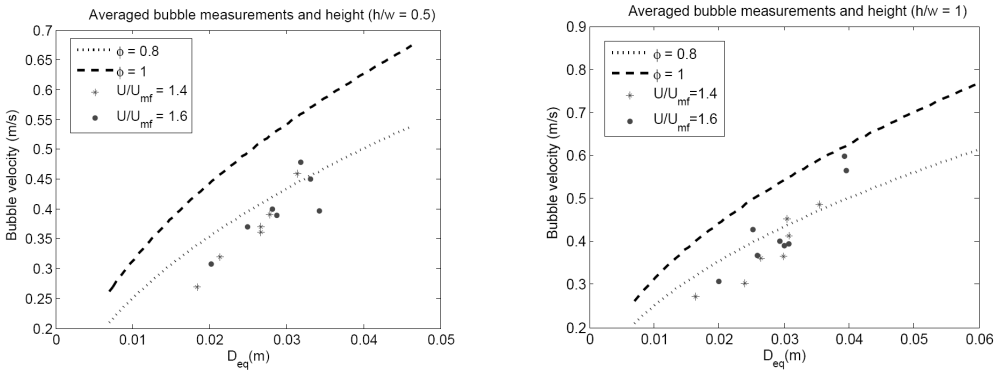

(a) (b)

Figure 2.8: Averaged bubble measurements and height

agreement to the theoretical correlation, 2.4. Therefore, the DIA technique can be used as a reliable technique for the bubble phase to characterize bubbles diameter and bubble velocity.

2.4.3 Dense phase velocity and recirculation regions

The dense phase velocity fields were obtained using the PIV technique correlating images of samples 1 and 2. The values obtained for each pair of images were summed obtaining the time-average dense phase velocity field along the bed; this procedure was applied for the six experimental cases. Fig. 2.9, shows the dense phase velocities distribution for all cases.

The dense phase velocity maps show the transport phenomenon induced by the ascending bubbles from the bottom to the top of the bed. They also address how the dense phase velocity increases due to, mainly, the bubble coalescence. When the superficial gas velocity increases, the bubbles suffer an increase in size. As a consequence of this increase in size, and knowing that the bubble velocity is proportional to the square root of its diameter Shen et al. (2004), the bubble velocity is higher, and bubbles transport the particles in their wakes with higher velocities. This dense phase transports from the bottom to the top of fluidized bed, needs to be compensated by a downwards movement of solid, creating recirculation regions. Figure 2.10 shows zones of interest where these recirculation regions are identified (Xiangfeng F. et al., 2008) in the two bed aspect ratios studied in this work.

With the information presented in figures 9 and 10 is possible to represent, schematically, the time-averaged dense phase movement. Figure 2.11.

Figure 2.11 (a) represents the dense phase pattern for high relation between width and bed height $h/w = 1$, on the other hand, figure 2.11 (b) represents, schematically, the time-averaged dense phase movement for smaller values of the bed aspect ratio

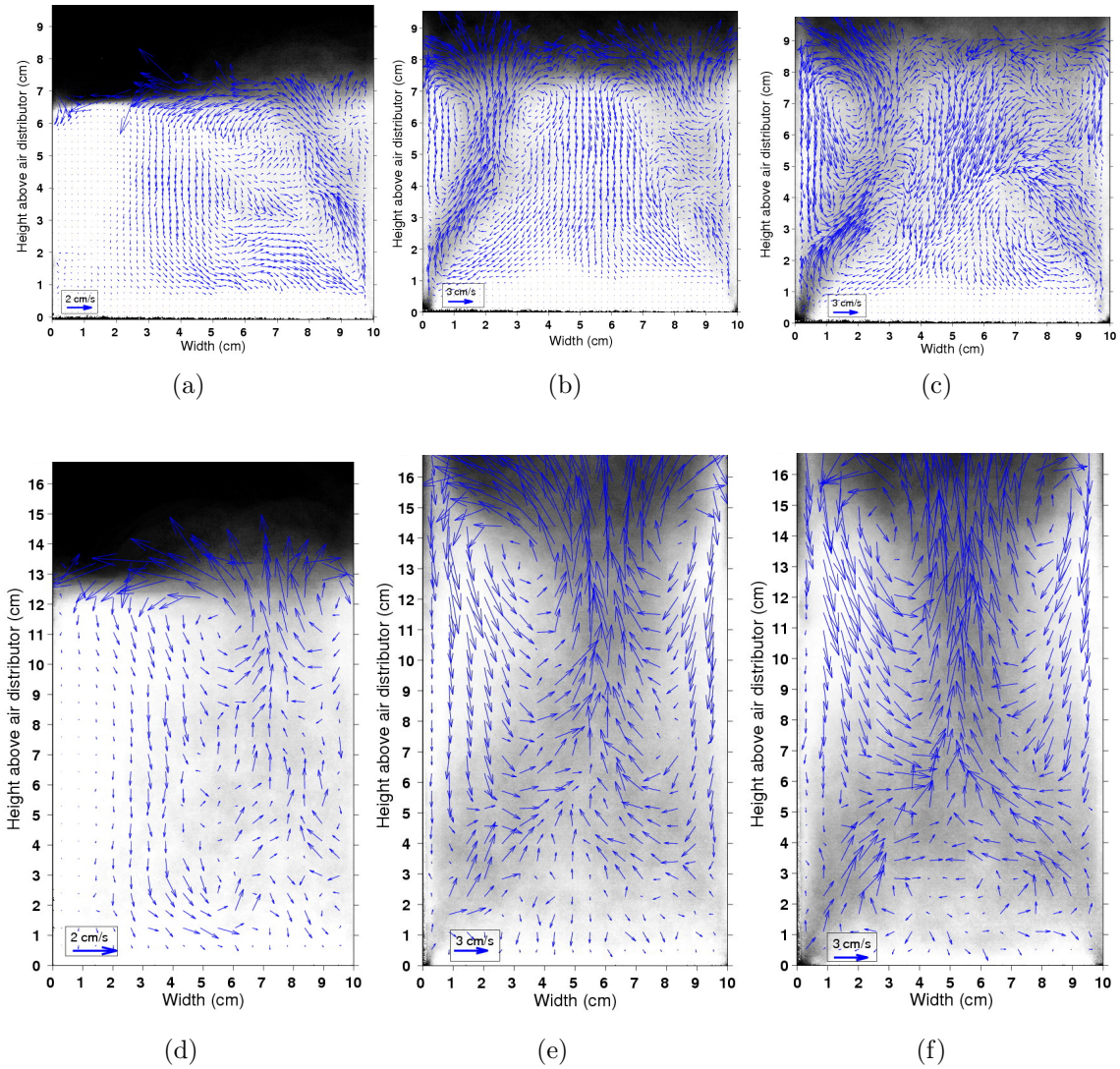

Figure 2.9: Time-averaged dense phase velocity for different cases. $a = case1$, $b = case2$, $c = case3$, $d = case4$, $e = case5$, $f = case6$

$h/w = 0.5$. As can be seen, figure 2.11 is in concordance with figure 2.5, solid circulation pattern in bed of different height-to-diameters ratios proposed by Werther J. and Molerus O. (1973)

The effective bubble path section can be obtained with the time-averaged PIV data. As stated above, the dense phase velocity vectors describe the transport phenomena induced by the ascending bubbles, and the dense phase velocity fields provide information about particle movement in all directions, not just the ascending movement but also the particle ingestion from the bubble wake. Therefore, is possible to distinguish the time-averaged regions of the ascending and descending particles and also to quantify their size. Figure 2.12 illustrates the dense phase velocity vectors, clearly showing regions of the ascending and descending particles.

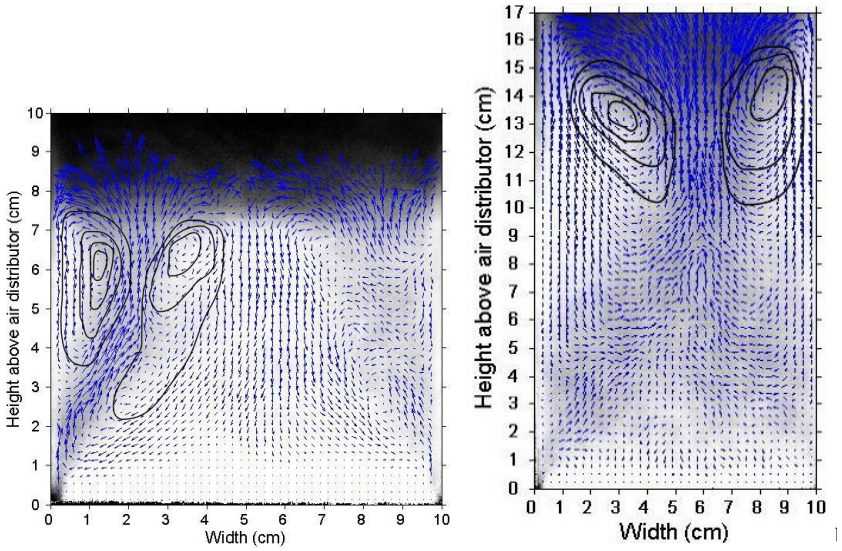

(a) (b)

Figure 2.10: Mean velocity path lines for the dense phase in cases 2 and 5, a) b), respectively

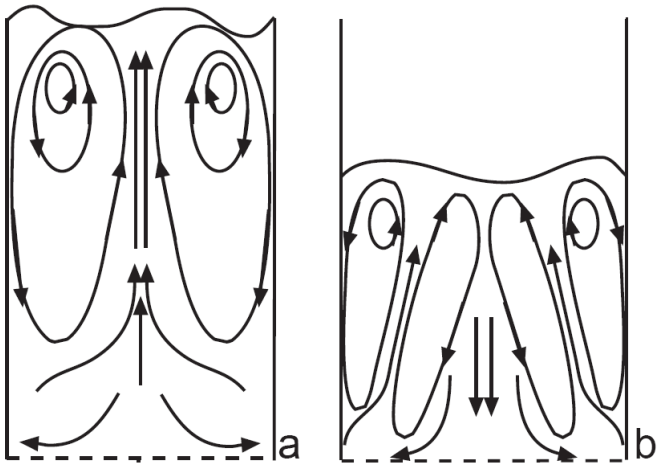

Figure 2.11: Schematics of the time averaged dense phase movement

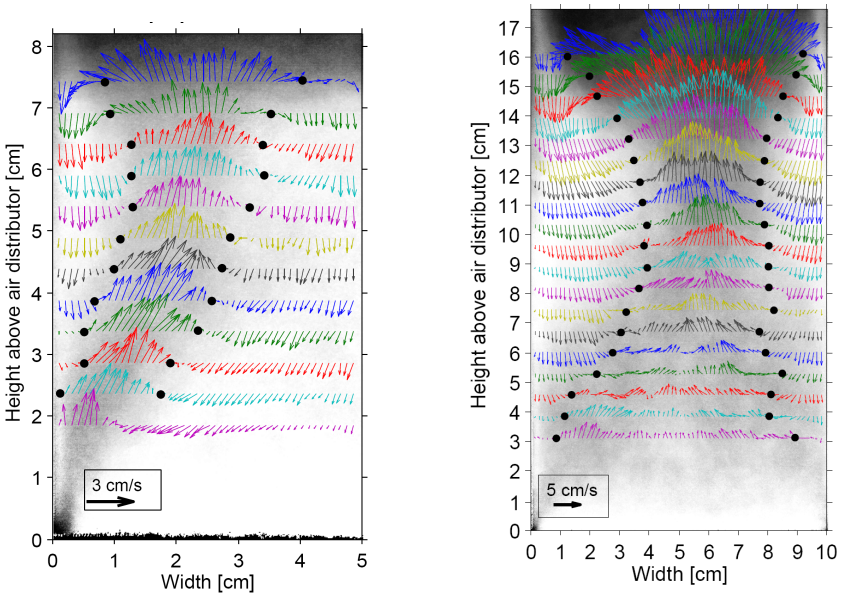

(a) (b)

Figure 2.12: Ascending and descending dense phase regions for *case*2 and 5, a and b respectively.

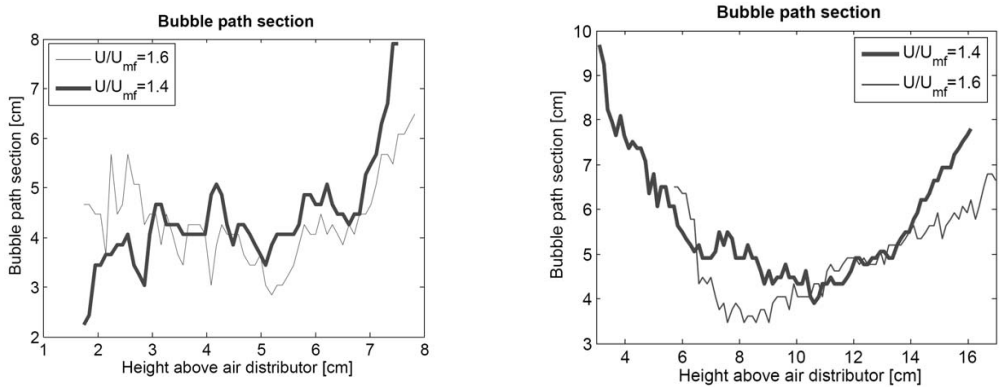

(a) (b)

Figure 2.13: Air path sections for the different heights above the air distributor. a) $h/w = 0.5$ b) $h/w = 1$

In this figure, black points represent the coordinates (x, y) where the sign of the vertical velocity vector changes for each row. Therefore, for the same row, the size of the most probable bubble path is delimited as the distance between black points. Note that Figure 2.12(a) only represents the half of the bed width, and that the complete air path region size is actually twice the represented size. The ratio between the height and the width of the bed h/w has an important influence on the air region development. Higher values of this parameter generate only a wide air channel in the middle of the bed, due to the coalescence effect. The width of the channel decreases as bubbles ascend from the bottom to the top, until the minimum width is reached, just under the bed surface. Then, the width increases until the freeboard is reached. However, for $h/w = 0.5$ the width of the air path increases continuously from the bottom to the freeboard. The influence of the superficial gas velocity on the size of the air path was also analyzed. Figure 2.13 shows, for different bed aspect ratios and different superficial gas velocities, the variation of the size of the air path section with the height above the air distributor.

Figure 2.13 (b) shows the influence of the superficial gas velocity on the bubble path section, or equivalently on the bubble coalescence: when the superficial gas velocity increases, the coalescence effect takes place closer to the air distributor Darton et al. (1977). Although the equivalent diameter of the bubble increases with the superficial gas velocity (see, Figure 2.7(b), the air path section decreases, reaching the minimum value at a smaller distance from the bottom of the bed. This result could be attributed to the elongated shape acquired by the bubbles when their size increases Goldsmith and Rowe (1975). However, this clear trent is not observed in the bubble path section depicted in figure 2.13(a).

Figures 2.9 and figure 2.12, show, for our experimental conditions, that the parti-

cles in the fluidized bed ascend in one or two paths. This ascending movement of the particles is produced by the excess of gas over minimum fluidization conditions that traverses the bed in the form of bubbles; as was previously commented, these bubbles transport particles in their wakes from the bottom to the bed surface. A descending movement of particles, in opposite direction to the main bubble flow, appears close to the walls towards the base of the fluidized bed in order to replace the particles that have been dragged by the bubbles. Obviously the amount of particles that ascends must balance with the particles that descend over a sufficiently large period of time. Therefore, the size and intensity of these ascending and descending transport of particles is intrinsically connected with the time-averaged dense phase values ($\overline{D}$) within the excess of air path delimited in Figure 2.12, and outside this path.

The combination of figure 2.10(b) and 2.12(b), give us qualitative information about the regions where it is more probable that the particles leave the bubble path and where it is more probable that they are dragged again by bubble. These regions are schematized in Figure 2.14 for cases 5 and 6 ($h/w = 1, U/Umf = 1.4, 1.6\, respectively$)

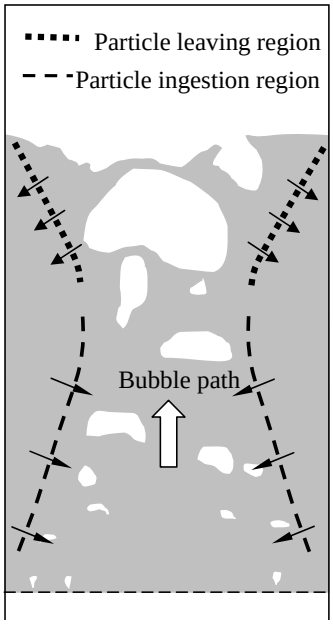

Figure 2.14: Interaction between the bubble path and the dense phase displacement,black arrows, in a 2-D fluidized bed.

2.4.4 Averaged particle circulation time

Some information about the particle circulation time within the bed can be obtained from the PIV data for the dense phase velocity shown in previous sections. These results are based in a short communication reported by Rowe (1973) summarized as follows:

Rowe P.N. reports that the upwards drift is roughly conical sphere of volume approximately 0.35 of the bubble volume V_b. The wake volume averages 0.25 of the bubble volume. Thus, each bubble displaces upwards a volume of particles of $0.6V_b$, Fig. 2.15 illustrates this model.

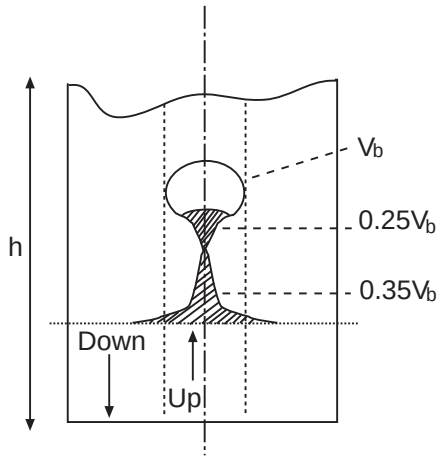

Figure 2.15: Model of particle movement

The volumetric bubble flow Q_b is defined as:

$$Q_b = V_b n \tag{2.5}$$

where n is the $bubble/sec$ cross a horizontal plane. The residence time of a single bubble in the bed is given by

$$t_b = h/U_b \tag{2.6}$$

and therefore the hold-up of bubbles by

$$Q_b t_b = nV_b h/U_b \tag{2.7}$$

and the fraction of bubble space in the bed

$$\epsilon_b = Q_b/U_b A \tag{2.8}$$

This is also the fraction of the bed cross-sectional area occupied by bubbles, A_b/A. A_b is that area through which the upwards particle flow of $0.6Q_b$. The averaged upward particle velocity then is given by

$$U_{up} = 0.6Q_b/A_b = 0.6U_b \tag{2.9}$$

and since there is no net particle movement out of the bed

$$U_{down} = 0.6Q_b/(A - A_b) = 0.6/\left(\frac{A}{Q_b} - \frac{1}{U_b}\right) \tag{2.10}$$

The averaged particle circulation time around the bed will be

$$t_c = h\left(\frac{1}{U_{up}} + \frac{1}{U_{down}}\right) = hA/0.6Q_b \tag{2.11}$$

The model proposed can be related with the expanded bed height and therefore with the minimum fluidization velocity U_{mf} in which case eq. 2.11 reduces to

$$t_c = h_{mf}/\left(0.6(U - U_{mf})\left(1 - \frac{U - U_{mf}}{U_b}\right)\right) \tag{2.12}$$

In the present work, the U_{up} and U_{down} have been calculated using the PIV technique, reporting a time-averaged results for upwards and downwards velocity for the dense phase in each case. Once the U_{up} and U_{down} have been obtained, the eq. 2.11 is calculated reporting the results presented in the next table:

h/w	U/U_{mf}	U_{up} (cm/s)	U_{down} (cm/s)	t_c (s)
	1.2	0.96	1.01	10.15
0.5	1.4	1.93	1.92	5.19
	1.6	3.14	3.18	3.16
	1.2	1.46	1.57	13.2
1	1.4	4.15	5.03	4.39
	1.6	4.58	5.77	3.91

Table 2.2: Averaged particle circulation time around the bed for different cases

Next figure shows the results presented in table 2.2

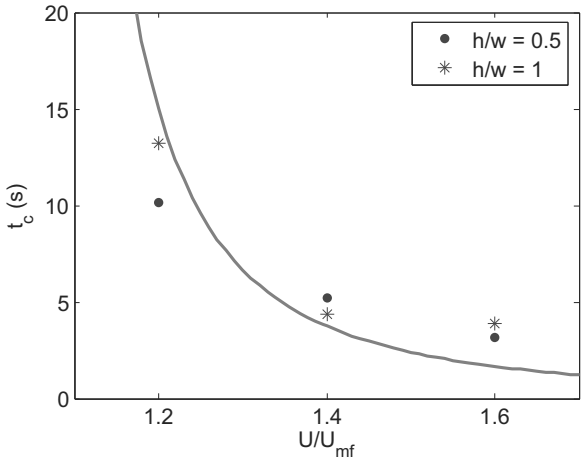

Figure 2.16: Averaged time particle circulation time vs.flow rate

The PIV technique is useful to calculate the averaged particle circulation time (Eq. 2.11) based in experimental results. Avoiding to use the expression 2.12 where

the throughflow effect is not taken into account.

2.5 Conclusions

In this work, different measurement techniques have been applied over a 2-D fluidized bed, getting fluid-dynamic information from the dense phase as well as bubble phase. The techniques include the measurement and visualization of the time-average bubble distribution, bubble velocity, and dense phase velocity maps. An analysis of the influence of the bed aspect ratio and the superficial gas velocity in the formation of fluid-dynamic structures in a fluidized bed is included. The main conclusions of the article are described in this section.

The black and white scale generated from the 100 acquired images provides complete information about proportion of time that a point is occupied by solid and bubble path. It is therefore possible to analyze the bubble distribution in the fluidized bed and whether an internal time-average fluid-dynamic structure exists.

The procedure calculates the mass center position and bubble velocity vector, to characterize the ascending movement of the bubbles through the bed and the coalescence effect. Cases 2 and 3, with a small geometrical relationship ($h/w = 0.5$), have two preferred airways clearly identified. In contrast, cases 5 and 6 ($h/w = 1$), have only one path for the ascending bubble, forcing the excess air to through to the center of the fluidized bed. In cases of low air supply ($U/Umf = 1.2$), a non uniform air distribution along the fluidized bed width is observed.

The time-average dense phase velocity fields obtained using the PIV technique over correlating images of sample 1 and 2, give us information about the dense phase movement. The excess air channel is identified and measured, and the recirculation regions close to these regions can be identified. This map provides information about the most probable path of a particle inside a fluidized bed.

The influence of the gas supply air over the excess air channel has also been analyzed. An increase has two effects: a faster coalescence effect along the bed and more elongated bubbles in the region. The combination of these two effects generates a reduction in the size of the excess air channel. The results show the most probably locations where the particles leave the bubble path and where the particles are ingested again into the bubble path.

Finally, this is in a close relation with the solid circulation rate, it was shown that when the gas supply is increasing, the averaged particle circulation time decreases, besides in a first approximation the effect of the bed aspect ratio in the averaged particle circulation time it seems to be not relevant.

2.6 Notation

A Cross sectional area of the bed, $[m^2]$

A_b Cross sectional area occupied by bubble, $[m^2]$

ΔP_{bed} Gas pressure drop through the bed $[Pa]$

$\overline{B}$ Fraction of time that a point is occupied by bubble$[-]$

d_p Particle diameter, $[\mu m]$

$\overline{D}$ Fraction of time that a point is occupied by solid$[-]$

h Fixed bed height, $[cm]$

n Number bubble per second crossing a horizontal plane$[sec^{-1}]$

N Number of images used for the calculation of the mean quantity$[-]$

N_b Cumulative number of bubbles$[-]$

Q_b Volumetric bubble flow $[m^3/s]$

R_{eq} Equivalent radius of the bubble$[m]$

t_c Averaged particle circulation time, $[s]$

U Superficial gas velocity, $[m/s]$

$\overrightarrow{U}$ Dense phase velocity vector$[m/s]$

$\overline{\overrightarrow{U}}$ Time averaged dense phase velocity vector$[m/s]$

U_{mf} Minimum fluidization velocity, $[m/s]$

U_{up} averaged particle velocity up, $[m/s]$

U_{down} averaged particle velocity down, $[m/s]$

V_b Bubble volume, $[m^3]$

w Bed width, $[cm]$

x Horizontal coordinate, $[cm]$

y Height above distributor, $[cm]$ *Greek symbols*

λ geometrical parameter$[-]$

ε Dense phase voidage$[-]$

ϵ_b fraction of bed occupied by bubble,$[-]$

ρ_p Particle density, $[Kg/m^3]$

Bibliography

Almendros-Ibáñez J.A., Sobrino C., de Vega M. and Santana D., A new model for ejected particle velocity from erupting bubbles in 2-D fluidized beds. *Chemical Engineering Science*,2006. vol. 61, pp. 5981-5990

Almendros-Ibáñez J.A., Sánchez-Delgado S., Sobrino C., and Santana D., Experimental observations on the different mechanisms for solid ejection in gas-fluidized beds.*Chemical Engineering and Processing.* 2009, 48, 734-744

Busciglio A., Vella G., Micale G. and Rizzuti L., "Analysis of the bubbling behaviour of 2-D gas solid fluidized beds Part I: digital image analysis technique". *Chemical Engineering Journal.* 2007, 140, 398-413

Darton R.C., LaNauze R.D., Davidson J.F. and Harrison D., 1977. Bubble growth due to coalescence in fluidised beds. *Transactions of the Institute Chemical Engineering*, vol. 55, pp. 274-280

Davidson J.F. and Harrison D., 1963. *Fluidised particles.* Cambridge University Press

Geldart D., 1973. Types of gas fluidization, *Powder Technology*, vol. 7, pp. 285-292

Goldsmith J.A. and Rowe P.N., The shape of the bubbles in a two-dimensional gas fluidised bed. *Chemical Engineering Science*, 1975, 30, 440-442.

Grace J.C. Chem. Engng. Prog. Symp. Ser. 1971. 67, 116-159

Grace J.R. and Clift R., 1974. On the two-phase theory of fluidization. *Chemical Engineering Science*, vol. 29, pp. 327-334

Grasa G. and Abanades J.L., The use of two different models to describe the axial mixing of solids in fluidised beds. *Chemical Engineering Science*. 2002, 57, 2791-2798

Johnsson F., Zijerveldb R.C., Schoutenb J.C., van den Bleek C.M., Leckner B., Characterization of fluidization regimes by time-series analysis of pressure fluctuations, *International Journal of Multiphase Flow.* 2000,26, 663-715.

Kunii D. and Levenspiel O., 1969. *Fluidization Engineering.* John Wiley & Sons

Laverman J. A., Roghair I., Van Sint Annaland M. and Kuipers H. Investigation into the hydrodynamics of gas-solid fluidized beds using particle image velocimetry coupled with digital image analysis. *The Canadian journal of chemical engineering.* 2008, 86, 523-535

Lim C.N , Gilbertson M.A. and Harrison A.J.L., Bubble distribution and behaviour in bubbling fluidised beds. *Chemical Engineering Science*, 2007, 62 56-59

Müller C.R., Davidson J.F., Dennis J.S. and Hayhurst A.L., 2007. A study of the motion and eruption of a bubble at the surface of a two-dimensional fluidized bed using particle image velocimetry (PIV), *Industrial & Engineering Chemistry Research*, vol. 46, pp. 1642-1652

Otsu N., 1979. A threshold selection method from gray-level histograms, *IEEE Transactions on Systems Man and Cybernetics*, 9 (1979) 62-66

Pallarès D. and Johnsson F., A novel technique for particle tracking in cold 2-dimensional fluidized beds-simulating fuel dispersion. *Chemical Engineering Science* 2006, 61, 2710 - 2720

Rodríguez-Rodríguez J., Martínez-Bazán C. and Montañes J.L.,A novel particle tracking and break-up detection algorithm: application to the turbulent break-up of bubbles. *Measurements Science and Technology*, 2003, 14, 1328-1340

Rowe P.N., A note on the motion of a bubble rising through a fluidized bed. *Chemical Engineering Science*, 1 (1964) 75-77

Rowe P.N. et al.*Trans. Instn Chem. Engrs*, 43 (1965) 271

Rowe P.N., Estimation of solid circulation rate in bubbling fluidised bed. *Chemical Engineering Science* 28 (1973) 979-980

Sasic S., Johnsson F., Leckner B., Fluctuations and waves in fluidized bed systems: the influence of the air-supply system, *Powder Technology*, 2005, 153, 176-195.

Shen L., Johnsson F. and Leckner B., 2004. Digital image analysis of hydrodynamics two-dimensional bubbling fluidized beds. *Chemical Engineering Science*, vol. 59, pp. 2607-2617

Sveen J.P., http://www.math.uio.no/∼jks/matpiv (Last modified in August, 2004. Accesed in 2008)

Tzeng J.W., Chen R.C. and Fan L.S., Visualization of flow characteristics in a 2-D bubble column and three phase fluidized bed, *AIChe Journal*, 1993, 39, 733-744

van Demeter J.J., in A.A.H. Drinkerburg (ed.), Proceeding of the international symposium on fluidization, Netherlands, Amsterdam. 1967

Wei F.,Cheng Y.,Jin Y. and Yu Z. Axial and lateral dispersion of fine particles in a binary-solid riser. *The Canadian Journal of Chemical Engineering*, 1998, 76, 19-26

Wei X., Sheng H. and Tian W., "Characterizing particle dispersion by image analysis in ICFB", *International Journal of Heat and Mass Transfer*. 2006, 49, 3338-3342

Werther J. and Molerus J., The local structure of gas fluidized beds-II. The spacial distribution of bubbles. *International Journal of Multiphase Flow*, 1973, 1, 123-138.

Xianfeng Fan, David J. Parker, ZhufangYang, Jonathan P.K. Seville and Jan Baeyens, The effect of bed materials on the solid/bubble motion in a fluidised bed, *Chemical Engineering Science*, 2008, 63, 943-950

Chapter 3

On the minimum fluidization velocity in 2D fluidized beds: variable thickness

Contents

3.1 Abstract

This work presents a new correlation to obtain the minimum fluidization velocity in 2D fluidized beds, based on experimental results for different particle sizes, bed thicknesses and heights of the fixed bed. The correlation proposed only depends on the

nondimensional variable t/d_p being t the bed thickness and d_p the particle size. This correlation has been compared with other experimental results that can be found in the literature and the comparison clearly shows two different tendencies: one group of experimental results that seems to follow the proposed correlation and other group that obtains higher minimum fluidization velocities than the ones predicted with the proposed correlation. In view of the differences in the experimental conditions of the different researchers, the influence of the electrostatic charge and the particle shape could explain the observed discrepancies.

In addition, the fluidization-defluidization curves measured experimentally have been compared with the curves predicted by Jackson model, fitting the model parameters to the experimental data. Nevertheless, for a fixed particle size and bed thickness, the one dimensional assumption of the model precludes to obtain general parameters due to the two dimensional voidage distribution in the bed and the electrostatic forces, which are not included in the model.

3.2 Introduction

The study of fluidized beds dynamics is a complex and not easy task. Different experimental techniques have been developed during the years to study it, such as pressure, capacitance, optical and /or heat transfer probes, Cheremisinoff (1986); Werther (1999); van Ommen and Mudde (2008). Other researchers have used imaging techniques to *"observe"* the interior of the bed. Simons Simons (1995) made a review of radiation and capacitance imaging and more recently various works have been published about the use of Magnetic Resonance Imaging (MRI) to measure time average particle velocity Müller et al. (2008), time average voidage in the bed Holland et al. (2008) and/or to measure the mean length of the jets formed in perforated plate distributors Rees et al. (2006).

On the other hand, 2D fluidized beds have been also widely used to study fluidized bed hydrodynamics since the pioneering works during the early 60's Massimilla and Westwater (1960); Rowe et al. (1964); Rowe and Partridge (1965); Grace and Harrison (1969) up the 21^{st} century, where different studies can be found in the literature. For example, Trsiakti et al. Trisakti et al. (2001) and Pallarès and Johnsson Pallarès and Johnsson (2006) followed the motion of an artificial fuel particle with a camera in a 2D fluidized bed in order to characterize fuel dispersion and fuel motion within the bed, Shen et al. Shen et al. (2004) and Busciglio et al. Busciglio et al. (2007) measured the bubble size and velocity along the bed height, Santana et al. Santana et al. (2005), Müller et al. Müller et al. (2007) and Almendros-Ibáñez et al. Almendros-Ibanez et al.

(2009) applied Particle Image Velocimetry (PIV) technique to obtain the instantaneous particle velocity around erupting bubbles in 2D fluidized beds, Almendros-Ibanez2 et al. (2009) combined PIV technique with computational calculations to characterize the particle-fluid motion around bubbles and Link et al. Link et al. (2004) and Busciglio et al. Busciglio et al. (2009) used the experimental results obtained in 2D fluidized beds to compare them with their numerical simulations.

Thus, 2D fluidized beds have been and are still successfully used to study particle-fluid dynamics in fluidized beds, contributing important qualitative information. Moreover, in 2D fluidized beds high speed cameras can be easily used Busciglio et al. (2007); Santana et al. (2005); Müller et al. (2007); Almendros-Ibanez et al. (2009); Almendros-Ibanez2 et al. (2009), which obtain higher spatial and temporal resolution than other techniques used in 3D beds (radiation and capacitance imaging and MRI). Nevertheless, it is still not clear how the results obtained in 2D fluidized beds can be quantitatively extrapolated to real 3D beds Grace and Baeyens (1986); Rowe and Everett (1972). Geldart Geldart (1970) and Clift Clift (1986) observed that the bubble size distribution obtained in 2D fluidized beds can not be directly extrapolated to 3D beds due to the differences in bubble coalescence between both geometries and wall effects. More recently, the experimental results of Shen et al. Shen et al. (2004) corroborate these results. In a different work, Briongos and Guardiola Briongos and Guardiola (2005) proposed a new method for scaling 2D hydrodynamics based on the chaos scale-up methodology.

Minimum fluidization velocity U_{mf} is one of the main parameters that characterize a fluidized bed. Ramos Caicedo et al. Ramos et al. (2002) observed that the minimum fluidization velocity in 2D fluidized beds varies with both bed thickness and bed height, observing important differences in U_{mf} (up to 500 %) when the bed height is varied from $h = 8\,cm$ to $h = 60\,cm$ (bed thickness $e = 6\,mm$ and particle size $d_p = 250 - 400\,\mu m$). Ramos Caicedo et al. proposed a correlation to extrapolate U_{mf} in 2D fluidized beds to a 3D geometry, although the correlation proposed was not for general use because the proposed constants depend on the particle size. Geldart Geldart (1970) observed also that the minimum fluidization velocity increases with the fixed bed height, although an increment of only 43 % in U_{mf} was observed when the bed height was increased from 5 to $80\,cm$. These differences observed in U_{mf} could be attributed to wall effects, because theoretically minimum fluidization velocity does not depends on bed height.

In this work a new correlation is proposed to quantify the influence of the 2D geometry on the measurement of the minimum fluidization velocity, showing that the minimum fluidization velocity in a 2D geometry increases as the ratio between the particle size and the bed thickness (d_p/t) increases, although no important differences

were observed with the fixed bed height (in contrats with the results observed by Ramos Caicedo et al. Ramos et al. (2002)). In addition, the model of Jackson Jackson (1998) was used to characterize the wall effects, although the 1D assumption of this model (the voidage varies with the bed height $\varepsilon(z)$) precluded to obtain general conclusions because the voidage distribution during the fluidization-defluidization process in a 2D bed varies with both height and width ($\varepsilon(x, z)$).

In the following, the experimental set-up and the particles employed during the experiments are described, then the experimental results are presented and finally the last sections discuss the experimental results and expose the main conclusions of the work.

3.3 Experimental setup

The experiments were carried out in a 2D cold fluidized bed of dimensions $500 \times 2000\,mm$ width w and high h Sanchez-Delgado et al. (2009), respectively. The third dimension, the thickness t, was variable. The rear of the bed was removable permitting to add or eliminate columns at the frame of the bed, which allows to vary the thickness of the bed. In this work three different bed thickness were employed: 5, 10 and $20\,mm$. The gas flow was introduced through both sides of the plenum in order to assure a proper distribution of the gas flow. Figure 3.1 shows a sketch of the 2D bed.

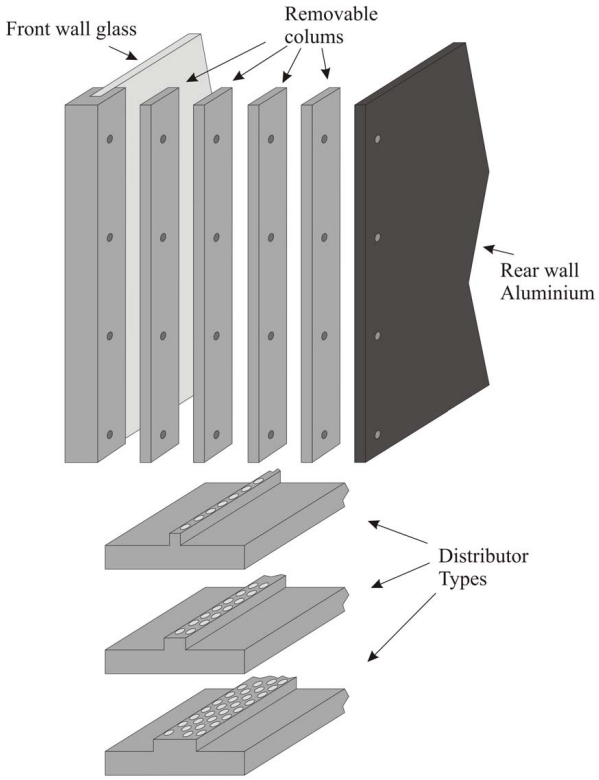

Figure 3.1: Scheme of the 2D fluidized bed with variable thickness

Three different distributors were employed for the three different bed thicknesses. The distributors were perforated plates with holes of $1\,mm$ of diameter with a gap of $1\,cm$ between them. In this way, the ratio between the open and the total distributor area was maintained constant for the three distributor, resulting in $1.57\,\%$ of open area. As a consequence, the characteristic curve of the distributor ($\Delta P_{dist} - U$) is the same for all of them. Figure 3.2(a) shows a scheme of the distributors and Figure 3.2(b) shows their characteristic curve.

The gas pressure drop was measured with a pressure transmitter (PTX 1400 model, GE industrial), with an operating pressure range from 0 to $6\,atm$, which was connected to the probe situated in the plenum, with a sample frequency of $100\,Hz$. The two particle types employed were spherical glass particles with a density of $\rho_p = 2500\,kg/m^3$ (type B according to Geldarts classification Geldart (1973)). Both particle size distributions are normal, with the mean particle size and the standard deviation showed in figure 3.3. In addition to the 2D measurements, some measurements were carried out in 3D bed, similar to the one described in more detail in Sobrino et al. (2008). These data were used for obtaining the minimum fluidization velocity in a 3D bed, as explained latter on.

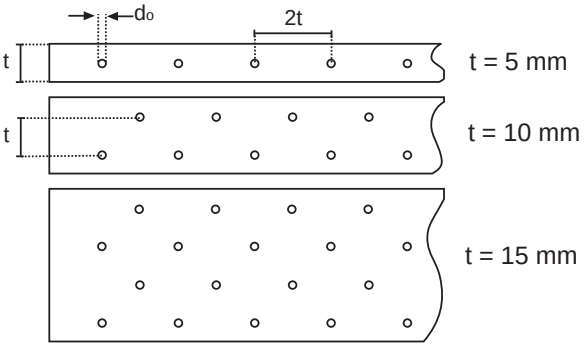

(a)

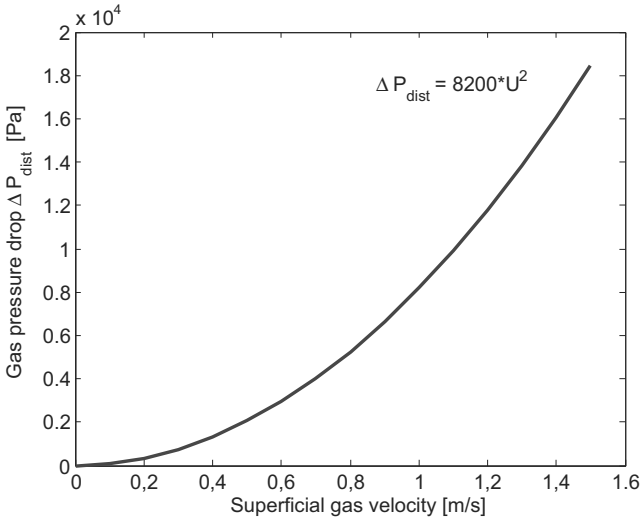

(b)

Figure 3.2: Distributor types, and characteristic curve of the distributor

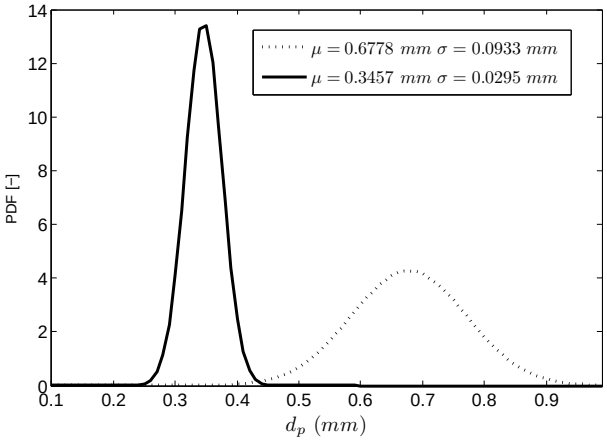

Figure 3.3: Particle size distributions for the two particles types used in this work

3.4 Mathematical Modeling

This works summarizes the main ideas of the model of fluidization-defluidization process including wall effects and particle-particle interactions, developed by Jackson (1998),Jackson (2000) The development of Sarra (2005) will be followed. In a fixed

bed the general momentum equations for the gas phase and the solid phase in the volume showed in figure 3.4 are respectively

$$\frac{\partial}{\partial t}\iiint_{\mathcal{V}} \epsilon\rho_g\, u_g\, dV + \iint_{\mathcal{S}} \epsilon\rho_g\, u_g\, \boldsymbol{u_g}\cdot\boldsymbol{n}\, dA = -\iint_{\mathcal{S}} p_g\, \boldsymbol{n}\, dA + \iint_{\mathcal{S}} \bar{\boldsymbol{\tau}}_{\boldsymbol{g}}\cdot\boldsymbol{n}\, dA + \iiint_{\mathcal{V}} \rho_g \boldsymbol{f_m} dV \quad (3.1)$$

$$\frac{\partial}{\partial t}\iiint_{\mathcal{V}} \phi\rho_s\, u_s\, dV + \iint_{\mathcal{S}} \phi\rho_s\, u_s\, \boldsymbol{u_s}\cdot\boldsymbol{n}\, dA = -\iint_{\mathcal{S}} \sigma_s\, \boldsymbol{n}\, dA + \iint_{\mathcal{S}} \bar{\boldsymbol{\tau}}_{\boldsymbol{s}}\cdot\boldsymbol{n}\, dA + \iiint_{\mathcal{V}} \rho_s \boldsymbol{f_m} dV \quad (3.2)$$

where ϵ is the voidage fraction and $\phi = 1 - \epsilon$ is the particle concentration. Assuming steady state conditions and plug flow and neglecting voidage variations in the control volume, the left side of equation (3.1) is equal to zero. If the bed is fixed, the particle velocity is zero and consequently the left side of equation (3.2) is also null.

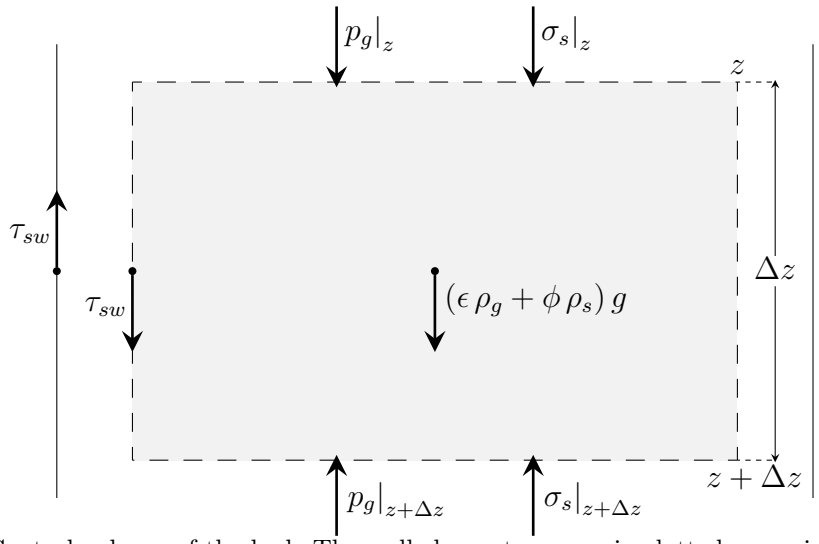

Figure 3.4: Control volume of the bed. The wall shear stress τ_{sw} is plotted assuming that the bed is being fluidized.

Therefore, with these simplifications, the sum of the both equations (3.1) and (3.2) is equal to

$$0 = A\left[-(\sigma_s + p_g)|_{z+\Delta z} + (\sigma_s + p_g)|_z\right] \pm (\tau_{sw} + \tau_{gw})\, P\, \Delta z + (\epsilon\rho_g + \phi\rho_s)\, gA\Delta z, \quad (3.3)$$

where A is the cross sectional area and P is its perimeter. The positive sign in the second term applies when the particles are moving up (the bed is fluidizing), while the negative sign applies when the particle are moving down (the bed is compacting).

Dividing equation (3.3) by Δz and taking the limit as Δz goes to zero, the following differential equation is obtained

$$-\frac{d\sigma_s}{dz} - \frac{dp_g}{dz} \pm \frac{P}{A}(\tau_{sw} + \tau_{gw}) + (\epsilon\rho_g + \phi\rho_s)\, g = 0. \quad (3.4)$$

Equation (3.5) can be further simplified neglecting the body forces and the wall shear stress for the gas phase. In this way, equation (3.5) reduces to

$$\frac{d\sigma_s}{dz} = -\frac{dp_g}{dz} \pm \frac{4}{D_h}\tau_{sw} + \phi\rho_s g, \tag{3.5}$$

where the concept of hydraulic diameter D_h has been introduced.

On the other hand, gas momentum equation (equation (3.1)), with the assumed simplifications, reduces to Darcy's law for porous media. This equation can be written in the following form

$$\frac{dp_g}{dz} = \beta(\phi)\frac{u_g}{1-\phi}, \tag{3.6}$$

where the function $\beta(\phi)$ can be obtained from Richardson-Zaki equation (Richardson and Zaki, 1954)

$$\beta(\phi) = \frac{\rho_s \phi\, g}{v_t}\frac{1}{(1-\phi)^{n-1}}, \tag{3.7}$$

where v_t is the particle terminal velocity and n is a parameter that correlates with terminal particle Reynolds number. In the viscous limit $n = 4.8$ whereas in the inertial limit $n = 2.4$. Between both limits n adquieres intermediate values. Khan and Richardson (1989) obtained the following relationship between n and the Archimedes number

$$\frac{4.8-n}{n-2.4} = 0.043\, Ar^{0.57}, \tag{3.8}$$

with $Ar = g\, d_p^3\, \rho_g\, (\rho_s - \rho_g)\, /\mu_g^2$.

The wall shear stress τ_{sw} can be related with the solid pressure perpendicular to the wall by the use of the coefficient of friction (Sarra, 2005) as follows

$$\tau_{sw} = \mu\sigma_{sw}, \tag{3.9}$$

and the value of σ_{sw} is also proportional to the pressure in a section perpendicular to the mass flow σ_s

$$\sigma_{sw} = j\,\sigma_s, \tag{3.10}$$

where j is the Janssen coefficient, which can be related with the angle of internal friction of the particles δ applying the Mohr stress circle analysis as follows

$$j = \frac{1-\sin\delta}{1+\sin\delta}. \tag{3.11}$$

Introducing equations (3.9) and (3.10) into equation (3.5) and taking into account

equations (3.6) and (3.7), the following expression is obtained

$$\frac{d\sigma_s}{dz} = -\frac{\rho_s\, g\, u_g}{v_t}\frac{\phi}{(1-\phi)^n} \pm \frac{4}{D_h}\mu\, j\sigma_s + \phi\rho_s g. \tag{3.12}$$

The compressive yield stress σ_s could be expected to increase monotonically with the particle concentration ϕ. Johnson et al. (1990) and Loezos at al. (2002) proposed a expression in the form

$$\sigma_s = \begin{cases} F\dfrac{(\phi-\phi_{min})^a}{(\phi_{max}-\phi)^b} & \text{if} \quad \phi_{min} \le \phi \le \phi_{max} \\ 0 & \text{if} \quad \phi < \phi_{min} \end{cases} \tag{3.13}$$

where a, b and F are constants to be adjusted experimentally.Jackson (1998, 2000) and Srivastava and Sundaresan (2002) simplified expression (3.13) assuming $a = b = 1$.

Defluidization cycle

Consider a freely bubbling fluidized bed with a superficial gas velocity $u_g > u_{g,mf}$. The superficial gas velocity is slow and progressively reduced up to $u_g = 0$. For a given value of u_g, equation (3.12) can be rearranged in the following form

$$\frac{\partial\phi}{\partial z} = \frac{-\dfrac{\rho_s\, g\, u_g}{v_t}\dfrac{\phi}{(1-\phi)^n} - \dfrac{4}{D_h}\mu\, j\sigma_s + \phi\rho_s g}{\dfrac{\partial\sigma_s}{\partial\phi}}, \tag{3.14}$$

where $\partial\sigma_s/\partial\phi$ can be obtained from equation (3.13). Equation (3.14) can be integrated numerically to obtain the voidage distribution along the bed height. The integration starts at $z = 0$ (free surface of the bed), where $\sigma_s = 0$ ($\phi = \phi_{min}$) and finish at $z = H$ (the bottom of the bed). At this position the following condition must be fulfilled

$$A\,\rho_s \int_0^H \phi\,(z)\, dz = m, \tag{3.15}$$

where m is the mass of particles in the bed.

Once the voidage distribution along the bed is known, the gas pressure drop along the bed height can be obtained from equation (3.6) as follows

$$\Delta p_g = u_g \int_0^H \frac{\beta\,(\phi)}{1-\phi}\, dz = \frac{u_g\rho_s g}{v_t}\int_0^H \frac{\phi}{(1-\phi)^n}\, dz \tag{3.16}$$

Fluidization cycle

Now consider the fluidization process. The gas velocity is increased from $u_g = 0$ until a critical velocity $u_g = u_c$, when the gas pressure drop overcomes the weight of

the particles in the bed and the additional pressure due to wall effects. For gas velocity higher than u_c the gas pressure drop is reduced to a value approximately equal to the mass of particles in the bed.

Jackson (1998, 2000) argued that the the value of σ_s at the bottom of the bed decreases as the gas velocity is increased up to u_c. When $u_g = u_c$ the whole bed is lifted as a block and the particles in the lower surface will rain due to the change in the gas velocity and will re-compact to form a new bed. At this point the yield stress at the bottom of the bed is equal to zero $\sigma_s|_{z=H} = 0$.

To obtain the critical velocity u_c equation (3.12) has to be integrated. During the fluidization process, the particle concentration along the bed height can be assumed equal to the one obtained at the end of the defluidization branch with $u_g = 0$. Operating in equation

(3.12)

$$\begin{aligned}
\frac{d\sigma_s}{dz} - \frac{4}{D_h}\mu\, j\, \sigma_s &= \rho_s\, \phi\, g - \frac{\rho_s\, \phi\, g}{v_t}\frac{u_g}{(1-\phi)^n}, \\
e^{-J\,z}\left[\frac{d\sigma_s}{dz} - J\,\sigma_s\right] &= e^{-J\,z}\left[\rho_s\, \phi\, g - \frac{\rho_s\, \phi\, g}{v_t}\frac{u_g}{(1-\phi)^n}\right], \\
\frac{d}{dz}\left(\sigma_s\, e^{-J\,z}\right) &= e^{-J\,z}\left[\rho_s\, \phi\, g - \frac{\rho_s\, \phi\, g}{v_t}\frac{u_g}{(1-\phi)^n}\right], \\
\sigma_s\,(z=H)\, e^{-JH} - \sigma_s\,(z=0) &= \rho_s\, g \int_0^H \phi e^{-Jz} dz - \frac{\rho_s\, g\, u_g}{v_t}\int_0^H \frac{\phi}{(1-\phi)^n} e^{-Jz} dz,
\end{aligned} \tag{3.17}$$

where $J = (4/D)\,\mu\, j$. At the point when the bed rises, σ_s is null at both at the top and at the bottom of the bed. Therefore, u_c can be obtained as follows

$$\frac{u_c}{v_t} = \frac{\displaystyle\int_0^H \phi\, e^{-Jz} dz}{\displaystyle\int_0^H \frac{\phi}{(1-\phi)^n} e^{-Jz} dz}. \tag{3.18}$$

Once u_c is known equations (3.6) and (3.12) can be integrated numerically along the bed height for different superficial gas velocities. The particle concentration along the bed $\phi\,(z)$ can be assumed as the one obtained at the end of the defluidization cycle. Jackson (1998, 2000); Sarra (2005) and Srivastava and Sundaresan (2002) assumed the value of the Janssen's coefficient j (and consequently the value of J) equal during both the defluidization and the fluidization cycle, as it is a property of the material. Other authors (Loezos at al., 2002) assumed different values of j in the fluidization j_f and defluidization j_{df} cycle due to the results of the model fits better their experimental

data.

3.5 Experimental results

The two types of particles were fluidized in the 2D fluidized bed for different fixed bed heights and different bed thicknesses. The different bed heights tested were 0.1, 0.2 and $0.3\,m$, resulting in bed aspect ratios $h/w = 0.2$, 0.4 and 0.6 respectively and the bed thicknesses were 0.5, 1.0 and $2.0\,mm$. The process followed during the experiments was always the same: the bed was fluidized with a superficial was velocity around $1.2 - 1.5$ times the minimum fluidization velocity, then the gas flow was progressively reduced until $U = 0$. The bed was maintained at these conditions during 20 minutes before the gas flow was progressively increased until the bed was freely bubbling again. The curve decreasing the gas flow was used to obtain U_{mf}, whereas the ascending curve was used to observe the hysteresis predicted by Jackson's model Jackson (1998) due to wall effects, as it is explained latter on.

In order to measure the minimum fluidization velocity the same procedure followed by Kathuria and Saxena Katuria and Saxena (1987) was used in this work. Firstly, the pressure drop between the plenum and the exit of the bed was measured for different superficial gas velocities, in order to obtain the characteristic curve of the empty system, as explained in the previous section. Then, the bed was filled with bed material until a certain height and the pressure was measured for different superficial gas velocities. In this way, the curve $\Delta P - U$ of the bed is obtained subtracting the the pressure drop of the empty system to the pressure drop of the system with bed material, according to Equation (3.19),

$$\Delta P = \Delta P_{s+p} - \Delta P_s \tag{3.19}$$

were ΔP_s is the gas pressure drop of the empty system, which was assumed approximately equal to the gas pressure drop through the distributor ΔP_{dist} (Figure 3.2(b)), and ΔP_{s+p} the gas pressure drop of the system filled with particles.

Figure 3.5 shows an example of defluidization-fluidization curve, for $d_p = 345.7\mu m$, $h = 20\,cm$ and $t = 0.5\,mm$. The circles represent the curve decreasing gas velocity and the squares the one when gas velocity is progressively increased. The straight lines are used to obtain U_{mf}. It is observed that the ascending curve is over the descending curve in the neighborhood of U_mf, in agreement with expected results predicted by Jackson's model Jackson (1998). This overpressure is due to the wall friction between the particles and the walls. During the fluidization process the gas pressure drop has to overcome not only the weight of the particles, but also the particle-wall friction,

resulting in the observed overpressure. This effect should be more important as the distance between walls decreases.

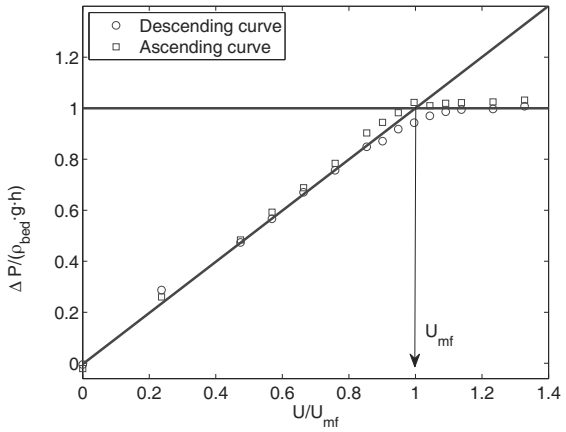

Figure 3.5: Defluidzation-fluidization curve for $d_p = 345.7\mu m$, $h = 20\,cm$ and $t = 0.5\,mm$

Table (3.1) shows the minimum fluidization velocities obtained for each combination of fixed bed height and bed thickness and each particle size. The results show how the minimum fluidization velocity seems not to be affected by the fixed bed height, because the small differences observed varying h are of the order of the uncertainties in the experimental measurements and there is not a clear tendency. Theoretically, minimum fluidization velocities only depends on the particle and gas properties, but not on the bed height. In contrast, experimental results of other researchers Geldart (1970); Ramos et al. (2002) showed noticeable differences on U_{mf} in 2D fluidized beds when the height of the fixed bed is increased. A possible explanation to this phenomena is discussed in the following section.

	Thickness $t\,[mm]$					
	5		10		20	
	Mean particle size $d_p\,[\mu m]$					
	345.7	677.8	345.7	677.8	345.7	677.8
$h = 10\,cm$	0.1403	0.3348	0.1234	0.2688	0.1241	0.2376
$h = 20\,cm$	0.1406	0.3540	0.1230	0.2846	0.1165	0.2591
$h = 30\,cm$	0.1366	0.3488	0.1366	0.2895	0.1197	0.2573

Table 3.1: Minimum fluidization velocities measured in the 2D fluidized bed. Units in m/s

The minimum fluidization velocity of the two types of particles were also measured in the 3D facility described in the previous section, following a similar procedure to the one used during the measurements in the 2D bed. Table 3.2 shows the results obtained, together with the mean minimum fluidization velocity obtained in the 2D facility for each bed thickness and particle size. The influence of the bed thickness

is clearly observed: the minimum fluidization velocity increases as the bed thickness is decreases. This tendency is sharper when the highest particles are fluidized, which suggest that $U_{mf,2D}$ could be correlated with the nondimensional parameter t/d_p.

		$U_{mf,2D}$	$U_{mf,3D}$
$d_p = 345.7\,\mu m$	$t = 5\,mm$	$0.1392\,m/s$	$0.1244\,m/s$
	$t = 10\,mm$	$0.1277\,m/s$	
	$t = 20\,mm$	$0.1201\,m/s$	
$d_p = 677.8\,\mu m$	$t = 5\,mm$	$0.3459\,m/s$	$0.2446\,m/s$
	$t = 10\,mm$	$0.2810\,m/s$	
	$t = 20\,mm$	$0.2513\,m/s$	

Table 3.2: Minimum fluidization velocities measured in the 3D bed and mean minimum fluidization velocities obtained in the 2D bed

In order to obtain a general correlation for the ratio $U_{mf,2D}/U_{mf,3D}$ as function of mean particle size and bed thickness, expression (3.20) is proposed, which fulfills the condition that $U_{mf,2D}$ tends to $U_{mf,3D}$ when $t \gg d_p$. Fitting the data of Table 3.2 to Equation 3.20 the values of $a = 8.492$ and $b = 1.598$ are obtained.

$$\frac{U_{mf,2D}}{U_{mf,3D}} = \exp\left(a \cdot \left(\frac{d_p}{t}\right)^b\right) \tag{3.20}$$

Figure 3.6 shows the data of Table 3.2 represented by circles together with the fitting curve (equation 3.20) and the results obtained by other researchers Busciglio et al. (2007); Rowe and Everett (1972); Geldart (1970); Saxena and Jadav (1983); Glicksman and McAndrews (1985); Katuria and Saxena (1987); Mudde et al. (1994). Two data obtained by Saxena and Jadav Saxena and Jadav (1983), represented by empty lozenges, seem to follow the tendency of the proposed equation. The experimental data were obtained for spherical glass beds and red silica sand particles with a mean particle size of $d_p = 427\,\mu m$ and $788\mu m$ respectively, being the bed thickness $t = 1.57\,mm$. Busciglio et al. Busciglio et al. (2007) observed no differences between the minimum fluidization velocity measured in their 2D bed and the result obtained from Ergun equation, thus a value of $U_{mf,2D}/U_{mf,3D} = 1$ was assumed and it is represented by a cross in Figure 3.6 and the data represented by an empty square (Rowe and Everett, 1972) correspond to a bed with a very large thickness of $14.3\,cm$, which fulfils the condition that $\lim_{d_p/t \to 0} U_{mf,2D} = U_{mf,3D}$. A different point, obtained by Saxena and Jadav (1983) represented by a filled lozenge (silica sand with a mean particle size of $d_p = 488\,\mu m$) departs from the tendency of the other data obtained by the same authors, who suggest the higher friction with the wall of sand particles (due to its non-spherical shape) in comparison with glass beds of a similar size as a possible

reason to this difference. With a dashed line the range of data measured by Geldart (1970). This data correspond to the variation of $U_{mf,2D}$ with the fixed bed height between 5 and 80 cm, because the particle size and the bed thickness were the same. The other data Rowe and Everett (1972); Glicksman and McAndrews (1985); Katuria and Saxena (1987); Mudde et al. (1994) represented in Figure 3.6 departs from the proposed equation.

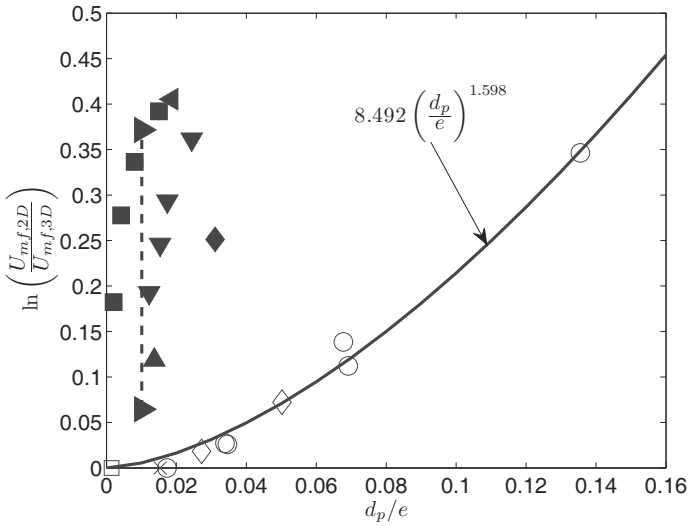

Figure 3.6: Plot representing $\ln(U_{mf,2D}/U_{mf,3D})$ vs d_p/t for different works. The solid line shows represents the equation obtained after adjust equation (3.20) to the data obtained in this work, represented by circles in the graph, and the dashed line representes the range of variation of the results obtained by Geldart Geldart (1970) varying the bed height h for the same value of d_p/e. ◯ data of this work (Table 3.2), × Busciglio et al. Busciglio et al. (2007), ◊ Saxena and Jadav Saxena and Jadav (1983), □ Rowe and Everett Rowe and Everett (1972), ♦ Saxena and Jadav Saxena and Jadav (1983), ▲ Glicksman and McAndrews Glicksman and McAndrews (1985), ▼ Kathuria and Saxena Katuria and Saxena (1987), ◄ Mudde et al. Mudde et al. (1994), ► Geldart Geldart (1970), ■ Rowe and Everett Rowe and Everett (1972)

Figure 3.6 clearly shows a group of experiments (represented with filled symbols) that departs from the experimental results of this work (represented with circles) and other researchers (represented with empty symbols and a cross). Some of the experiments could be unexpected, as the results obtained by Rowe and Everett (1972), whose results are represented by filled squares and correspond to particles with $d_p = 210\mu m$ fluidized in beds with thickness of 1.4, 2.6, 5.0 and 10.2 cm respectively; and its not until a thickness of 14.3 cm (point represented by an empty square) when the wall effects seems to do not influence on the minimum fluidization velocity. A possible explanation to these discrepancies is discussed in the following section.

Data	Authors	Particles	d_p [μm]	t [mm]	walls material	$\frac{U_{mf,2D}}{U_{mf,3D}}$
○	this work	glass spheres	345.7	5.0	glass	1.12
				10.0		1.03
				20.0		1.00
			677.8	5.0		1.41
				10.0		1.15
				20.0		1.03
×	Busciglio et al. Busciglio et al. (2007)	glass ballotoni	215	15.0	glass	1.00
◊	Saxena and Jadav Saxena and Jadav (1983)	glass spheres	427	15.7	glass	1.02
		sand	788			1.08
□	Rowe and Everett Rowe and Everett (1972)	alumina	210	143.0	—	1.00
♦	Saxena and Jadav Saxena and Jadav (1983)	sand	488	15.7	glass	1.29
■	Rowe and Everett Rowe and Everett (1972)	alumina	210	14.0	—	1.48
				26.0		1.40
				50.0		1.32
				102.0		1.20
▲	Glicksman and McAndrews Glicksman and McAndrews (1985)	sand	1040	76.0	plexiglass	1.13
▼	Kathuria and Saxena Katuria and Saxena (1987)	sand	774	31.7	plexiglass	1.44
				44.4		1.34
				50.4		1.28
				63.5		1.21
◄	Mudde et al. Mudde et al. (1994)	polystyrene spheres	560	30.0	perspex	1.50
►	Geldart Geldart (1970)	sand	128	12.7	perspex	1.07-1.45

Table 3.3: Experimental conditions of the data showed in Figure 3.6

3.6 Discussion

3.6.1 Wall effects influence during the defluidization-fluidization process

Equations (3.13)-(3.18) predicts properly the hysteresis and the overpressure due to wall effects in fluidized beds of small diameters, as was observed by various researchers Srivastava and Sundaresan (2002); Loezos at al. (2002); Liu et al. (2008). Srivastava and Sundaresan Srivastava and Sundaresan (2002) and Loezos et al. Loezos at al. (2002), fluidized particles in cylindrical beds with internal diameters between 10 and 50 mm and Liu et al. Liu et al. (2008) , used microfluidized beds of internal diameters ranging between 12 and 32 mm. In contrast, in this work Jackson model has been adjusted to experimental data obtained in 2D beds.

In this way, the value of the coefficient n of the equation 3.18 was fitted to the experimental data following the same methodology used by Srivastava and Sundaresan (2002) and Loezos at al. (2002). The value of ϕ_{min} was assumed equal to the average value at minimum fluidization conditions ϕ_{mf}, which was estimated measuring the mass of particle introduced in the bed and the fixed bed height. Following the works of Srivastava and Sundaresan Srivastava and Sundaresan (2002) and Loezos et al. Loezos at al. (2002), two different values of J were used, one for the defluidizaton curve

, J_{df}, and the other one for the fluidization curve, J_f. The value of J_f was obtained directly from Equation (3.18), where u_c is known, and the parameters J_{df} and ϕ_{max} were optimized to the values that better fits the experimental data. Table 3.4 summarized the values obtained for the data represented in Figure 3.7.

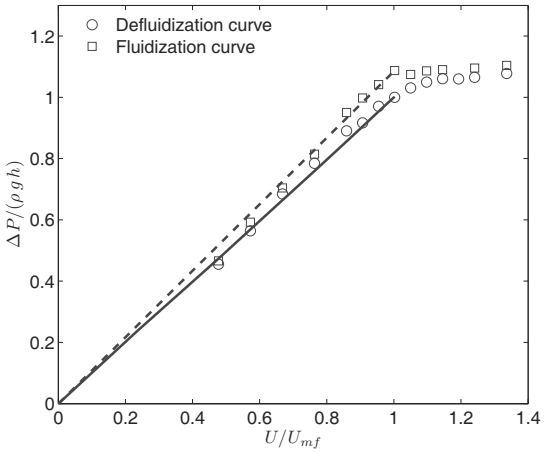

Figure 3.7: Fluidization-defluidization curve for $d_p = 345.7\mu m$, $h = 10\,cm$ and $t = 0.5\,mm$. The solid and the dashed lines represent the curves obtained with Jackson model for the defluidization and fluidization processes respectively.

Parameters	**Values**
F	$2500\,N/m^2$
ϕ_{min}	0.54
ϕ_{max}	0.56
ρ_s	$2500\,kg/m^3$
n	2
J_{df}	$1000\,m^{-1}$
J_f	$800\,m^{-1}$

Table 3.4: Summary of the Jackson model parameters for the data represented in Figure 3.7.

Nevertheless, the optimum values of J_f, J_{df} and ϕ_{max} varies notably for each experimental condition. For example, for the same particles and experimental conditions of the data showed in Figure 3.7, varying the bed height to $h = 30\,cm$, a optimum values of $J_{df} = 1\,m^{-1}$ and $n = 6$ are obtained. These contradictory results precludes to obtain general values for a fixed particle size and bed thickness.

One explication to these differences could be attributed to application of a one dimensional model ($\phi = \phi(z)$), in a 2D bed, where the voidage distribution is clearly bidimensional ($\phi = \phi(z, x)$) being x the horizontal coordinate. In a two dimensional bed, if the distributor pressure drop is high enough (as it is the case) bubbles appear uniformly along the distributor length, but the coalescence along the bed height force

bubbles to move to the center of the bed, being the sides of the bed regions of particles moving down completely free of bubbles, as it is schematized in Figure 3.8(a)[1]. The continuous bubble pass in the central region of the bed results in higher local porosities in this region than in the sides of the bed when the gas flow is being reduced under minimum fluidization conditions. As a consequence, when the fixed bed is being fluidized increasing progressively U from zero to U_{mf}, the voidage distribution is not uniform along the bed and the gas preferably percolates through the central region of the bed, where particles are less compacted. Figure 3.8(b) shows an scheme of the voidage profiles in the bed when it is being fluidized and the preferential gas flow, which is perpendicular to the constant voidage profiles. The voidage is higher in the center and in the top of the bed.

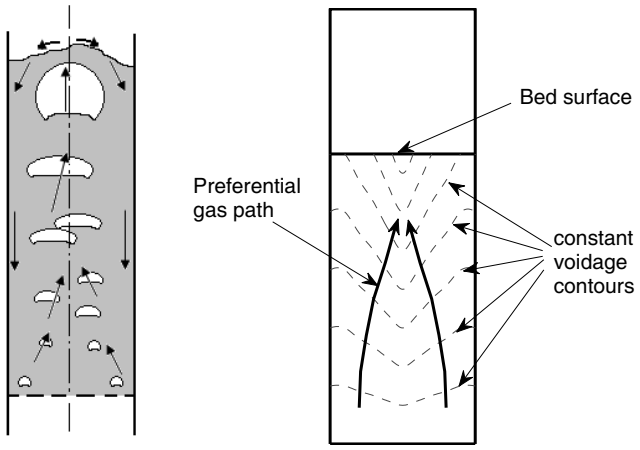

Figure 3.8: (a) Scheme of the bubble motion in the bed when is freely bubbling, the arrows indicate the transport of particles, and (b) scheme of the constant voidage profiles and gas path in the bed when it is being fluidized

This effect is observed when the particles are being fluidized in a bed of large fixed height, as the serie of photographs of Figure 3.9 show. In Figure 3.9(a) small bubble are observed at the top-center region of the bed, where the bed is less compacted, while the rest of the bed seems to be undisturbed. Slightly increasing the gas velocity the small bubble grow up and appear from deeper regions (see Figure 3.9(b)) and finally bubbles are observed from the distributor up to the bed surface, although they are observed only in the central region of the bed (see Figure 3.9(c)), due to the higher permeability to gas flow of this region. The sides of the bed in Figure 3.9(c) are free of bubbles. If the gas flow is increased again, the bubbles will appear along the width of the bed, but for a gas velocity around U_{mf} gas tends to percolate through the central

[1]Depending on the ratio between the height and the width of the bed a different bubble path configuration, with two main bubble paths, could be observed Sanchez-Delgado et al. (2008)

region of the bed due to its lower resistance to the gas flow.

The one-dimensional assumption of Jackson's model implies that $\phi = \phi(z)$ and U is uniform along the bed section. The experimental observations of this work show that these assumptions limit the applicability of the model in 2D beds, although wall effects and hysteresis can be observed in some experiments, as the one showed in Figure 3.5. Nevertheless, the influence of wall effects on the minimum fluidization velocity is clearly observed in Figure 3.6, where walls influence is introduced by the nondimensional variable d_p/t. As the ratio between the particle size and the bed thickness decreases, the minimum fluidization velocity increases.

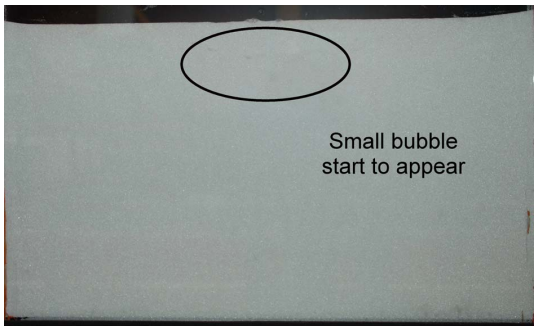

(a) $U = 0.140\,m/s$

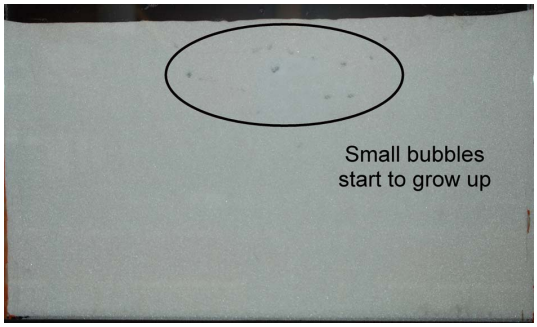

(b) $U = 0.147\,m/s$

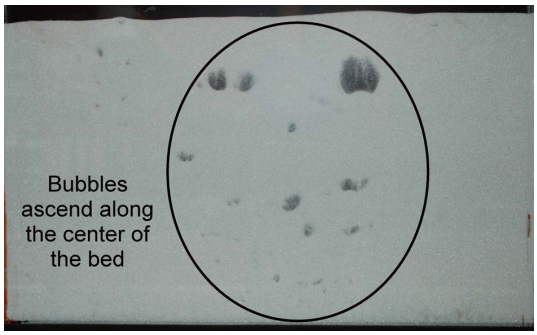

(c) $U = 0.160\,m/s$

Figure 3.9: Sequence of photographs captured during the fluidization branch for $d_p = 345.7\mu m$, $h = 30\,cm$, $t = 5\,mm$

3.6.2 Discussion of Figure 3.6

Figure 3.6 shows high discrepancies between the minimum fluidization velocities measured by different researchers. On the one hand, the experimental results of this work, together with others marked with empty symbols or a cross, seem to adjust to the proposed exponential relationship between $U_{mf,2D}$ and $U_{mf,3D}$ (Equation (3.20)). On the other hand, the results marked with filled symbols, clearly depart from the proposed equation, showing values of $U_{mf,2D}$ much higher for particle size to thickness ratios in the range between 0 and 0.04.

The differences are very high to be attributed to uncertainties in the experimental measurements or to the experimental techniques employed. Nevertheless taking a look on Table 3.3, we can check that all the experiments that seems to follow the correlation proposed (Equation (3.20)) were fluidized in 2D beds with the walls made of glass, except the data of Rowe and Everett (1972), marked with an empty square. Nevertheless this point can be considered almost a 3D experiment due to the large thickness of the bed. In addition, Busciglio et al. (2007) although used a bed made with perspex, the walls of the bed in direct contact with the fluidized particles were made of glass with the intention of avoiding electrostatic charge problems, which preclude to observe properly the interior of the bed because the particles deposite on the walls surface. Saxena and Jadav (1983) grounded both walls of the bed in order to assure no static charge on the walls surface. In this work no problems with the electrostatic charge were observed during the experiments.

In contrast the rest of data were obtained in 2D beds whose walls were made with plastic materials (either perspex or plexiglass). Under this conditions electrostatic charge could be important. Moreover, Mudde et al. (1994) fluidized also plastic particles, resulting in the highest velocities ratio ($U_{mf,2D}/U_{mf,3D} = 1.5$) of all the data of Table 3.3, for a not very small bed thickness of $t = 30\,mm$. The unique exception is the point marked with a filled lozenge, which departs from the other data obtained by the same authors. As was commented previously, Saxena and Jadav (1983) attributed this difference to differences in the particle geometry.

The electrostatic charge in fluidized bed is a very complex phenomenon and depends of multitude of variables Rojo et al. (1986); Guardiola et al. (1996): bed height, particles size, fluidization velocity, relative humidity of the fluidizing air, etc.. The results of Rojo et al. (1986) showed that for bubbling conditions the electrostatic charge increased with the fixed bed height, which could explain the increase of minimum fluidization velocity with the bed height observed by Ramos et al. (2002) and by Geldart (1970). Guardiola et al. (1996) observed the increase of electrification increasing particle size and air velocity and also remarked the importance of the relative humidity of the air. In 2D beds, the influence of the interaction walls-particles on the electrostatic charge, which was usually neglected in 3D beds Rojo et al. (1986), could be also an important variable. Therefore, electrostatic charge could be an additional force to take into account in the momentum equation (Equation (3.12)), but the multitude of involved variables and the experimental conditions of the data summarized in Table 3.3 preclude to quantify this force.

In view of the experimental conditions showed in Table 3.3, another parameter that could also influence the results is the sphericity ϕ_p of the particles Geldart (1970).

Most of the results that adjust to Equation (3.14) were obtained for spherical particles ($\phi_p = 1$), and in contrast, most of the experiments represented with a filled symbol were obtained for non spherical particles ($\phi_p \neq 1$). Only the point obtained by Mudde et al. (1994) were obtained with spheres, but these particles were made of plastic material and electrostatic charge could notably influence on this result, as it was commented previously. The particle sphericity is a parameter difficult to measure, and most of the experimental results that can be found in the literature are based on an indirect measurement from Ergun equation Kunii and Levenspiel (1991), which results in high uncertainties. As a consequence, Equation (3.20) should be used with caution when non-spherical particles are being fluidized, as the constants $a = 8.492$ and $b = 1.598$ were obtained for spherical particles.

3.7 Conclusions

Equation proposed a simple correlation to predict minimum fluidization velocity in 2D fluidized beds. This equation has been obtained for spherical particles fluidized in a 2D bed, varying the bed thickness (between 0.5 and 2.0 mm) and the fixed bed height (between 10 and 30 cm). Nevertheless the comparison of Equation (3.20) with results of other works suggest that the correlation predicts properly the minimum fluidization velocity for spherical particles and 2D beds made of glass walls, rather than plastic walls, where electrostatic charge could have a great influence on U_{mf}.

In addition, Jackson model for wall effects has been fitted to the experimental fluidization-defluidization curves. Although the parameters of the model can be adjusted to one specific experiment, the one dimensional assumption of the model precludes to obtain general conclusions.

3.8 Notation

A Section of the bed perpendicular to the gas flow $[m^2]$

D_h Hydraulic diameter $[m]$

d_p Particle size $[m]$

F Constant in Equation (3.13) $[Pa]$

H Bed height $[m]$

h Fixed bed height $[m]$

J Constant defined in Equation (3.18) $[m^{-1}]$

j Janssen coefficient $[-]$

t Bed thickness $[m]$

g Gravity constant $[9.81\, m/s^2]$

U Superficial gas velocity $[m/s]$

U_{mf} Minimum superficial gas velocity $[m/s]$

u_c Critical gas velocity $[m/s]$

u_g Interstitial gas velocity $[m/s]$

v_t Particle terminal velocity $[m/s]$

w Width of the bed $[m]$

x Horizontal coordinate

z Vertical coordinate, measured from the top of the bed

Greeks letters

ΔP Gas pressure drop due to the particles $\Delta P = \Delta P_{s+p} - \Delta P_s$ $[Pa]$

ΔP_{dist} Gas pressure drop in the distributor $[Pa]$

ΔP_g Gas pressure drop including wall effects (Equation (3.6)) $[Pa]$

ΔP_s Gas pressure drop in the empty system $[Pa]$

ΔP_{s+p} Gas pressure drop in the system filled with particles $[Pa]$

ε Voidage in the bed $[-]$

μ Friction coefficient $[-]$

ρ_s Solid density $[kg/m^3]$

σ_s Compressive yield stress of the particles $[Pa]$

ϕ Particle concentration $\phi = 1 - \varepsilon$ $[-]$

ϕ_p Particle sphericity $[-]$

Subscripts

$(\ )_{2D}$ Magnitude refereed to the 2D bed

$(\ )_{3D}$ Magnitude refereed to the 3D bed

$(\ )_{df}$ Defluidization curve

$(\ )_{f}$ Fluidization curve

$(\ )_{min}$ Minimum

$(\ )_{max}$ Maximum

Bibliography

Almendros-Ibáñez J.A., Sánchez-Delgado S., Sobrino C., and Santana D., Experimental observations on the different mechanisms for solid ejection in gas-fluidized beds.*Chem. Eng. Proc.* 2009, 48, 734-744

Almendros-Ibáñez J.A., Pallarès D., Johnsson F., Santana D., Novel approach to characterize fluidized bed dynamics combining Particle Image Velocimetry and Finite Element Method, *Ind. & Eng. Chem. Res.*, 48(2009), 5010-5023

Briongos J.V., Guardiola J., Newmethodology for scaling hydrodynamic data from a 2D-fluidized bed, *Chem. Eng. Sci.*, 60(2005), 5151 5163

Busciglio A., Vella G., Micale G. and Rizzuti L., Analysis of the bubbling behaviour of 2-D gas solid fluidized beds Part I: digital image analysis technique. *Chemical Engineering Journal.* 2007, 140, 398-413

Busciglio A., Vella G., Micale G. and Rizzuti L., Analysis of the bubbling behaviour of 2D gas solid fluidized beds. Part II. Comparison between experiments and numerical simulations via Digital Image Analysis Technique, *Chem. Eng. J.*, 148(2009), 145-163

Cheremisinoff N.P., Review of experimental methods for studying the hydrodynamics of gas-solid fluidized beds, *Ind. Eng. Chem. Process Des. Dev.*, 25(1986) 329-351

Clift R., in D. Geldart (ed.), Gas Fluidization Technology. Wiley, Chichester, 1986, p. 53

Geldart D., The size and frequency of bubbles in two- and three-dimensional gas-fluidised beds, *Powder Tech.*, 4(1970), 41-55

Geldart D., Types of gas fluidization, *Powder Technol.* 7(1973), 285292

Glicksman L.R. and McAndrews G., The effect of bed width on the hydrodynamics of large particle fluidized beds, *Powder Technol.*, 42(1985), 159-167

Grace J.R., Harrison D., The behaviour of freely bubbling fluidised beds, *Chem. Eng. Sci.*, 24(1969), 497-508

J.R. Grace and J. Baeyens, in D. Geldart (ed.), Gas Fluidization Technology. Wiley, Chichester, 1986, p. 415

Guardiola J., Rojo V., Ramos G., Influence of particle size, fluidization velocity and relative humidity on fluidized bed electrostatic, *J. Electrost.*, 37(1996), 1-20

Holland D.J., Müller C.R., Sederman A.J., Mantle M.D., Gladden L.F., Davidson J.F., Magnetic resonance imaging of fluidized beds: Recent advances, *Theor. Found. Chem. Eng.*, 42(2008) 469-478

Jackson R., in L.S. Fan and T.M. Knowlton (eds.), Fluidization IX: Proceedings of the Ninth Engineering Foundation Conference of Fluidization. New York, 1998, p. 1

Jackson R., *The Dynamics of Fluidized Particles*, Cambridge University Press, 2000

Johnson P.C., Nott P.R., Jackson R., 1990. Frictional-collisional equations of motion of particulated flowsand their aplications to chutes, *Journal of Fluid Mechanics*, vol. 210, pp. 501-536.

Khan A.R., Richardson J.F. ,1989. Fluid-particle interactions and flow characteristics of fluidized beds and sttling suspensions of spherical-particles, *Chemical Engineering Science*, vol. 78, pp. 111-130.

Kathuria D.G. and Saxena S.C., A variable-thickness two-dimensional bed for investigating gas-solid fluidized bed hydrodynamics, *Powder Technol.*, 53(1987), 91-96

D. Kunii and O. Levenspiel, *Fluidization Engineering (2nd edition)*, Butterworth-Heinemann, 1991

Link J., Zeilstra C., Deen N., Kuipers H., Validation of a discrete particle model in a 2D spout-fluid bed using non-intrusive optical measuring techniques, *Can. J. Chem. Eng.*, 82(2004), 30-36

Liu X., Xu G., Gao S., Micro fluidized beds: Wall effect and operibility, *Chem. Eng. J.*, 137(2008), 302-307

Loezos P.N., Costamagna P., Sundaresan S., The role of contact stresses and wall friction on fluidization, *Chem. Eng. Sci.*, 57(2002), 5123-5141

Massimilla L., Westwater J.W., Photographic study of solid-gas fluidization, *AIChE J.*,6(1960), 134-138

Mudde R.F., Schulte H.B.M., van den Akker H.E.A., Analysis of a bubbling 2-D gas-fluidized bed using image processing, *Powder Technol.*, 81(1994), 149-159

Müller C.R., Davidson J.F., Dennis J.S. and Hayhurst A.L., 2007. A study of the motion and eruption of a bubble at the surface of a two-dimensional fluidized bed using particle image velocimetry (PIV),*Ind. & Eng. Chem. Res.*, vol. 46, pp. 1642-1652

C.R. Müller, D.J. Holland, A.J. Sederman, M.D. Mantle, L.F. Gladden, J.F. Davidson, Magnetic Resonance Imaging of fluidized beds, *Powder Technol.*, 183(2008) 53-62

Pallarès D. and Johnsson F., A novel technique for particle tracking in cold 2-dimensional fluidized beds-simulating fuel dispersion. *Chem. Eng. Sci.* 2006, 61, 2710 - 2720

Ramos Caicedo G., García Ruiz M., Prieto Marqués J.J., Guardiola Soler J., Minimum fluidization velocities for gas/solid 2D beds, *Chem Eng. Proc.*, 41(2002) 761-764

Rees A.C., Davidson J.F., Dennis J.S., Fennell P.S., Gladden L.F., Hayhurst A.N., Mantle M.D., Muller C.R., Sederman A.J., The nature of the flow just above the perforated plate distributor of a gas-fluidised bed, as imaged using magnetic resonance, *Chem. Eng. Sci.*, 61(2006) 6002-6015

Richardson J.F., Zaki W.N., 1954. Sedimentation and fluidisation, *Transaction of the Institution of Chemical Engineers*, vol. 32, pp. 35-53.

Rojo V., Guardiola J., Vian A., A capacitor model to interpret the electric behaviour of fluidized beds. Influence of apparatus geometry, *Chem. Eng. Sci.*, 41(1986), 2171-2181

Rowe P.N., Partridge B.A., Lyall E., Cloud formation around bubbles in gas fluidized beds, *Chem. Eng. Sci.*, 19(1964), 973-985

Rowe P.N., Partridge B.A., An x-ray study of bubbles in fluidised beds, *Trans. Inst. Chem. Eng.*, 43(1965), 157-175

Rowe P.N., Everett D.J., Fluidised bed bubbles viewed by x-rays. Part II-The transition from two to three dimensions of undisturbed bubbles, *Trans. Instn. Chem. Engrs.*, 50(1972), 49-54

Sánchez-Delgado S., Almendros-Ibáñez J.A., Soria-Verdugo A., Santana D., Ruiz-Rivas U., in J. Werther, W. Nowak, K.E. Wirth, E.U. Hartge, (Eds.). TuTech Innovation GmbH, Hamburg, 2008, p. 1007

Sánchez-Delgado S., Acosta-Iborra A., Santana D., Dense phase velocity fluctuation in a 2-D fluidized bed. Submmited for publication to *Powder Technol.*

Santana D., Nauri S., Acosta A., García N., Macías-Machín A., Initial particle velocity spatial distribution from 2-D erupting bubbles in fluidized beds. *Powder Tech.*, 150(2005), 1-8

Sarra A., Miller A.L., Shadle L.J., 2005. Experimentally measured shear stress in the standpipe of a circulating fluidized bed, *AIChE Journal*, vol. 51, pp.1131-1143.

Saxena S.C., Jadav S., A two-dimensional gas fluidized bed for hydrodynamic and elutriation studies, *Powder Technol.*, 36(1983), 61-70

Shen L., Johnsson F. and Leckner B., 2004. Digital image analysis of hydrodynamics two-dimensional bubbling fluidized beds. *Chemical Engineering Science*, 59 (2004), 2607-2617

Simons S.J.R., Imaging techniques for fluidized bed systems: a review, *Chem. Eng. J. Biochem. Eng. J.*, 56(1995) 83-93

Sobrino C., Almedros-Ibáñez J.A., Santana D.and de Vega M., Fluidization of group B particles with a rotating distributor, *Powder Technol.*, 181(2008), 273280

Srivastava A. and Sundaresan S., Role of wall friction in fluidization and standpipe flow, *Powder Technol.*, 124(2002), 45-54

Trisakti B., Oshitani J., Tanaka Z., Circulating particle flow and air bubble behavior at various superficial gas velocities in two-dimensional gas-solid fluidized beds, *Adv. Powder Technol.*, 12(2001), 507-519

van Ommen J.R., Mudde R.F., Measuring the gas-solids distribution in fluidized feds A review, *Int. J. Chem. React. Eng.*, 6(2008) Review R3

Werther J., Measurement techniques in fluidized beds, *Powder Technol.*, 102(1999) 15-36

Chapter 4

Dense-phase velocity fluctuation in a 2-D fluidized bed

Contents

4.1 Abstract

This work presents an investigation of the perturbations induced by the bubbles in a 2-D fluidized bed. A combination of Digital Image Analysis (DIA) and Particle Image Velocimetry (PIV) techniques was developed to characterize the dense and bubble phases. The analysis of the mean and the instantaneous fluctuations of the velocity of the dense phase, together with the solid movement around bubbles, allowed for the measurement of the influence region, distinguishing an upward moving dense phase in the nose and the wake of the bubble (drift) and a downward moving dense phase in the

sides of the bubble. For an isolated bubble, we measured the drift area within the total influence region and related the size of these regions to the equivalent diameter of the bubble. This work also presents results on the volumetric dissipation of kinetic energy, where we concluded that the energy dissipation in the dense phase is proportional to the square of the bubble velocity.

4.2 Introduction

Understanding the processes involved in the mixing of solids is essential for the design of fluidized bed reactors. Lacey (1954) distinguished three components in a mixing process: 1) convective, 2) diffusive and 3) shear mixing. Generally, these mechanisms are combined in most processes, although in some processes one of them predominates. Convective mixing mechanism involves the transfer of a group of particles from one location to another, diffusive mixing involves the random movement of particles and shear mixing involves the formation of slip planes within the mixture.

Later, Shen et al. (1995) presented an investigation of the dynamics of solids mixing in fluidized beds. Their mechanistic model of a gas-solid fluidized bed was based on the models of Kunii and Levenspiel (1969) and Fan et al. (1986). This model assumed that the fluidized bed consists of three phases, a dilute phase containing no solids (the bubble phase), an upward moving dense phase (the wake phase) and a downward moving dense phase (the emulsion phase). To solve the convection-diffusion equation, they used a power-law difference method; the numerical results were in satisfactory agreement with the previously existing experimental data.

Recently, Lu et al. (2008) employed a Discrete Element Method (DEM) to simulate the motion and mixing behavior of granular materials in three-dimensional vibrated beds. In their work, a study of the importance of the mixing mechanisms is also presented, using the index, M, defined by Lacey (Lacey, 1954) as the parameter to quantify the mixing quality.

Digital Image Analysis (DIA) and Particle Image Velocimetry (PIV) are two of the most common techniques applied to 2-D fluidized beds to analyze the bubble and emulsion phases. 2-D fluidized beds allow for bubble visualization, making it possible to obtain relevant bubble parameters (center of mass, velocity, equivalent diameter, etc.) to characterize the bubbling behavior of the fluidized bed. Additionally, the emulsion phase velocity can be characterized using the PIV technique. Recently, Sanchez-Delgado et al. (2008) studied the time-averaged bubble concentration and time-averaged particle velocity in a 2-D fluidized bed to characterize the behavior of fluidized beds with different bed aspect ratios and superficial gas velocities. These

techniques were applied by Almendros-Ibanez et al. (2009) to study the different mechanisms for solid ejection in gas-fluidized beds. Busciglio et al. (2007) presented a digital image analysis technique developed to study the fluidization dynamics of a lab-scale bubbling bed. They compared the main bubble parameters (bubble size and bubble velocity distribution) with correlations presented in the literature and confirmed the applicability of the DIA technique. Laverman et al. (2008) combined the DIA and the PIV techniques to study the bubble behavior and to characterize the emulsion phase. Specifically, they studied the influence of particles raining through the bubble on the time-averaged velocity profile of the emulsion phase.

In this work, the perturbation region generated by a bubble in a 2-D fluidized bed has been studied using the time-averaged emulsion velocity field and the calculation of fluctuating velocity component of the dense phase as proposed by Liu et al. (2005). Applied to fluidized beds, this technique is able to establish the region of the dense phase where the effect of the bubble rise is important in terms of solids mixing. Furthermore, for an isolated bubble, it is possible to identify two phases containing the entire solid: the upward moving dense phase in the wake of the bubble and the downward moving dense phase at the sides of the bubble. The experimental results are in satisfactory agreement with the mechanistic model proposed by Shen et al. (1995)

Although the attrition phenomena depend on many factors, such as the physical-chemical nature of the particles and the process conditions, one fundamental variable related to fluidized bed dynamics is the shear between particles Werther and Reppenhagen (2003). With the results obtained using the proposed techniques, valuable information about the shear can be obtained to improve attrition modeling in fluidized beds. In this work, the application of non-intrusive techniques in a 2-D fluidized bed allows to calculate the total influence region in the dense phase, A_t , and the size of the drift region, A_d , within the total influence region.

In addition, a parameter, σ , is defined as the ratio of the volumetric dissipation of kinetic energy and the apparent viscosity. It will be demonstrated that this parameter is proportional to the square of the bubble velocity, U_b^2 . Therefore, the volumetric dissipation of kinetic energy in the dense phase can be related to the kinetic energy of the bubble. This relation represents an initial quantification of bubble kinetic energy in the attrition phenomena in fluidized beds.

4.3 Experimental set-up

Fig. 4.1 shows a schematic diagram of the image acquisition system and the fluidized bed apparatus employed in the experiments.

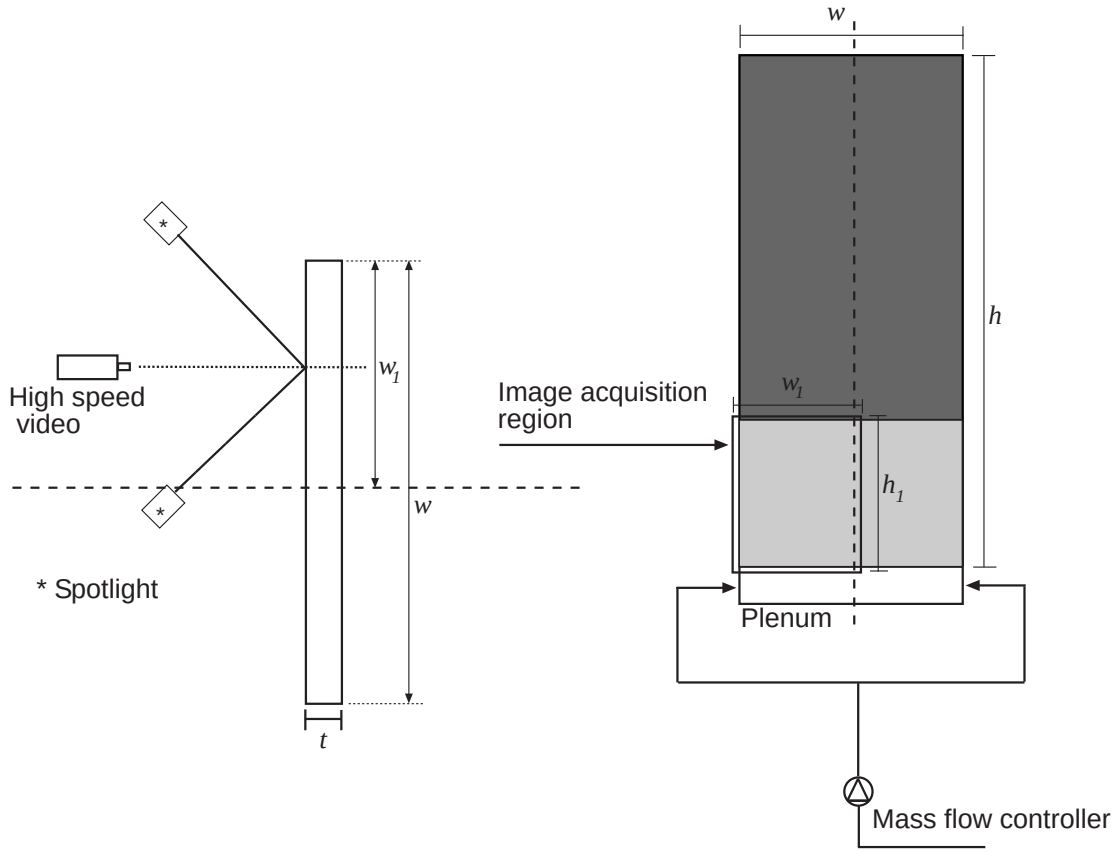

Figure 4.1: Scheme of experimental facilities

The experiments were carried out in a 2-D cold fluidized bed $50\,cm$ wide w, $200\,cm$ high h and $0.5\,cm$ thick t. The front wall was made of glass whereas the back panel was made of aluminum and covered by a black card to obtain a higher contrast in the images. Two $650\,W$ spotlights were used to provide uniform illumination. The bed was filled with a mixture of black and white Geldart-B glass particles (Geldart, 1973), with a density, ρ_p, of $2500\,kg/m^3$ and a diameter, d_p, of $600 - 800\ \mu m$, previously sieved, following a normal distribution, with a mean and standard deviation of 677.8 μm and 93.3 μm, respectively. The ratio between the superficial gas velocity, U_g, and the minimum fluidization velocity, U_{mf}, was equal to 1.75 ($U_{mf} = 35\,cm/s$).

Only the left side of the fluidized bed was recorded due to the symmetric configuration of the bed; the imaged area was: $h_1 \times w_1 = 30\,cm \times 25\,cm$ and the images were recorded at a frame rate, f_a, of $125\,fps$ with a camera resolution of $1270 \times 992\,pixels$.

The air distributor consisted of a perforated plate with 50 holes of $1\,mm$ diameter spaced $1\,cm$ apart. The characteristic curve of the air distributor is shown in Fig. 4.2

During the experiments, the gas pressure drop through the bed was ΔP $4500\,Pa$ and the mean superficial gas velocity was around $0.62\,m/s$. Therefore, the distributor and the bed pressure drops during experiments were of the same order. Under these

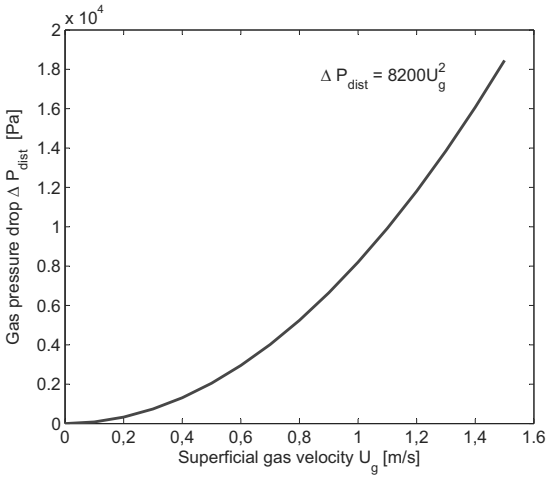

Figure 4.2: Characteristic curve of the distributor

operating conditions the bed and the air-supply system are independent, Johnsson et al. (2000), Sasic et al. (2004), Sasic et al. (2005).

In this work, a special PIV code, *MatPIV* 1.6.1 (Sveen, 2004), has been used to obtain the dense velocity field. Interrogation windows of $16 \times 16\, pixels$ with a 0.5 overlap were typically used in the PIV analysis performed to compute the velocity fields of the dense phase. Recently, several authors have used this application on 2-D fluidized beds to calculate particle velocities Almendros-Ibanez et al. (2009), Müller et al. (2007). For these experiments, the fluidized bed column was filled with a total weight of $1600\, g$, $1568\, g$ of white particles and $32\, g$ of black ones to improve the measuring technique, Müller et al. (2007). DIA was applied to establish the boundaries between the dense phase and the bubble phase. The analysis was based on the calculation and application of a threshold level over each image, Otsu (1979). Using this technique, not only are the phases clearly identified (dense phase and bubble phase), but also different bubble properties could be calculated, such as the equivalent diameter based on bubble area, $D_{eq} = \sqrt{(4A_b/\pi)}$, the mass center or the bubble velocity Caicedo et al. (2003).

4.4 Results and discussion

During the rise of a single bubble, it is possible to identify solid particles that are influenced by that motion. When a pair of bubbles is rising vertically, the trailing bubble is accelerated under the influence of the leading bubble; eventually, the dome of the trailing bubble enters into the wake of the leading bubble and they become a single bubble (Almendros-Ibanez et al., 2009) (Davidson and Harrison, 1963). During coalescence, it is difficult to establish the influence region of each bubble.

4.4.1 Bubble induced particle velocity

Typically, when a bubble is traveling toward the top of the bed, the particles in the dense phase can either rain through the bubble or move downward, surrounding the bubble. The particles located in the wake of the bubble are accelerated due to the wake effect on the dense phase. Applying PIV techniques to the recorded images, we can obtain the variations of the dense phase velocity.

Snapshots of the bubbling bed are displayed in Figs. 4.3 (a)-(e). In these figures, the rectangular region and the horizontal line were drawn to show where the calculations were performed. We defined $t = 0$ Fig. 4.3a as the instant of time when the bubble enters the study region.Fig. 4.3(f) shows the vertical velocity of the dense phase, U_y, at the horizontal line for those snapshots.

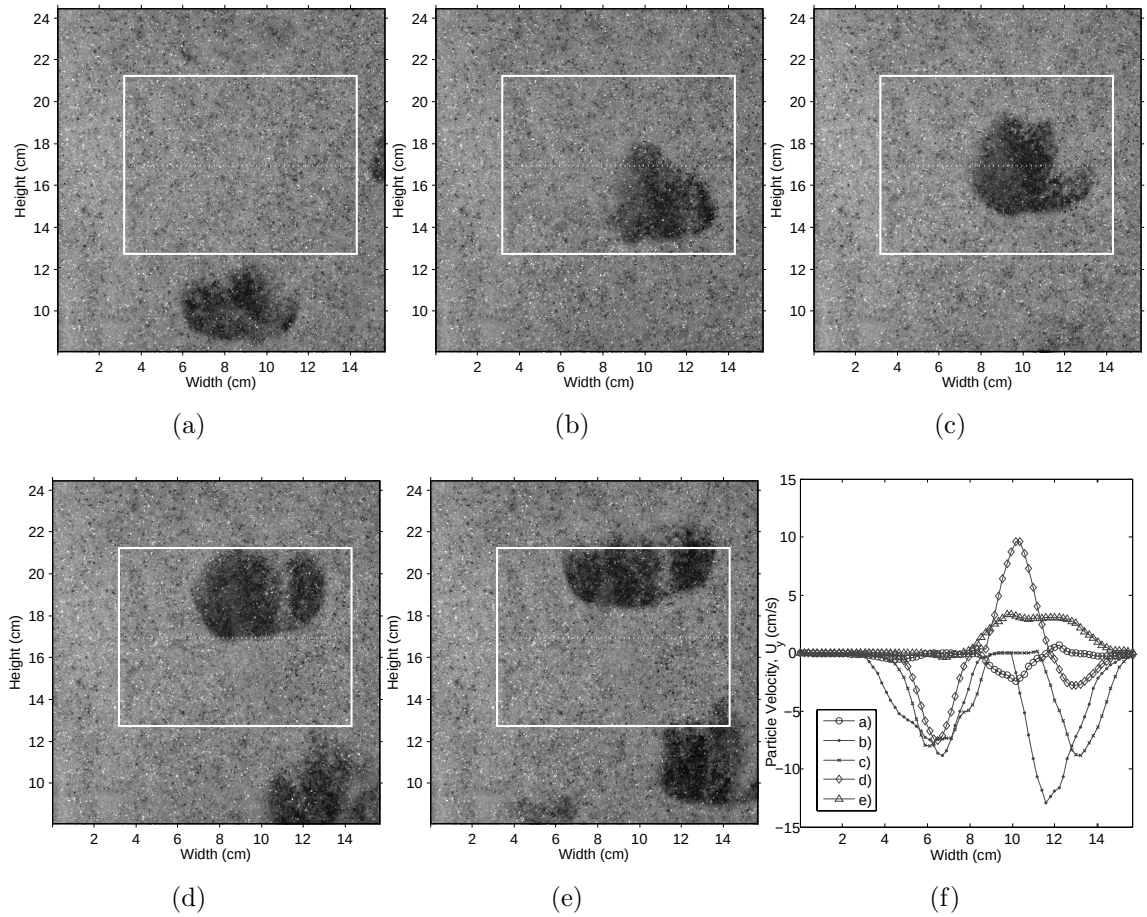

Figure 4.3: PIV results of the dense phase in a fixed line when an isolated bubble crosses the kine at different times. Figs. 3 (a-e) are at times t = 0, 48, 104, 160 and 216 ms respectively

When a bubble reaches the horizontal line (Figs. 4.3 (b)-(c)) the dense phase has a downward movement around the bubble. Fig. 4.3(d) shows the instant of time at which the wake of the bubble is crossing the line; it can be observed that the solids in this region have an upward motion.

Considering T as the time interval between $t = 0$ and the moment at which the bubble leaves the study region, the time-averaged dense-phase velocity fields can be calculated as follows:

$$\overline{\mathbf{U}(\mathbf{x})} = \frac{\sum_{n=1}^{N} \mathbf{U}_n(\mathbf{x}, t)}{N} \tag{4.1}$$

where N is the number of images corresponding to the time interval considered to calculate the average velocity ($N = f_a T$).

As stated above, a threshold level was calculated to transform the grayscale image into black and white to aid in distinguishing the dense phase and the bubble phase, Otsu (1979). For each image, the pixels representing the dense phase are given a value of 1 ($C_n(\mathbf{x}) = 1$) and the pixels representing the bubble phase are given a value of 0 ($C_n(\mathbf{x}) = 0$). Then, the fraction of time that a point, $\mathbf{x}$, is occupied by solids can be calculated as follows:

$$\overline{C(\mathbf{x})} = \frac{\sum_{n=1}^{N} C_n(\mathbf{x})}{N} \tag{4.2}$$

For the images analyzed in Fig. 4.3, the velocity fields in the selected region are represented in Figs. 4.4 (a-e). Additionally, Fig. 4.4(f) represents a superposition of $\overline{C}$ (the color map) and the time-averaged velocity of the dense phase.

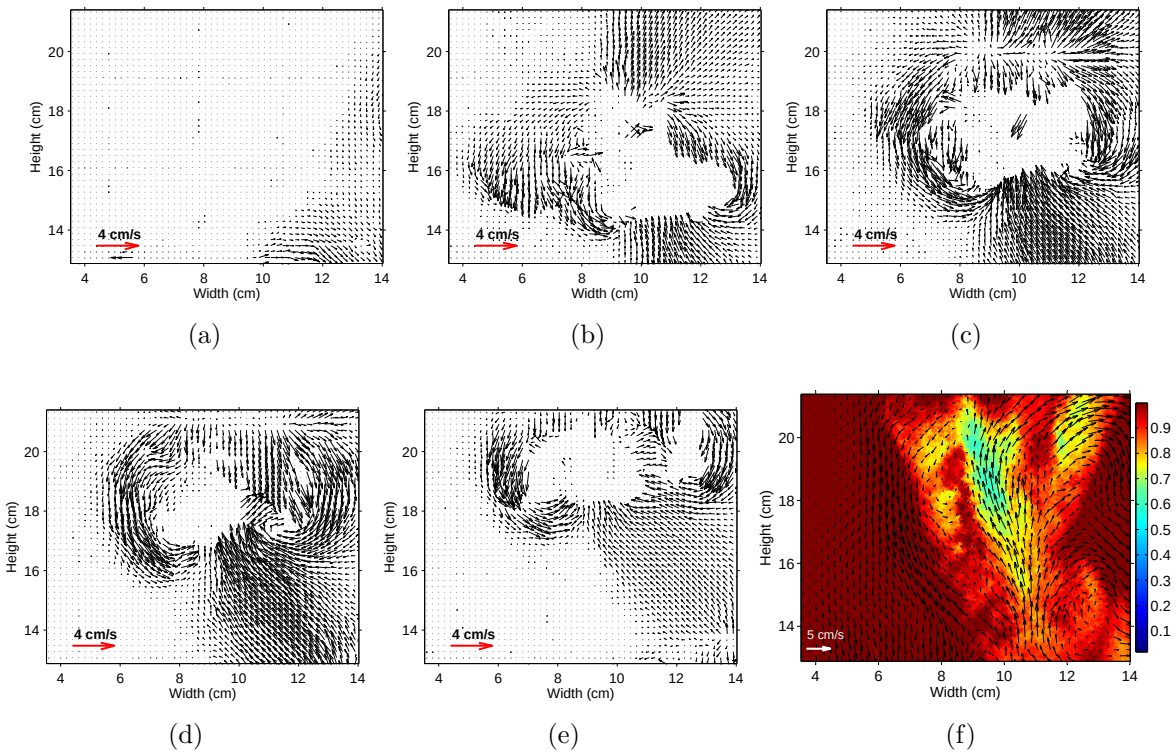

Figure 4.4: PIV results at different times (a,b,c,d and e) and a superposition of the time-averaged dense-phase velocity field with the fraction of time that a point is occupied by solids (f)

Figs. 4.4(b-e) show the effect of an isolated bubble on the dense phase. It can be seen that the particles located at the sides of the bubble move downward and the particles in the wake of the bubble move upward. The time-averaged velocity field of the dense phase,$\overline{\mathbf{U}}$, together with the fraction of time that a point is occupied by solids, $\overline{C(\mathbf{x})}$, are represented in Fig. 4.4(f). Taking a closer look at this figure, three different zones can be distinguished in terms of solids transport mechanisms: (i) a region that is always occupied by solids ($\overline{C} = 1$), where the dense phase is moving downward, (ii) an upward moving dense phase with the lowest values of $\overline{C}$, and (iii) an interface layer between these two regions, where vortices appear. According to Shen et al. (1995), solids mixing is composed of two components: the first is the convection component between the upward and the downward moving regions of the dense phase and the second is the diffusion component in the downward dense phase.

For the same fluidization conditions, $U_g/U_{mf} = 1.75$, the same procedure was performed to analyze the bubble-coalescence phenomenon (Fig. 4.5). The velocity fields shown in Figs. 4.6(a-e) correspond to the flow visualizations presented in Figs. 4.5(a-e). Fig. 4.6(f) shows a superposition of the fraction of time that a point is occupied by the emulsion phase and the time-averaged dense-phase velocity field. In this case, it is also possible to distinguish the three regions of the solids mixing mechanism described above. It can be observed that the interface layer for the coalescing bubble is narrower than for the case of the isolated bubble. Furthermore, due to this coalescing effect, the velocities in the dense phase reach higher values and the effect of the two wakes increase the solids transport.

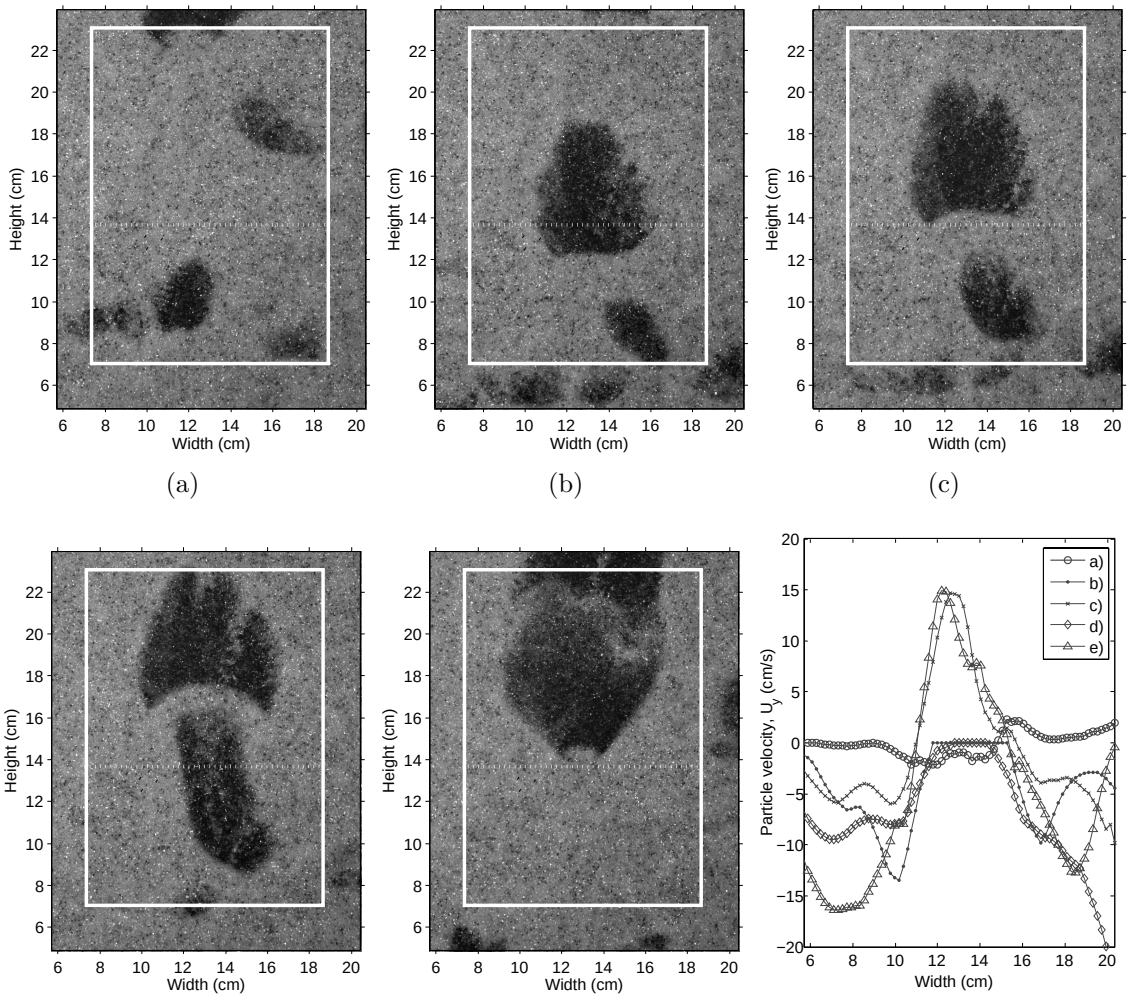

Figure 4.5: PIV results of the dense phase in a fixed line when two coalescing bubbles cross the line at different times. Fig. 5 (a-e) are at times t = 0, 80, 120, 168, and 256 ms, respectively

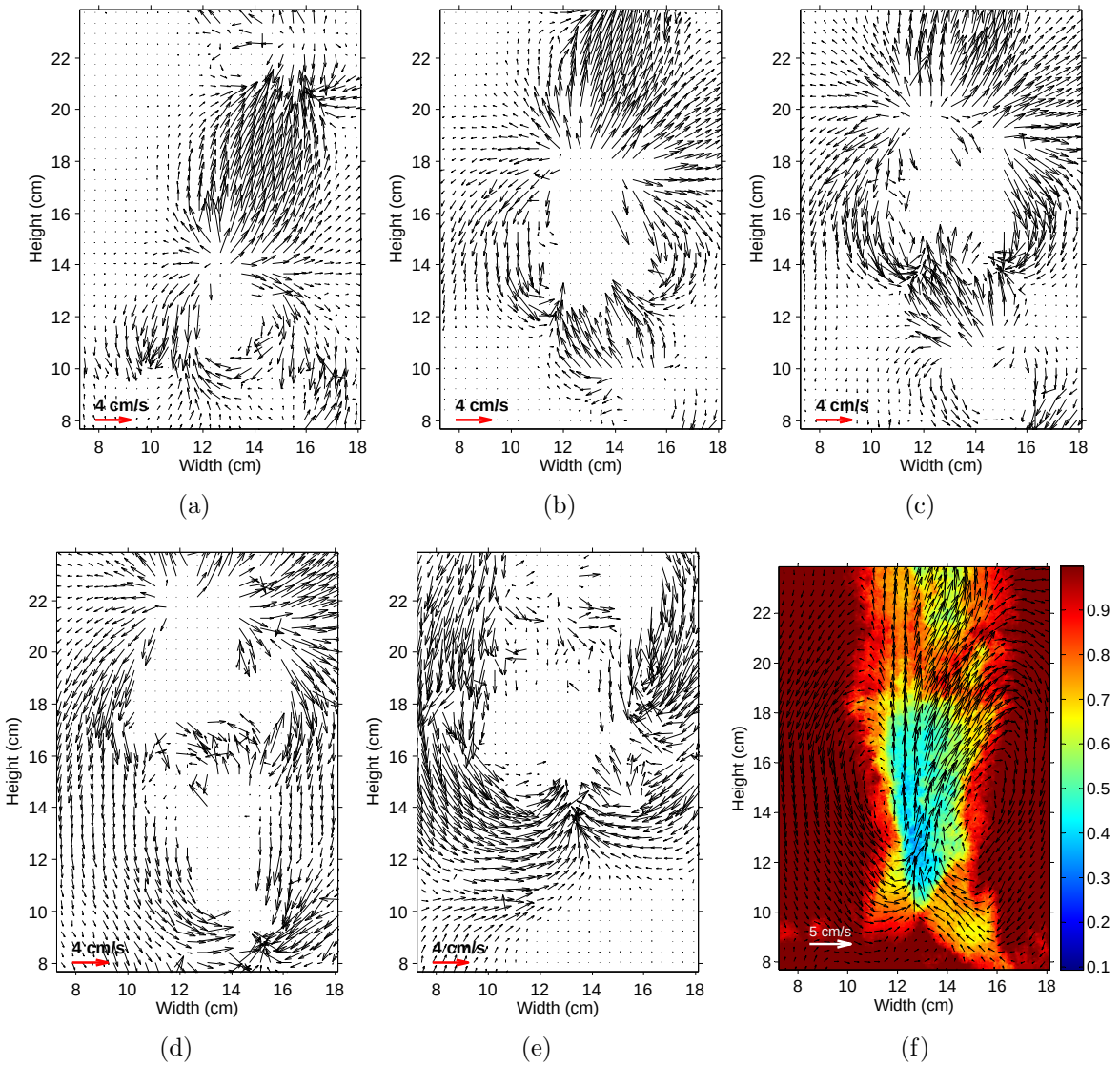

Figure 4.6: PIV results at different times (6 a, b, c, d and e), and a superposition of the time-averaged dense-phase velocity field with the proportion of time that a point is occupied by solids (f) for a coalescing bubbles

4.4.2 Bubble influence and dense phase velocity perturbation

Once the effect of a rising bubble on the dense phase has been characterized, it is important to quantify the size of the region in the dense phase where the effect of the bubble rise is important in terms of solids mixing (i.e., the influence region).

In this section, the dense-phase velocity perturbation is analyzed. With this aim, the absolute fluctuating velocity,$|\mathbf{U}'(\mathbf{x}, t_n)|$, was obtained by:

$$|\mathbf{U}'(\mathbf{x}, t_n)| = |\mathbf{U}(\mathbf{x}, t_n) - \overline{\mathbf{U}}(\mathbf{x})| \tag{4.3}$$

Fig. 4.7a shows a snapshot of a bubble moving upward in our 2-D bed. The absolute

fluctuation velocity of the emulsion region was calculated at that instant of time (Fig. 4.7(b)).

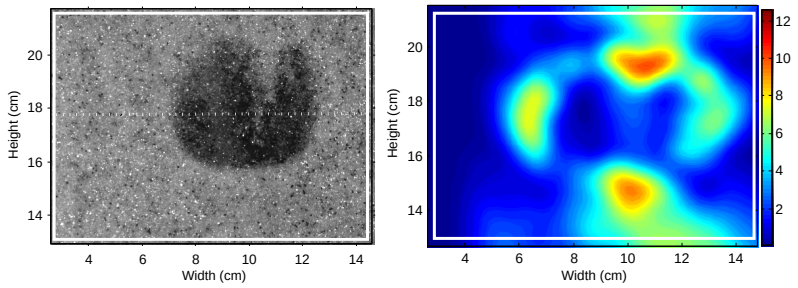

(a) (b)

Figure 4.7: (a) Flow visualization of a bubble; (b) Absolute vertical velocity perturbation of the dense phase.

Three regions can be identified surrounding the bubble. In the dense phase at the top of the bubble, a region of high magnitude velocity perturbation appears due to the effect of the nose of the bubble. A second region can be distinguished where the particles move upward, affected by the wake of the bubble, and finally at the bubble sides, two zones of high absolute perturbation values are identified, corresponding to the downward moving dense phase. This visual inspection is complemented with a numerical analysis to define the influence region of a bubble rising over the dense phase. Fig. 4.8 represents the absolute velocity perturbation along the horizontal line defined in Fig. 4.7a as well as the horizontal derivative of that magnitude.

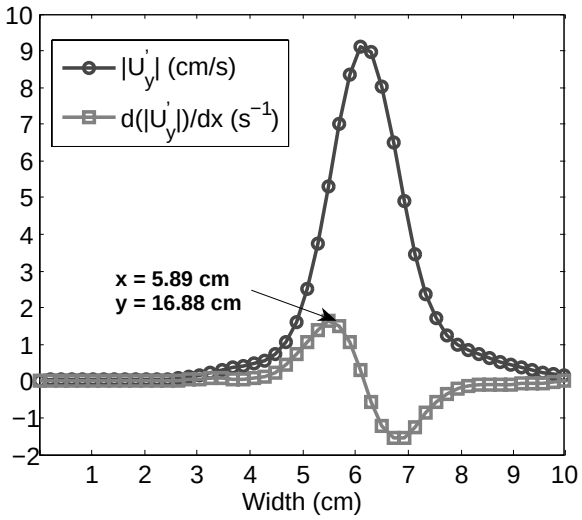

Figure 4.8: Absolute velocity perturbation of the dense phase, and horizontal derivative along the line of Fig. 7(a)

In this analysis, the perturbation values denote, quantitatively, the influence of a rising bubble and the derivate of the perturbation provides information about the bubble influence region.

The position where the derivative reaches a maximum is considered as the boundary of the influence region (marked by black dots in Fig. 4.9), and therefore the value of $|\mathbf{U}'(\mathbf{x})|$ at this position would be the threshold value designated to establish that the dense phase is affected by the bubble. Fig. 4.10a shows the points at which the dense-phase velocity perturbations are larger than the threshold value previously calculated.

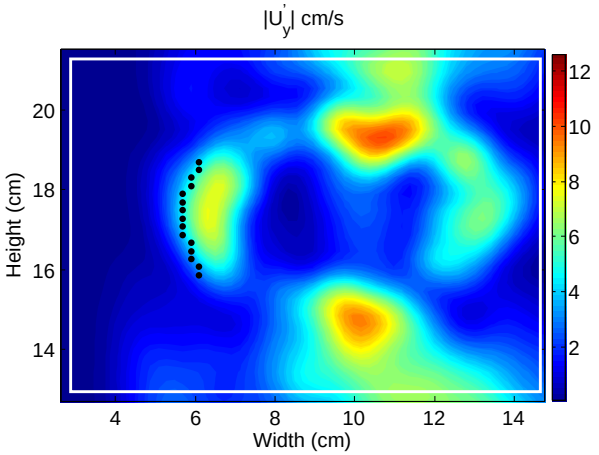

Figure 4.9: Boundary of the influence region at the left side of the bubble shown in Fig. 4.7

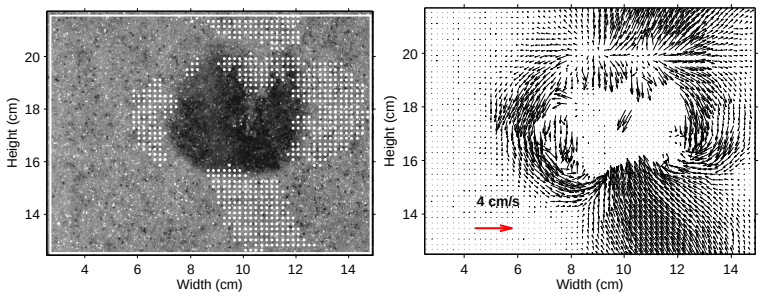

(a) (b)

Figure 4.10: (a) Representation of the influence region over the original image; (b) PIV results for Fig. 10a

Fig. 4.10(b) shows the two emulsion phases defined according to the direction of movement: an upwardly moving dense phase in the bubble wake dominated by convective mechanisms and a downwardly moving dense phase where the diffusion effect is the most relevant mixing mechanism Shen et al. (1995). These regions are in accord with the influence regions plotted in Fig. 4.10a.

The same analysis applied to an isolated bubble has been applied for two coalescing bubbles. Fig. 4.11 shows the flow visualization of two coalescing bubbles, the absolute vertical velocity perturbation of the dense phase, $|\mathbf{U}'_y(\mathbf{x})|$, and the total influence region generated by the bubble chain. This analysis does not allow for the distinction of the influence region generated by each bubble.

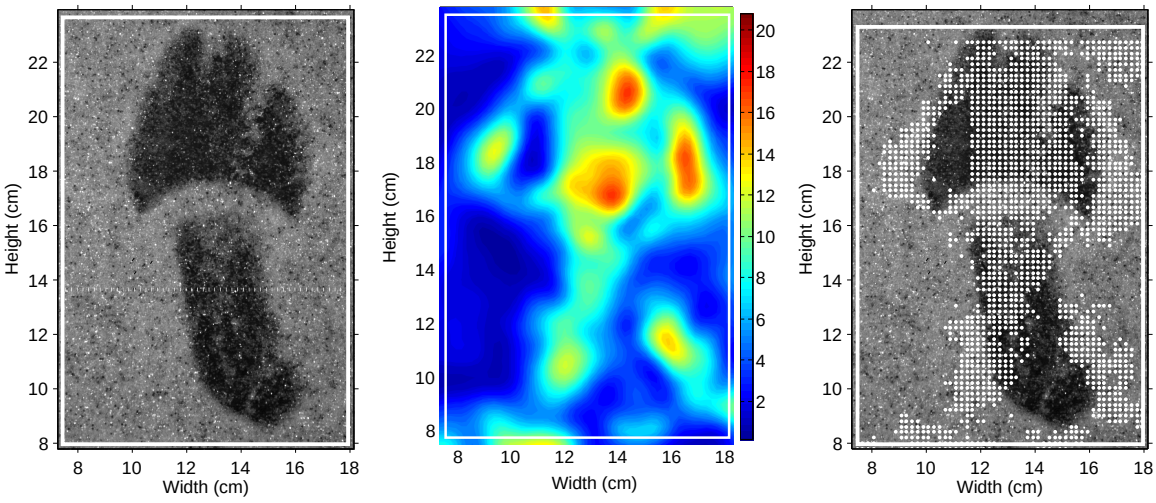

(a) (b) (c)

Figure 4.11: (a) Coalescing bubbles in a 2-D fluidized bed. (b) Absolute velocity perturbation of the dense phase. (c) Total influence region generated by the bubbles.

4.4.3 Influence region measurement and dissipation of kinetic energy

In this section, different bubble parameters were calculated and compared for a total of 20 isolated bubbles: equivalent bubble diameter, D_{eq}, center of mass, $\mathbf{x}_{cm}$, bubble velocity, U_b, influence region, A_t, and drift region, A_d. Fig. 4.12 shows an example of the calculation of these parameters for one bubble.

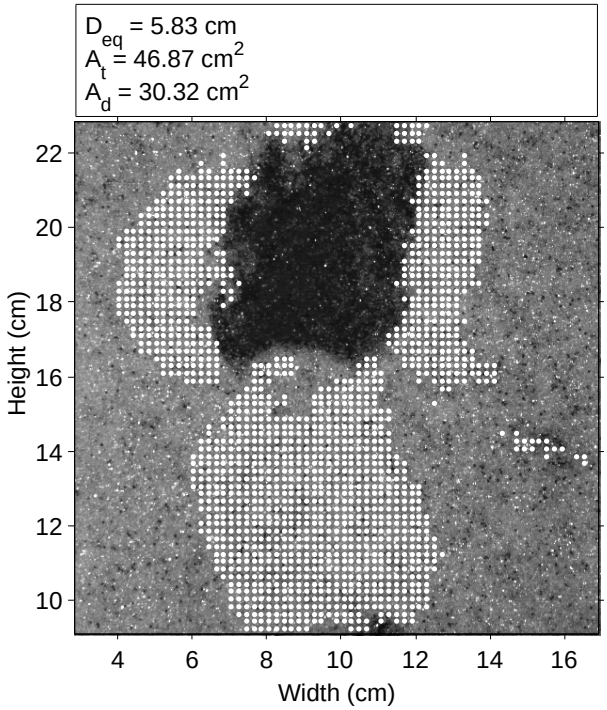

Figure 4.12: Results for an isolated bubble

Fig. 4.13(a) shows the relationship between the total influence region and the perturbation region occupied by the wake. A linear-regression fitting was applied to these data. It can be seen that the drift area represents around the half of the influence region. Fig. 4.13(b) shows the relationship between the total influence region and the equivalent diameter of the bubble. As expected, larger bubbles generate larger influence regions, and a linear relationship between total influence region and the equivalent square diameter, $A_t \propto D_{eq}^2$, was observed; Fig. 4.13(c) also shows a linear relationship between the drift area and the equivalent diameter, $A_d \propto D_{eq}$.

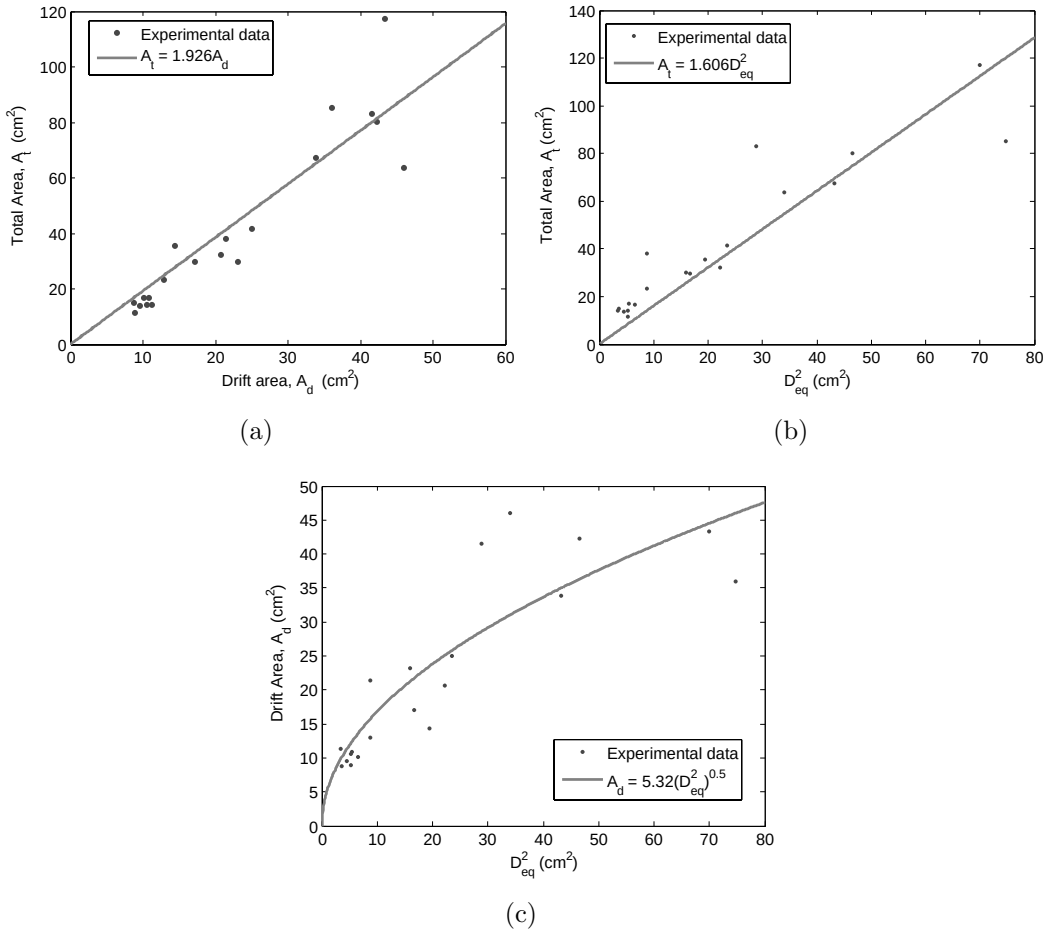

Figure 4.13: Experimental relationship between bubble size and influence-region size: (a) Total influence region and drift size; (b) Total influence region and bubble equivalent diameter squared; (c) Drift area and bubble equivalent diameter squared

In a bubbling fluidized bed, the mechanical power supplied by the air system is given by the product of the volumetric flow rate of gas times the pressure drop. This input energy can be divided into two terms: the energy to keep the particles in suspension and the input energy that remains for bubble formation, and thus for attrition, Werther and Reppenhagen (2003). Attrition promoted by bubbles takes place in regions where there are severe gradients in the dense-phase velocity. Under the model of dense-

phase behavior as an incompressible fluid, attrition can be interpreted as a mechanism of particle kinetic-energy dissipation that results in the fracture or degradation of particles. The energy equation shows that dissipation is related to the particle velocity gradients along the x and y directions:

$$\sigma = \frac{\phi_v}{\mu} = 2\left(\frac{\partial u}{\partial x}\right)^2 + 2\left(\frac{\partial v}{\partial y}\right)^2 + \left(\frac{\partial u}{\partial y} + \frac{\partial v}{\partial x}\right)^2 \tag{4.4}$$

where ϕ_v is the volumetric dissipation of kinetic energy and is the apparent dense-phase viscosity. Therefore, it seems reasonable to assume that a relationship exists between attrition and particle-velocity gradients. Hence, in regions of high velocity gradient attrition will be higher. Fig. 4.14 shows the maximum value of σ as a function of the total influence region.

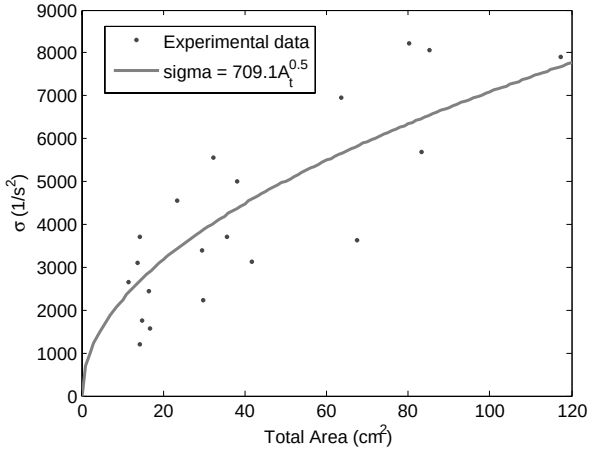

Figure 4.14: σ vs. total influence region previously calculated.

Fig. 4.14 shows that the volumetric dissipation of kinetic energy is proportional to the square root of the total influence region. Fig. 4.13(b) shows a linear relationship between the total influence region, A_t, and the square of the equivalent bubble diameter. Therefore, the volumetric dissipation of kinetic energy is proportional to the equivalent diameter of the bubble: $\sigma \propto D_{eq}$. As the bubble velocity is related to the bubble diameter by the expression $U_b = \phi\sqrt{gD_{eq}}$ Davidson and Harrison (1963), we can conclude that the volumetric dissipation of kinetic energy of the dense phase is related to the kinetic energy of a rising bubble: $\sigma \propto U_b^2$.

4.5 Conclusions

PIV and DIA techniques were employed in a 2-D fluidized bed in order to distinguish the dense phase from the bubble phase and obtain the time-averaged velocity of the dense phase as well as the proportion of time that a region was occupied by a bubble. The

perturbation in the dense phase induced by a rising bubble and the quantification of the area of influence of a bubble in the dense phase were obtained from the experimental results.

The present work has shown that there are three regions clearly defined around a bubble in terms of its velocity fluctuation: 1) a region above the bubble dome, 2) a region with an upward moving dense phase in which particles are transported into the drift of the bubble and 3) a region with a downwardly moving dense phase in which particles surround the bubble towards its wake. For coalescing bubbles, it was not possible to distinguish which regions corresponded to each bubble due to the interference between the wakes of the leading and the trailing bubbles. It is also shown that the velocity fluctuation of the dense phase diminishes sharply beyond the influence region. Hence, the horizontal derivative of the vertical velocity fluctuation around a bubble can be used to delimit the region of influence of a bubble. Using this procedure, the experimental results indicate that the area perturbed by the velocity of the dense phase is proportional to the square of the bubble diameter. As the ascent velocity of bubbles is related to their diameter, the region of influence of a bubble in the dense phase is linked to the dissipation of the bubble kinetic energy.

4.6 Notation

A_d drift region, $[cm^2]$

A_t influence region, $[cm^2]$

$C_n(\mathbf{x})$ dense phase (level = 1) or bubble phase (level = 0) for a point at position $\mathbf{x}$

$\overline{C(\mathbf{x})}$ fraction of time that a point is occupied by dense phase

d_p particle diameter, $[cm]$

f_a acquisition frequency, $[Hz]$

h fluidized-bed height, $[cm]$

h_1 recorded height of the fluidized bed, $[cm]$

M mixing degree

N number of images selected for analysis

t fluidized-bed thickness, $[cm]$

T time interval of the measurement, $[s]$

U_g superficial gas velocity, $[cm/s]$

$\overline{\mathbf{U}(\mathbf{x})}$ time-averaged dense-phase velocity, $[cm/s]$

U_b bubble velocity, $[cm/s]$

U_y vertical dense-phase velocity, $[cm/s]$

$\mathbf{x}_{cm}$ center-of-mass coordinates of the bubble, $[cm]$

$\mathbf{U}(\mathbf{x}, t)$ dense-phase velocity, $[cm/s]$

$\mathbf{U'}(\mathbf{x}, t)$ fluctuating velocity component, $[cm/s]$

U_{mf} minimum fluidization velocity, $[cm/s]$

w fluidized-bed width, $[cm]$

w_1 recorded width of the fluidized bed, $[cm]$

$\mathbf{x}$ horizontal and vertical coordinates for a point $\mathbf{x} = x\,\overrightarrow{i} + y\,\overrightarrow{j}$, $[cm]$

Greek letters

μ apparent dense-phase viscosity, $[kg/(ms)]$

ρ_p particle density, $[kg/(m^3)]$

σ ratio between the volumetric dissipation of kinetic energy and the apparent viscosity, $[1/(s^2)]$

ϕ_v volumetric dissipation of kinetic energy, $[kg/(ms^3)]$

Bibliography

Almendros-Ibáñez J.A., Sánchez-Delgado S., Sobrino C., and Santana D., Experimental observations on the different mechanisms for solid ejection in gas-fluidized beds. *Chem. Eng. Proc.* 2009, 48, 734-744

Busciglio A., Vella G., Micale G. and Rizzuti L., "Analysis of the bubbling behaviour of 2-D gas solid fluidized beds Part I: digital image analysis technique". *Chemical Engineering Journal*. 2007, 140, 398-413

Caicedo G.R., Juan J. Prieto Marqués, Mónica García Ruíz and Jesús Guardiola Soler. A study on the behaviour of bubbles of a 2D gas-solid fluidized bed using digital image analysis. *Chem. Eng. Process*.42 (2003) 9-14

Davidson J.F. and Harrison D., 1963. *Fluidised particles*. Cambridge University Press

Fan L.T., Song J.C. and Yutani N., Radial particle mixing in gas-solids fluidized beds. *Chem. Eng. Sci.* 41 (1986) 117

Geldart D., 1973. Types of gas fluidization, *Powder Technology*, vol. 7, pp. 285-292

Johnsson F., Zijerveldb R.C., Schoutenb J.C., van den Bleek C.M., Leckner B., Characterization of fluidization regimes by time-series analysis of pressure fluctuations, *International Journal of Multiphase Flow.* 2000,26, 663-715.

Kunii D. and Levenspiel O., 1969. *Fluidization Engineering*. John Wiley & Sons

Lacey P.M.C., Developments in the theory of particle mixing, *J. appl. Chem.*, 4, May, 1954, 257-268

Laverman J. A., Roghair I., Van Sint Annaland M. and Kuipers H. Investigation into the hydrodynamics of gas-solid fluidized beds using particle image velocimetry coupled with digital image analysis. *The Canadian journal of chemical engineering*. 2008, 86, 523-535

Liu Z., Zheng Y., Jia L. and Zhang Q., Study of bubble induced flow structure using PIV, *Chemical Engineering Science* 60 (2005) 3537-3552.

Lu L-S. and Hsiau S-S Mixing in a vibrated granular bed: Diffusive and convective effects. *Powder Technology*. 184 (2008) 31-43

Müller C.R., Davidson J.F., Dennis J.S. and Hayhurst A.L., 2007. A study of the motion and eruption of a bubble at the surface of a two-dimensional fluidized bed using particle image velocimetry (PIV),*Ind. & Eng. Chem. Res.*, vol. 46, pp. 1642-1652

Otsu N., 1979. A threshold selection method from gray-level histograms, *IEEE Transactions on Systems Man and Cybernetics*,vol. 9, pp. 62-66

Sánchez-Delgado S., Almendros-Ibáñez J.A., Soria-Verdugo A., Santana D., Ruiz-Rivas U., in J. Werther, W. Nowak, K.E. Wirth, E.U. Hartge, (Eds.). TuTech Innovation GmbH, Hamburg, 2008, p. 1007

Sasic, S., Johnsson, F., Leckner, B., Interaction between a fluidized bed and its air-supply system: Some observations 2004. *Industrial and Engineering Chemistry Research* 43 (18), pp. 5730-5737

Sasic, S., Leckner, B., Johnsson, F., Fluctuations and waves in fluidized bed systems: The influence of the air-supply system 2005 *Powder Technology* 153 (3), pp. 176-195

Shen L., Zhang M. and Xu Y. Solid mixing in fluidized beds. *Powder Technology*. 1995, 84, 207-212

Sveen J.P., http://www.math.uio.no/∼jks/matpiv (Last modified in August, 2004. Accesed in 2008)

Werther J. and Reppenhagen J. Handbook of fluidization and fluid-particle system. Attrition: Ed. Wen-Ching Yang. New York: Marcel Dekker Inc. 2003, 8 Elsevier, 1990, p 8, pp 97-106.

Chapter 5

Multiple orifice bubble generation in 2-D gas-solid fluidized beds: the activation region approach

Contents

5.1 Abstract

This work addresses the bubble generation mechanism at multi-orifice distributors in gas-solid fluidized beds. Different measurements devices such as high speed video camera and Kistler pressure transducers are applied to obtain information from both local and global bed dynamics. Pressure fluctuation time series are used for dynamic diagnosis of the 2-D facility employed during the study. The bed is operated at several bubbling conditions leading to different bubble flow patterns characterized by digital image analysis of both the dense and the bubble phases. In order to explain the bubble pattern developed within the bed and the measured bubble dynamics, a phenomenological discrete bubble model is used. The model proposes an activation region mechanism for multi-orifice bubble generation. The underlying hypothesis is that the bubble formation can be placed in a region above the distributor plate where the initial bubble size is the result of the simultaneous bubble generation of neighboring orifices. Aspects such as the distributor design and operating conditions define the characteristic bubble generation frequency and initial bubble size. Moreover, within the model, the bubbles are defined as spherical caps rising through the dense phase that is considered as a continuous, and the interactions between neighboring bubbles including the coalescence effect due to the wake acceleration forces are taken into account. As a result of the comparison between the experimental and the simulated data, it is concluded that the activation region mechanism proposed explains the observed bubble generation phenomena at multiple orifice generation. The use of the activation region mechanism instead of a multi-orifice generation model, based on the direct single-orifice bubble formation, leads to a substantial decrease of the computational cost to simulate bubbling fluidized beds. Moreover, it is shown how for uniform gas distribution across the distributor plate, bubble dynamic interactions play the main role as the driver of the resulting bubble flow pattern developed within the bed.

5.2 Introduction

The gas-solids fluidized beds can be used in many applications in industry such as gasifiers, combustors, dryers or catalytic cracking of hydrocarbons owing to the excellent rates of heat and mass transfer and the uniform and controllable temperature. In these systems, the design of the distributors is important to ensure the desired overall performance of the fluidized bed reactor.

The gas distributor (also called a grid) in a fluidized bed reactor is intended to induce a uniform and stable fluidization across the entire bed cross section, prevent

non fluidized regions on the grid, operate for long periods (years) without plugging or breaking, minimize the "rain" of solids into the plenum beneath the grid, minimize attrition of the bed material, and support the weight of the bed material during startup and shutdown. However, more recent studies now allow grid design based on scientific principles, Werther and Hartge (2003). One problem in designing the fluidized bed and the distributor is understanding and predicting the mixing pattern of solids just above the distributor, the mixing at the distributor region is mainly influenced by the nature and length of jets directly related with separation and diameter of the orifices, the properties of the fluidized bed particles and the flow-rate of the gas (Rees et al., 2006)(Müller et al., 2009)The interaction between these jets have a direct influence in the bubble formation and in the global behavior of the fluidized bed. In gasliquidsolid fluidization systems, bubble dynamics plays a key role in dictating the transport phenomena and ultimately affects the overall rates of reactions. It has been recognized that the bubble wake, when it is present, is the dominant factor governing the system hydrodynamics (Fan and Tsuchiya, 1999). In general, consideration of the flow associated with the bubble wake near the bubble base, whether laminar or turbulent, is essential to characterize the complete behavior of the rising bubble, including its motion. Conversely, examining the shape, rise velocity, and motion of a bubble can provide an indirect understanding of the dynamics of the liquidsolid flow around the bubble (Yang et al., 2007)

Bubble formation phenomena will influence the distributor performance as well as the final bubble pattern developed within the bed, however, whereas bubble generation at a single orifice has been widely studied, and some models have been proposed for computing the bubble volume at the detachment (Davidson and Harrison, 1963) (Caram and Hsu, 1986) (Vakhoshouri and Grace, 2009) the information reported in literature regarding the multi-orifice bubbling formation in gas−solid fluidized beds is rather scarce (Leung, 1971) (Rees et al., 2006) (Müller et al., 2009). In principle, the natural approach for multi-orifice bubbling generation would be to address the case of multiple orifices as an extension of single orifice bubble formation. However, several factors such as gas leakage and the rapid formation of doublets and triplets by coalescence of the emerging bubbles, make the previous discrete bubble models appearing in the literature use instead empirical correlation to estimate the initial bubble size. Besides, other critical aspects of bubble formation, such as the bubble injection frequency and the subsequent injection pattern, have been often left out of the discussion. Hence, it is clear that the bubble generation mechanism will play a major role which must be addressed with caution to satisfactorily explain the observed performance of distributors in fluidized beds (Briongos et al., 2009)

5.2.1 Motivation

In this work different techniques such as DIA−PIV and pressure probes have been used in a 2D fluidized bed to study the influence of the distributor performance in the bubble pattern, the dense phase velocity and the fluidized bed dynamic. Two perforated plate distributors, with an homogeneous distribution of holes along them, were compared under the same experimental conditions (superficial gas velocity, fixed bed height and particle type). The global behavior of the fluidized bed for both cases did not presented significant differences therefore it made us to consider that there might possibly exist a region where bubbles are generated, independently of the holes performance. To corroborate this hypothesis, a previous phenomenological model presented by Briongos et al. (2009) has been used. This model confirms that the bubble interaction in the dense phase controls the bubble pattern of the fluidized bed, being the orifice performance an irrelevant parameter in the study of the global behavior of the fluidized bed. The results obtained in the model are useful when the holes have a homogeneous distribution along the distributor. Previous works presented by Rees et al. (2006) and Müller et al. (2009) proved the existence of a jet region where the air is not considered as going into the bubbles. Bubbles are found in a region above jets and this region is not determined by the orifices performance, but by the interaction between neighboring orifices. The experimental dynamic results obtained in the fluidized bed were in agrement with the dynamic results generated with the model described by Briongos et al. (2009).

5.3 Experimental set-up

The experiments are carried out in a 2-D cold fluidized bed $50\,cm$ wide w, $200\,cm$ high h and $0.5\,cm$ thick t, Fig. 5.1.

The front wall is made of glass and the back panel is made of aluminum and covered by a black card to get a higher contrast in the images. Two 650 watts spotlights are used in order to have a uniform illumination of the bed. The bed was filled with white Geldart-B glass particles, Geldart (1973) , 2500 kg/m^3 density ρ_p , and $600 - 800\,mm$ diameter d_p, previously sieved. Two distributor types were used in the experiments, for each one, five different ratios between the superficial gas velocity, U, and the minimum fluidization velocity, U_{mf}, $(U/Umf = 1.5, 1.75, 2, 2.25, 2.5)$ and three different fixed bed heights, $(h_1 = 15, 30, 45cm)$ were used. Therefore, in this work, a total of 30 cases were studied.

For each case, 3271 images were acquired using a high speed video camera, Redlake Motion pro X3, with 4 Gb memory at 125 frames per second. Then, the same analysis techniques of chapter-2 (DIA-PIV), were used. As in other chapters, with these tech-

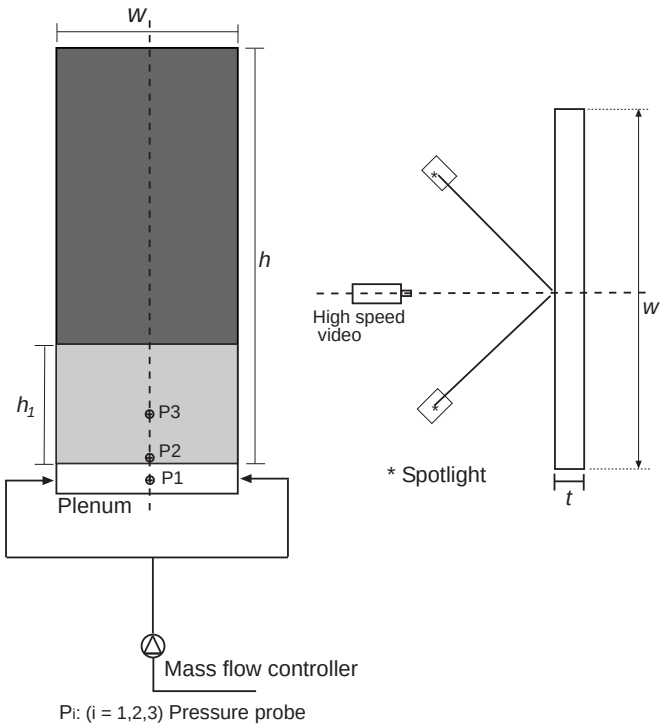

Figure 5.1: Scheme of experimental facilities

niques, not only the phases are clearly identified (dense phase and bubble phase), but also an image superposition reports the time that the points are occupied by bubbles or solids, and the mean dense phase velocity can be calculated (Sanchez-Delgado et al., 2008). As it can be seen, in Fig. 5.1, three pressure probes were used in the fluidized bed to get information about pressure fluctuations. Three piezoelectric pressure sensors, Kistler type 7261 connected to the probes were used, and three Kistler amplifier type 5011, were used to get the signal and transform into a dc voltage. The lowest frequencies were high-pass filtered with a cut-off frequency of 0.16 Hz, and the signals were low-pass filtered with a cut-off frequency of 100 Hz, satisfying the Nyquist criterion. By this filtering action the fluctuations of the pressure are measured relative to the local average pressure, i.e., the offset of the signal is zero. The sample frequency was of 200 Hz (Villa et al., 2003) (van Ommen et al., 2004).

5.3.1 Distributor types

For the experiments, two distributors, with different hole distributions, have been used. The distributors are perforated plates with holes of 1mm diameter. Fig. 5.2 shows this design.

As it can be seen, types I and II have an homogeneous distribution of holes along the distributor keeping constant the ratio between the open area and the total area;

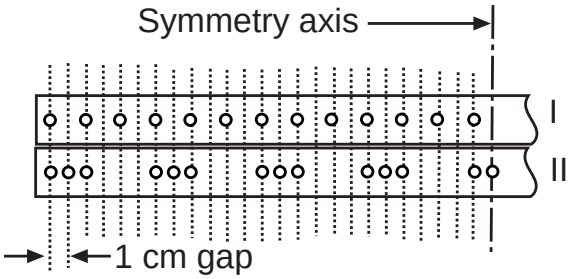

Figure 5.2: Distributor types

therefore they share the same characteristic pressure drop curve through the distributor vs. superficial gas velocity: $\Delta P = 30000U^2$, Fig. 5.3

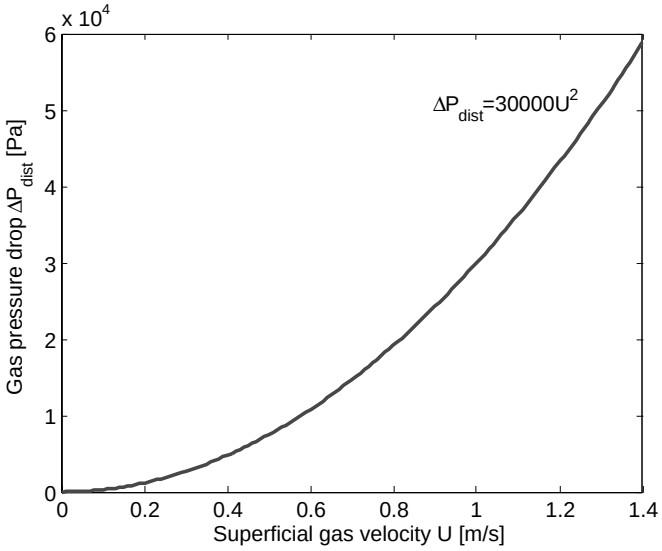

Figure 5.3: Characteristic curve for the distributors

For all the experiments, and for all the values of superficial gas velocity, gas pressure drop through the distributor was higher enough in comparison with the gas pressure drop through the bed: under these operation conditions the bed and the air-supply system are independent (Sasic et al, 2004),(Sasic et al, 2005).

5.4 Activation bubble model

The proposed model consist on a discrete phenomenological approach. This model is completely developed in a previous work of Briongos et al. (2009). Following, a summary of the bubble model will help the reader to understand the bubble model used.

5.4.1 Model basis and bubble generation

The superficial gas velocity of a fluidized bed, U, under bubbling conditions, can be divided in two terms, the air responsible to keep the fluidized bed in the minimum fluidization condition , U_{mf}, and the excess gas. Therefore, the excess gas, responsible of the bubble formation can be expressed as follows:

$$U_e = U - U_{mf} \tag{5.1}$$

The horizontal fluidized bed section is represented by A_{bed} , it is possible then to calculate the visible bubble flow, V_b:

$$V_b = \psi U_e A_{bed} \tag{5.2}$$

Where ψ is the dimensionless ratio between the observed bubble flow and the excess flow from the two phase theory, Kunii and Levenspiel (1991),Jonhsson et al. (1991)

For this work, the starting point of the bubble generation in a multi-orifice distributor plate is focused in the single orifice model proposed in Davidson and Harrison (1963).

When the air is blown steadily through an orifice into a liquid of small viscosity, a bubble can be formed. At very low air rates, the bubble formation is governed by a balance between surface tension and buoyancy forces, but at higher air rates the inertia of the liquid becomes more important that the surface tension, in fluidized beds the surface tension is zero. If the air rate is still higher, the momentum of the air will generate a permanent jet in the orifice before break-up into separated bubbles. Next figure, Fig. 5.4, shows an scheme of a bubble formation in the orifice. O represent the gas source and C represents the bubble center.

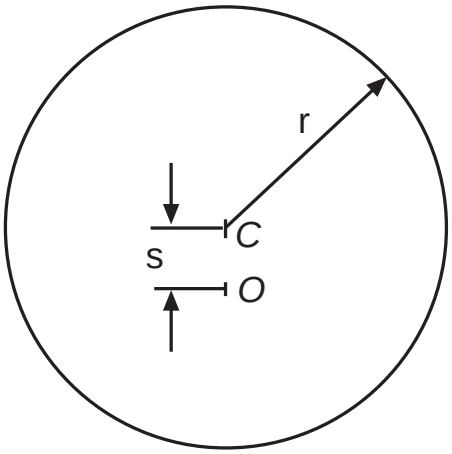

Figure 5.4: Bubble forming in a liquid; the gas source is at O(Davidson and Harrison, 1963)

The bubble is initially centered on O at time $t = 0$, the buoyancy forces make it

rise and at time t (Fig. 5.4) the bubble center O has risen a distance s from the center of the orifice C. If the gas flow rate G is considered constant, the bubble volume V_o at time t can be written as follows:

$$V_o = 4\pi r^3/3 = Gt \tag{5.3}$$

When the bubble base reaches the orifice, that is, when $r = s$, the bubble will detach. The motion is defined by balancing the buoyancy forces $\rho_L V_o g$, where ρ_L is the liquid density, against the rate of change of upward momentum of liquid surrounding the bubble, the inertia of the air within the bubble being neglected. For the forming bubble the upward momentum at any instant of time is therefore $\frac{1}{2}\rho_L V_o \frac{ds}{dt}$, and the equation of upward motion is

$$\rho_L V_o g = \frac{d}{dt}\left(\frac{1}{2}\rho_L V_o \frac{ds}{dt}\right) \tag{5.4}$$

Last equation shows that when a sphere moves in an inviscid fluid, with no separation of the flow, the effective mass added to the sphere by the surrounding fluid is half the displaced mass.

Now, by eliminating V_o from between 5.3 and 5.4 and integrating with respect to t, gives

$$\frac{ds}{dt} = gt \tag{5.5}$$

using the initial condition that $ds/dt = o$ when $t = 0$. Integrating 5.5 gives

$$s = \frac{1}{2}gt^2 \tag{5.6}$$

using the second initial condition that $s = 0$ when $t = 0$. Assuming that the bubble detaches from the orifice when $r = s$, we can, from 5.3 and 5.6 calculate the time of formation of the bubble

$$t = \frac{1}{g^{3/5}}\left(\frac{6G}{\pi}\right)^{1/5} \tag{5.7}$$

and substituting this value of t into 5.3 gives the bubble volume at detachment

$$V_o = \frac{1.138G^{1.2}}{g^{0.6}} \tag{5.8}$$

As stated above, G represent the visible flow per hole:

$$G = \frac{V_b}{N_{or}} = \frac{\psi U_e A_{bed}}{N_{or}} \tag{5.9}$$

With the combination of 5.3 and 5.4, the bubble frequency above the orifice can be estimated according to:

$$f_{b,or} = \frac{G}{V_o} \tag{5.10}$$

5.4.2 The activation region mechanism

In the last ten years, several studies reveal that the bubbling synchronicity is strongly related with the orifice distribution along the distributor, liquid depth and gas flow rate (Ruzicka et al., 1999) (Xiao and Tan, 2003), however, no explicit model is provided to account for that influence (bubble synchronization, doublets, triplets...). Despite the fact that there is not a known model, those studies also report the fact that the orifices active in one part of the distributor enhance the bubble generation within their nearest distributor region, making the orifices which belong to other distributor regions passive for bubble formation.

Recently, Rees et al. (2006) and Müller et al. (2009) have reported, using MRI (Magnetic Resonance Imaging), that in the case of multiple-orifice distributors and for $U/U_{mf} > 1$, the region near the distributor plate exhibits permanent jets, Fig. 5.5 where the upper parts of the jets merged with each other forming a central dilute core and the bubble detachment takes place in a closer region above the distributor. For the first time, a time-averaged velocity map over a horizontal plane was obtained; it demonstrated that the central core was rising upwards and that the surrounding material was descending.

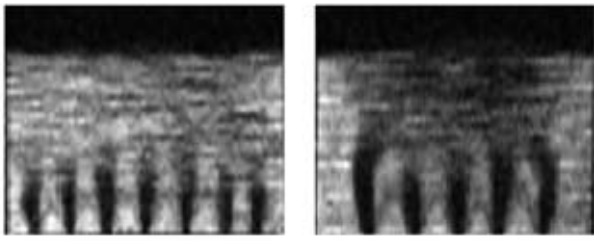

Figure 5.5: Mean jet pattern reported by Rees et al. (2006), for $U/U_{mf} = 1.4$ at different holes distribution.

That information serves here to propose the activation region mechanism, where the multi-orifice plate is seen as a discrete source of information where the bubbles are the dynamical message to be transmitted, Fig. 5.6. In the same way that the single orifice is characterized by a bubble injection frequency, the multi-orifice distributor is characterized by an overall bubble generation frequency, f_b. The overall bubbling frequency defines a rate of region activation, and according to that, bubble of volume

v_b is given by:

$$v_b = \frac{V_b}{f_b} \tag{5.11}$$

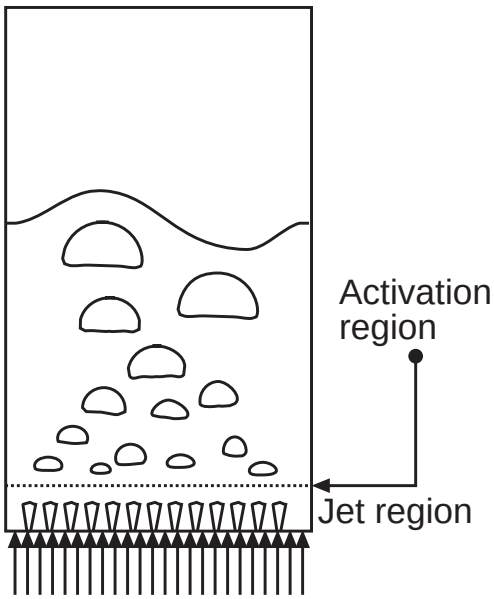

Figure 5.6: Scheme of the model proposed

Fig. 5.7 shows a picture of our experimental 2D fluidized bed system operating at bubbling conditions with a multi-orifice distributor, which serves to illustrate the idea behind the activation region mechanism.

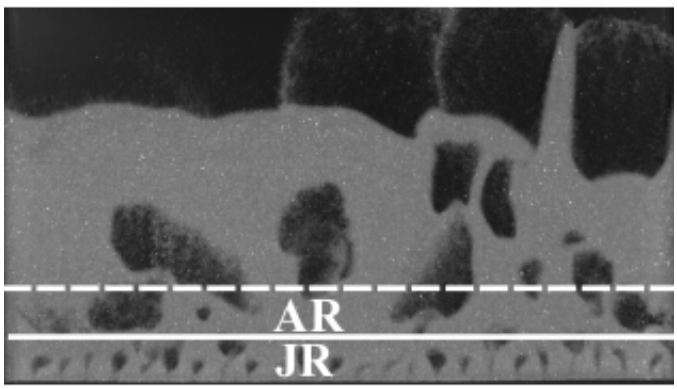

Figure 5.7: Two-dimensional Fluidized bed operating at bubbling regime. The solid line accounts for the limit of the orifice interaction region, JR (jet region); the active regions i.e bubbles, AR, will appear above the JR.

The bubbles will be generated at different regions on the distributor plate at a rate defined by f_b. Therefore, it is assumed that the resulting bubble size is the consequence of the coalescence of bubbles generated at neighboring orifices. In order to estimate f_b, two approaches were presented.

The synchronous model

This model assumes that the bubble generation frequency f_b is synchronized to the orifice bubble generation $f_{b,or}$, i.e. the overall bubble generation frequency, f_b, would be the same that the frequency resulting from the orifice bubble generation mechanism, $f_b = f_{b,or}$, but, in those conditions, the model erroneously predicts the expected dynamical behavior of the bed, therefore, the synchronous model assumption is not useful for designing purposes. However, it can be used as a dynamical matching tool. For this model, it can be concluded that the distributor performance needs to be taken into account in order to avoid the limitation of the synch-model for designing purposes.

The asynchronous model

With the aim to use the activation region mechanism for designing purposes, the asynch-approach assumes the distributor performance will produce a deviation on the predicted $f_{b,or}$ of the single orifice given by the previous synch-model as follows:

$$f_b = \phi f_{b,or} \tag{5.12}$$

where ϕ is defined as a ratio between the stirring effectα_{Da} of the distributor and the fraction of active area relative to the total distributor area f_a

$$\phi = \alpha_{Da}/f_a \tag{5.13}$$

α_{Da} has at least two contributions: the contribution due to jet stirring, α_j, and the mixing promoted by the bubbles formed at the distributor, α_b. Finally, the stirring capacity of the active area region of the distributor, α_{Da}, is given as the weighted mean of both two components:

$$\alpha_{Da} = w_j\alpha_j + w_b\alpha_b \tag{5.14}$$

where the weights w_j and w_b are estimated as follows:

$$w_i = \frac{\alpha_i}{\alpha_j + \alpha_b} \tag{5.15}$$

and

$$\alpha_j = \frac{\frac{1}{2}u_{or}^2}{\Delta P} \tag{5.16}$$

The factor α_j gives the ratio between the kinetic energy of the orifice jets and the

resistance of the bed, where u_{or} is the gas velocity through the orifice (It is well known that u_{or} has a closely relation with the pressure drop across the distributor ΔP) It has been reported that when $\alpha_j > 1$, the stirring capacity of the distributor is mostly due to the jets formed at the orifices, whereas for $0.09 < \alpha_j < 1$ the stirring capacity is due to both jets and bubbles formed at the distributor, and for $\alpha_j << 1$ the jets do not contribute much to bed stirring and bubbles should do the job. As it can be seen in the equation 5.14, there is another term to take into account in the stirring capacity of the activation region, α_b, this term shows a relation between the kinetic energy due to bubbles formed at the distributor plate and the resistance of the bed.

$$\alpha_b = \frac{\frac{1}{2}u_{b,or}^2}{\Delta P} \tag{5.17}$$

Where $u_{b,or}$ is the initial bubble velocity and it is estimated from the results of the synch-model as:

$$u_{b,or} = \frac{d_{b0}}{2t_d} \tag{5.18}$$

where t_d was defined as the detachment time in the model proposed. This expression 5.19 is the same expression proposed by Davidson and Harrison (1963), 5.7, where the gas flow rate per hole G is substituted by the visible bubble bubble flow V_b under the assumption that all the visible bubble flow V_b is concentrated in only one region during the time t_d.

$$t_d = \frac{1}{g^{3/5}}\left(\frac{6V_b}{\pi}\right)^{1/5} \tag{5.19}$$

d_{b0} represents the bubble diameter based on the bubble volume, taking into account the wake fraction f_w (Hoffmann et al., 1993)

$$d_{b0} = ((1 + f_w)\upsilon_b 6/\pi)^{1/3} \tag{5.20}$$

Coming back to eq. 5.13, the term f_a is defined as the fraction of active area relative to the total distributor area, and it is estimated as follows:

$$f_a = \frac{area\,of\,the\,active\,region}{bed\,area} = \frac{(\pi/4)d_{b0}^2}{A_{bed}} \tag{5.21}$$

This section can be summarized as follows:

- The multi-orifice distributor is characterized by an overall bubble generation frequency, f_b, based on the Davidson and Harrison (1963).

- The model proposes that the distributor performance will produce a deviation on the predicted orifice bubble generation frequency. $f_b = \phi f_{b,or}$.
- ϕ is defined as a ratio between the stirring effect of the distributor, α_{Da}, and the fraction of active area relative to the total distributor area, f_a
- The model modifies the time of formation of the bubble, t_d, proposed by Davidson and Harrison (1963), under the assumption that all the visible bubble flow, V_b, is concentred in only one region during the time t_d.

5.4.3 Bubble rise, trailing bubble and bubble coalescence

To characterized the bubble pattern within the fluidized bed, the bubble rise and the bubbles interaction have to be modeled.

Bubble rise

Following the results reported in Briongos et al. (2007), the proposed bubble model assumes that the bubbles are the driver of bubbling fluidized beds dynamics, which is in agreement with previous approaches reported in literature (Daw and Halow, 1992), (Pannala et al., 2004). In contrast to those previous models where the bubbles are considered as spherical elements, in the present approach, the bubbles are considered as spherical caps which rise according to their size and local condition. Moreover, instead of computing the bubble trajectory by integrating the bubble velocity in time from empirical correlations, the bubbles are tracked individually according to Bokkers et al. (2006), where the virtual mass force has been modified to account for the spherical cap (Kendoush, 2003)

$$\frac{d}{dt}\left[(m_b + m_v)U_b\right] = \left(\rho_g + C_v\rho_e\right)\nu_b\frac{d}{dt}U_b = F_B + F_D \tag{5.22}$$

Where F_B is the effective buoyancy force and F_D is the drag force acting on the bubble, which are given by:

$$F_B = F_b + F_g = \frac{\pi d_b^3}{6}\left(\rho_p - \rho_g\right)g(1-\varepsilon) \tag{5.23}$$

$$F_g = -\frac{\pi d_b^3}{6}\rho_g g \tag{5.24}$$

$$F_b = \frac{\pi d_b^3}{6}\left(\varepsilon\rho_g + (1-\varepsilon)\rho_p\right)g \tag{5.25}$$

$$F_D = -\frac{1}{2}C_D\rho_e\frac{\pi}{4}d_b^2U_b^2 \tag{5.26}$$

According to Bokkers et al. (2006), the drag coefficient for single bubble rising is computed from the steady state force balance giving:

$$C_D = \frac{4}{3}\frac{(\rho_e - \rho_g)}{\rho_e}\frac{d_b g}{U_b} \tag{5.27}$$

Thus, each bubble trajectory along the Z axis is estimated by integrating the eq. 5.22, whereas the dynamical coupling between rising bubbles that lead to the XY displacement is driven by the wake acceleration force that results from the trailing bubble effect.

Trailing bubble effect

The behaviour of bubbles in fluidized beds has received considerable attention, and expressions for estimating the rising velocities of bubbles have been previously reported (Davidson et al., 1985). Moreover, it is well known that bubbles rise more rapidly when rising in a bubble stream than in isolation due to the process of bubble coalescence (Grace and Harrison, 1969). Thus the wake of the leading bubble accelerates the trailing bubble before the coalescence process takes place. Accordingly, it is clear that in order to simulate the observed bed behaviour, the trailing effect should be taken into account to model the behaviour of an interacting stream of bubbles. In previous works, the dynamical coupling between neighbours bubbles was either neglected (Bokkers et al., 2006) or described through empirical relationships (Daw and Halow, 1992) (Pannala et al., 2004). In contrast, in this paper an interacting bubble model is proposed to describe the trailing bubble effect of the leading bubbles. The model is based on the pressure recovery in the wake below a spherical cap reported in Davidson and Harrison (1963), and on the idea suggested by Clift and Grace (1971) of adding to the isolated bubble velocity a component related to the particulate phase. The hypothesis is that the pressure drop originated by the wake of the leading bubble will cause acceleration of the corresponding trailing bubbles by means of a void propagation mechanism, thus the increase of velocity due to the wake acceleration force equals the velocity that the dense phase would have at the position of the trailing bubble. According to that, the pressure recovery is obtained by applying Bernoullis theorem. (Davidson and Harrison, 1963).

$$p_R = \rho_g g h - \frac{1}{2}\rho_g U_b^2 \tag{5.28}$$

Bernoullis theorem is applied again to estimate the void propagation velocity which corresponds to the increase of bubble velocity due to the wake acceleration force:

$$U_{void} = \sqrt{\frac{2p_R}{\rho_e}} \tag{5.29}$$

The bubble velocity of the trailing bubble is finally given as the sum of its isolation velocity plus the void propagation velocity:

$$U_{Tb} = U_{ib} + U_{void} \tag{5.30}$$

Bubble coalescence

The coalescence of bubbles is modelled following the approach reported in Daw and Halow (1992). Consequently, during the coalescence there is a net gas exchange between the lower and upper bubbles that governs the process. However, instead of defining the gas exchange rate, Q_c, as a function of bubble rise velocities, the through flow velocity across any plane through the bubble derived from the alternative analysis presented in Lockett et al. (1967) is used as constant gas transfer rate during the coalescence, being therefore as:

$$Q_c = 3U_{mf}\frac{\pi}{4}d_{Lb}^2 \tag{5.31}$$

Moreover, it is worth mentioning that neither the upper bubble nor the lower bubble are bound to the coalescence process; they are still free to interact with any neighbour bubble according to the phenomenological assumption presented below that ruled the interactions. That fact makes possible the splitting of the coalescing bubble pair to appear, giving rise to a final bubble size distribution resulting from coalescing and splitting processes.

Other phenomenological key assumptions

I. Bubbles grow only by coalescence.

II. Wall effects are not taken into account.

III. A bubble is a trailing bubble if it lies within the projected horizontal area defined by twice the diameter of its closest leading bubble and, if their center-to-center distance is less or equal than that of four times the leading bubble radii (Clift and Grace, 1971).

IV. In order for the coalescence processes to take place, the trajectory followed by the nose of the lower bubble should fall within the overlap region defined by one times the diameter of the upper bubble.

V. When the nose of the lower bubble enters the wake of the leading bubble (Hoffmann et al., 1993) the coalescence process begins by shrinkage of the lower bubble and subsequent increase of the upper bubble. Coalescence will continue until the complete depletion of the lower bubble or until the splitting of the coalescing pair as a result of the interaction with neighbour rising bubbles.

VI. Bubbles will exit the bed when their centers reach the bed surface.

VII. Either when a bubble leaves the bed or when a bubble disappears as a result of

the coalescence process, the total number of bubbles in the bed is reduced by 1.

5.5 Result and discussion

This section will be focused in the analysis of the bubble pattern, the time-averaged dense phase velocity and the dynamical analysis in the 2-D fluidized bed. As stated above two distributors were used during the experiments, therefore the influence of the distributor performance in the global behavior of the fluidized bed has been analyzed.

5.5.1 Bubble pattern and dense phase velocity for different distributors

Bubble pattern

First, the bubble pattern within the fluidized bed is obtained using the DIA technique previously used in chapter-2: once the images were acquired, a threshold transformation was applied over images, getting pixels of value $B_{i,j} = 1$ for the points occupied by the bubbles and pixels of value $B_{i,j} = 0$ for points occupied by dense phase, with the superposition of these transformed images, a time averaged maps were generated showing the time that the point (i, j) is occupied by bubbles or by dense phase, (Sanchez-Delgado et al., 2008):

$$\overline{B_{i,j}} = \frac{1}{N} \sum_{K=1}^{N} B_{i,j,K} \tag{5.32}$$

$$\overline{C_{i,j}} = 1 - \overline{B_{i,j}} \tag{5.33}$$

Next figure, Fig. 5.8, shows the time averaged results for images superposition for the two different distributors.

In a simple view, it is possible to appreciate the same time averaged bubble concentration for the two images presented, it is also possible to detect that the region close to the distributor presents some difference in the images. In order to compare the internal structure of the fluidized bed with these two different distributors, three cuts at different heights above the distributor are represented in the Fig. 5.9:

As it can be seen, there are no important differences in the bubble pattern of fluidized bed, at least for these heights. Now, the attention will be focused in the region just above the perforated distributor Fig. 5.10.

Fig. 5.10 shows the boundary line that divides the region where the points have never been occupied by bubbles and the region where, the points have at least been

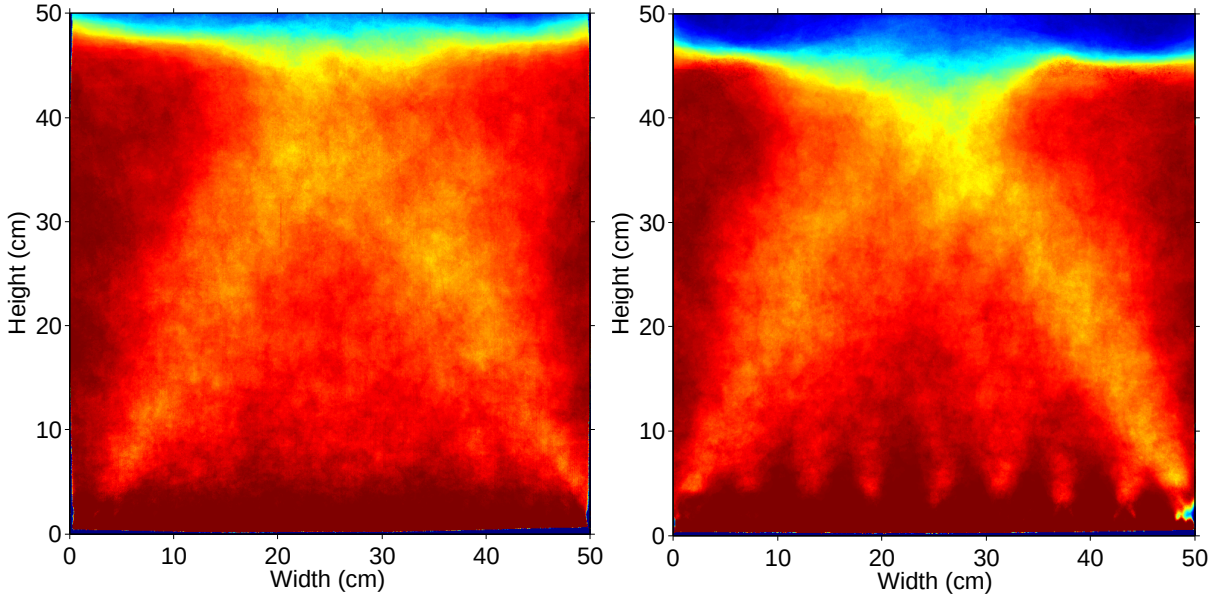

(a) (b)

Figure 5.8: a) Distributor type I, $h_1 = 45\,cm$,$U/U_{mf} = 2.25$, b) Distributor type II, $h_1 = 45\,cm$,$U/U_{mf} = 2.25$

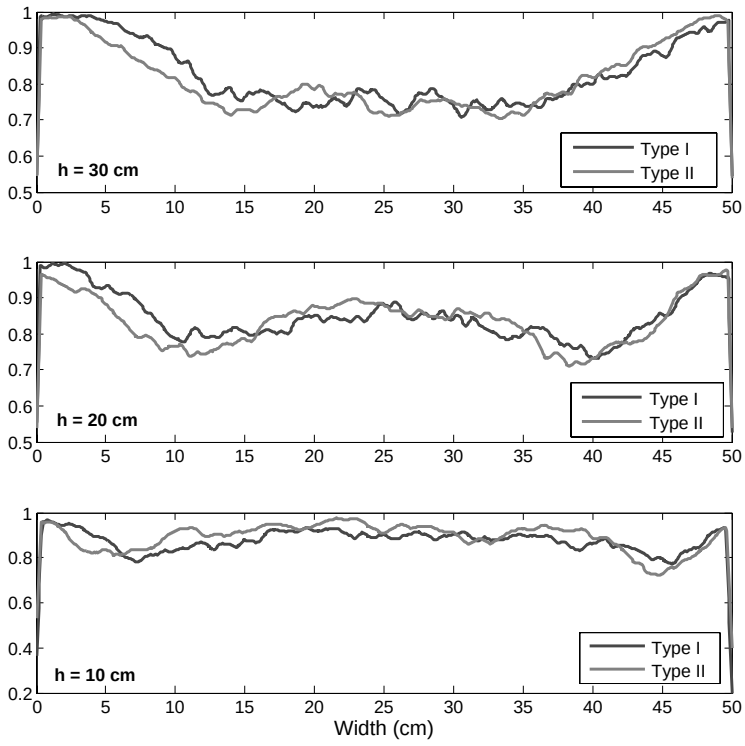

Figure 5.9: $\overline{C_{i,j}}$ results at different height above distributor for the two distributors, $h_1 = 45\,cm$, $U/U_{mf} = 2.25$

occupied by bubbles 1% of the times. It can be seen how the distributor type I presents a flat profile of $\overline{C_{i,j}}$, this is the consequence of the grid configuration because the separation between the orifices is the same. However, the type II presents an irregular

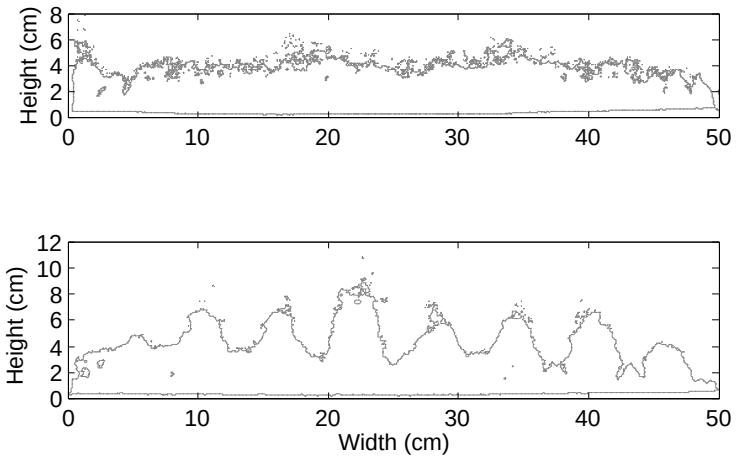

Figure 5.10: $\overline{C_{i,j}}$ Contour plot for small height above the distributor for the two distributors (Type I (up) and II (down)), $h_1 = 45\,cm$, $U/U_{mf} = 2.25$

contour of $\overline{C_{i,j}}$ because of the jet interaction; the orifices in this distributor are placed in groups of three, therefore the jet interaction makes that bigger jets penetrate more in the fluidized bed, generating dead zones between them (Rees et al., 2006).

Following, similar images as the images shown in Fig.5.8 are represented in Fig. 5.11. In this case, the bed aspect ratio has decreased ($h_1 = 15\,cm$) and two relations between superficial gas velocity and minimum fluidization velocity have been analyzed.

The same analysis of Fig. 5.9, at different heights of the fluidized, was applied in images of Fig. 5.11, corroborating that there is no influence of the orifice distribution along the distributor in the general bubble pattern of the fluidized bed beyond the activation region. Fig. 5.11 also shows the effect of the flow rate in the jet formation: as the the flow rate increases the activation region is located at less height above the distributor. Rees et al. (2006) reported that the jets grow in height with increasing gas flow-rate, hence the interaction between neighboring jets which start to define the activation region takes place closer to the distributor.

Dense phase velocity

As in chapter 2 the dense phase velocity vector is represented by $\overrightarrow{V}_{i,j,k}$ and the time-averaged dense phase velocity is calculated as follows:

$$\overline{\overrightarrow{V}_{i,j}} = \frac{1}{N}\sum_{k=1}^{N}\overrightarrow{V}_{i,j,k} \tag{5.34}$$

Fig. 5.12 shows the time-averaged dense phase velocity results for the same cases presented in Fig. 5.8 providing qualitative information about the distributor influence in the dense phase behaviour. It is clear the similarity between both cases, which have an upwards moving dense phase in the central section of the bed, and two downward moving dense phases on the walls of the FBs. Therefore, apparently they exhibit the

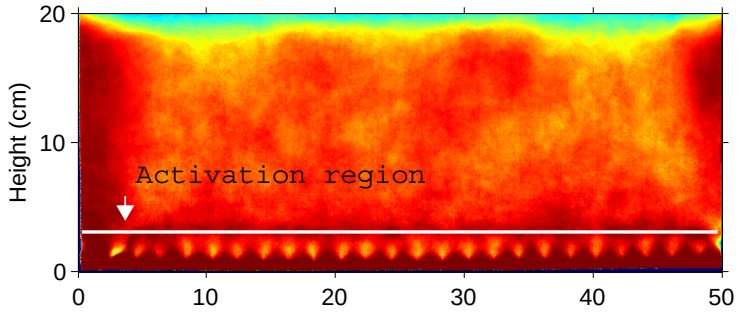

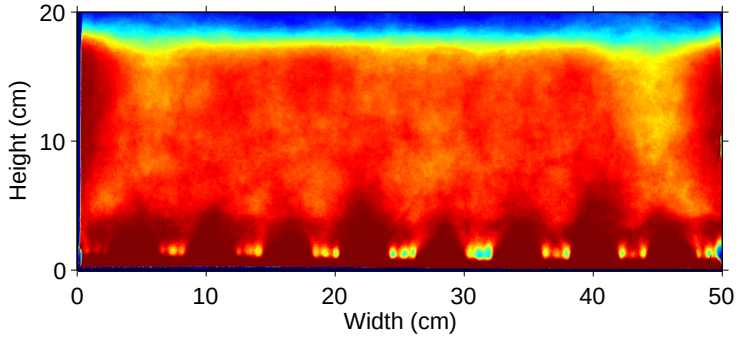

(a)

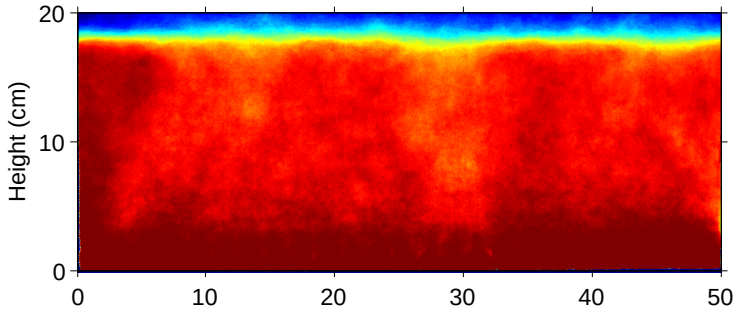

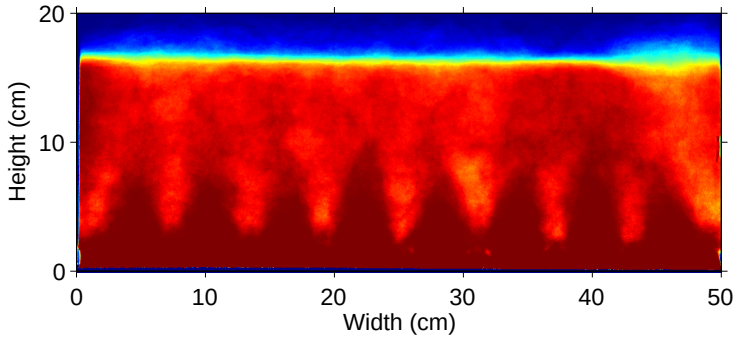

(b)

Figure 5.11: a-1) Distributor type I, fixed bed $h_1 = 15\,cm$, $U/U_{mf} = 2.25$, a-2) Distributor type II, fixed bed $h_1 = 15\,cm$, $U/U_{mf} = 2.25$, b-1) Distributor type I, fixed bed $h_1 = 15\,cm$, $U/U_{mf} = 1.75$, b-2) Distributor type II, fixed bed $h_1 = 15\,cm$, $U/U_{mf} = 1.75$

same internal flow structure.

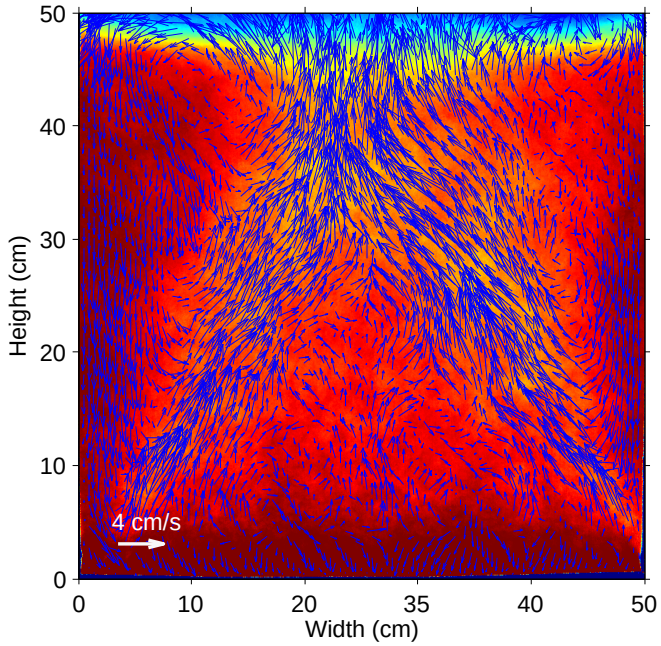

(a)

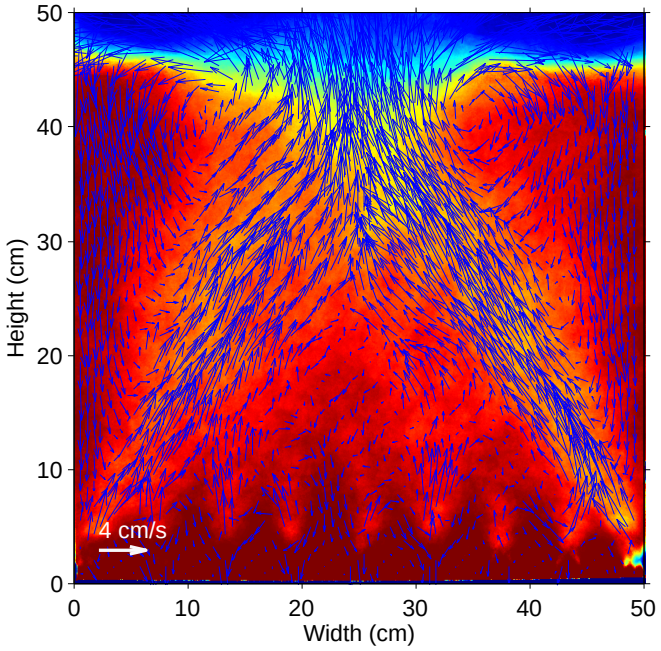

(b)

Figure 5.12: Time averaged dense phase velocity results and bubble pattern. a) Distributor type I, $h = 45\,cm$ and $U/U_{mf} = 2.25$ b) Distributor type II, $h = 45\,cm$ and $U/U_{mf} = 2.25$

Moreover, it is worth to point out that the vertical velocity values for both cases at different heights above the air distributor are very similar for both distributors as shown in Fig. 5.13.

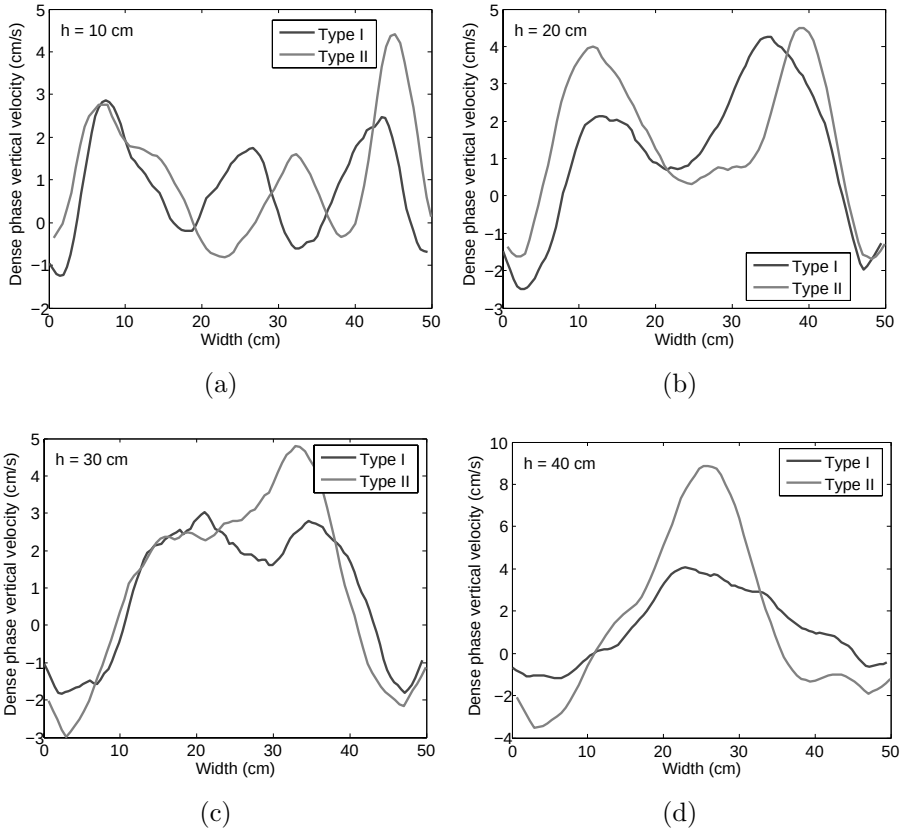

Figure 5.13: Vertical dense phase velocity values for the two distributors at different height, U/U_{mf})225

5.5.2 Dynamic analysis

Complementarily to the previous digital image analysis, the time series collected by means of the Kistler pressure transducers are used to compare the overall fluidized bed dynamics characterizing two beds operating with different distributor plates. Thus, frequency domain, mutual information function, and state space analysis are applied over the measured pressure fluctuation signal for dynamical comparison.

Frequency Domain Analysis

The spectral analysis of experimental time series has been widely applied to gas-solid fluidized bed dynamics diagnosis. In this study, it is used to provide information on the characteristic frequencies appearing within the measured signals. The frequency domain representation of the signal can be described by the estimation of its power spectral density, PSD. Here, the well known Welch's averaged periodogram method is used to compute the PSD (Johnsson et al., 2000). It should be noted that the energy of the spectrum is dimensionless, since the time series were previously normalized to time series having a mean of zero and a standard deviation of unity. This fact makes the ordinate of the power spectrum to be P_{xx}/σ^2. According to Brown and Brue (2001) in

order to get a good trade off between resolution and error, no less than 20 periodograms have been averaged to compute the PSD.

State Space Analysis

Gas-solid fluidized bed dynamics are governed by two-phase, non-linear interactions, which apparently exhibit low-dimensional deterministic chaotic features (Briongos and Guardiola, 2003). The state space analysis deals with the reconstruction of the attractor in the phase space, and the subsequent evaluation of their invariant properties, such as the Kolmogorov entropy, K, and the correlation dimension, D_2. The strangeness of the attractor is currently quantified in terms of computing either the homogeneity structure (i.e. D_2, numbers of degrees of freedom), or by measuring the sensitivity to the initial conditions (Kolmogorov entropy).

Reconstruction of the attractor:

The reconstructed attractor in the phase space has been considered as the 'finger print' of the fluidized bed dynamics. In this work the Broomhead and King (1986) method, which avoids the need to introduce statistical independence between points of the time series is used to reconstruct the attractor.

Correlation dimension:

Since the correlation dimension, D2, is related to the number of degrees of freedom of the system, it has been extensively used as a measure of the local structure of a strange attractor, being given by the correlation between random points on the corresponding attractor. The method used in this work to estimate de correlation dimension is based on the Grassberger and Procaccia (1983) algorithm.

Kolmogorov entropy:

The Kolmogorov entropy is a direct measure of the chaos level, providing qualitative and quantitative information on the underlying dynamics, by measuring the average surprise of one measurement by making a new measurement despite having knowledge about past history. The Kolmogorov entropy is usually expressed in units of bits/s, reflecting the rate of loss information by the system (unpredictability), in the way that for fully deterministic the Kolmogorov entropy is zero, whereas for random time series, the entropy should be infinite, among those situations, a positive Kolmogorov entropy value characterizes deterministic chaotic processes. There are several methods for estimating the Kolmogorov entropy from experimental time series, the algorithm used here is based on the well known maximum likelihood method (Schouten et al., 1994)

Mutual Information Function

Mutual information function, I, is based on the uncertainty concept developed by Shanon and Weaver (1949). According to that, the uncertainty associated with

any measure depends on probability from all possible outcomes. Thus, when dealing with deterministic signals the connection between successive measurements is repeated over fundamental frequency intervals, the future behavior is therefore completely predictable. For random processes there is not a deterministic connection among the successive measures and the knowledge over past history, does not have consequences on the future dynamic behavior of the signal. In contrast, deterministic chaotic processes are an intermediate situation, exhibiting short-term predictability. According to that, the Mutual Information Function provides information about the temporal evolution of the process, as the same as the autocorrelation function does. However, the fact the Mutual Information Function does not assumes any functional relationship between the data points, makes it more appropriated for studying non-linear dynamics (Karamavru and Clarck, 1997).

Dynamical comparison

The normalized frequency spectra of the measured pressure fluctuation time series are shown on Fig. 5.14. It is observed how the characteristic frequencies of the 2D bed operating with either distributor plate configurations (I, II), are very similar. Only slight differences can be observed in the spectra estimated from the signals measured in the middle and bottom bed regions, which seem to be more influenced by the jetting region. In contrast, the top bed dynamics exhibit a remarkable matching for both situations. According to that the dynamical regime developed in both systems exhibit a similar frequency structure characteristic of multiple bubbling regime. The multiple bubble regime is a well fluidized bubbling bed with a uniform bubble distribution and, with the bubbles evenly distributed over the cross-section of the bed.

The dynamical similarities drawn from the frequency domain analysis are confirmed by the state space analysis. Thus as Fig. 5.15 shows how the reconstructed attractor, eigenvalue spectra, and attractor properties such as the correlation dimension and Kolmogorov entropy almost match for the signals collected at different positions, in fact, as for the frequency domain analysis, the result extracted from the pressure probe located at the middle bed region ($h = 0.2\,cm$) exhibit slightly differences within both the eigenvalue spectra and reconstructed attractors.

Finally, the mutual information function analysis shown in Fig. 5.16 agree with the results obtained from the frequency and state space analysis, confirming the dynamic similarities found during the digital image analysis. Thus, it can be observed in Fig. 5.16 how the time series collected a different positions for the fluidized bed operating with the distributor I and II types, exhibit a similar short-term as well as long-term temporal structure, which explains the matching on the Kolmogorov entropy value.

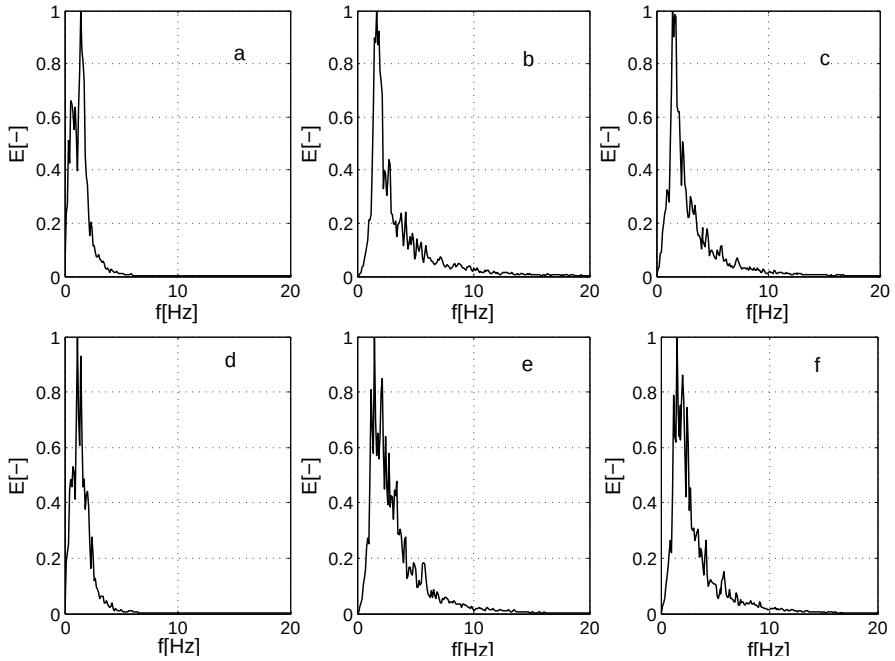

Figure 5.14: Normalized power spectral density estimation for distributor I (a, b, c) and II (d, e, f) from pressure fluctuation time series collected respectively at $h = 0m, 0.2m, 0.45m$

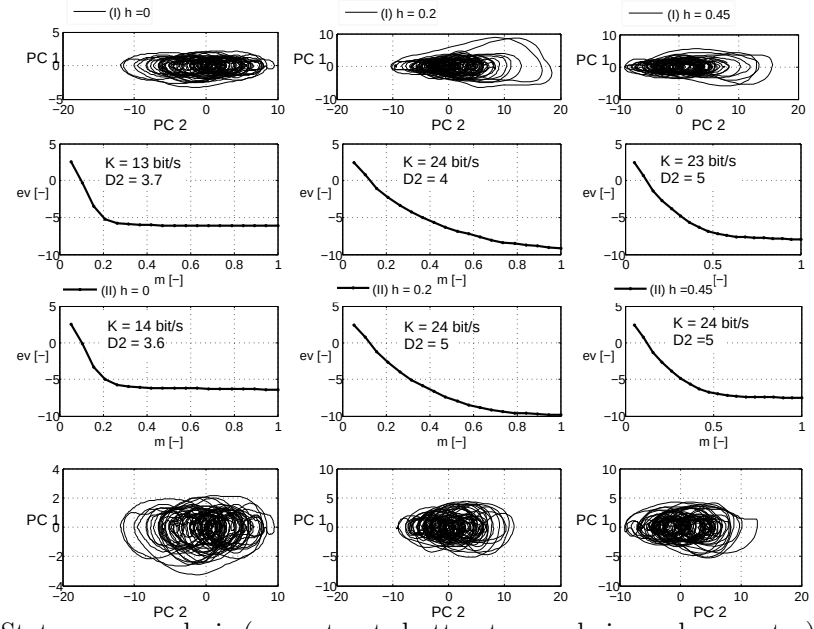

Figure 5.15: State space analysis (reconstructed attractors and eigenvalue spectra) for distributors I and II from pressure fluctuation time series collected respectively at $h = 0m, 0.2m, 0.45m$

5.6 Conclusion

It has been proved how two uniform multi-orifice distributor having the same pressure drop and different grid configuration, lead to the same dynamical bubble pattern and global bed behavior (above the activation region) when the beds are operated at the

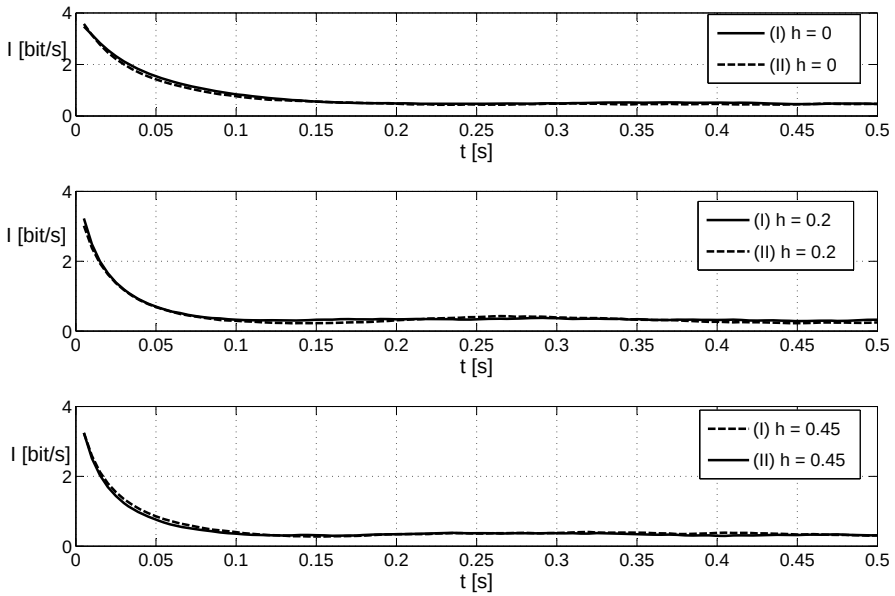

Figure 5.16: Time series explained the matching on the Kolmogorov entropy values

same fluidization conditions. Consequently, it is concluded that the bubble dynamics interactions play the main role as the driver of the resulting bed dynamics developed within the bed, and therefore, the overall bed dynamics for uniform gas distribution conditions does not depends on grid configuration for the fluidization condition covered.

5.7 Notation

A_{bed} Cross sectional area of the bed $[m^2]$

AR Activation region $[-]$

$B_{i,j}$ $Value = 0\, or\, 1$ for a pixel i, j occupied by dense phase or bubble phase respectively,$[-]$

$\overline{B_{i,j}}$ Proportion of time that the point i, j is occupied by bubbles,$[-]$

c Bubble center proposed by Davidson $[m]$

$C_{i,j}$ $1 - B_{i,j}$,$[-]$

$\overline{C_{i,j}}$ Proportion of time that the point i, j is occupied by solids,$[-]$

C_D Drag coefficient for a single bubble $[-]$

C_v Virtual mass force coefficient $[-]$

D_2 Correlation dimension $[-]$

D_b Bubble diameter $[m]$

d_{bo} Bubble diameter with the effect of the wake fraction f_w $[m]$

d_{Lb} Leading bubble diameter $[m]$

d_p Particle diameter $[m]$

E Power spectrum energy $[-]$

Δ_p Pressure drop through the distributor $[-]$

f_a Fraction of the active area relative to the total distributor area $[-]$

f_b Frequency generation bubble, $[s^{-1}]$

$f_{b,or}$ Bubble frequency above the orifice, $[s^{-1}]$

F_B Effective buoyancy force $[N]$

F_D Drag force $[N]$

f_w Wake fraction $[-]$

g Gravity constant $[9.81\, m/s^2]$

G Gas flow rate per hole $[m^3/s]$

h Fluidized bed height, $[cm]$

I Mutual information function $[bits]$

i, j Horizontal and vertical coordinates for a pixel, $[cm]$

JR Jet region $[-]$

K_c Kolmogorov entropy per cicle $[bits/cycle]$

N_{or} Number of orifices $[-]$

o Origin of the bubble proposed by Davidson $[m]$

P_R Pressure recovery $[Pa]$

Q_c Gas transfer rate during coalescence, $[m^3/s]$

r Bubble ratio proposed by Davidson $[m]$

s $c - o$ $[m]$

t_d Detachment time $[s]$

U Superficial gas velocity $[m/s]$

U_e Excess gas $[m/s]$

U_{ib} Isolated bubble velocity, $[m/s]$

U_{mf} Minimum fluidization velocity, $[m/s]$

U_b Bubble velocity, $[m/s]$

u_{b-or} Initial bubble velocity, $[m/s]$

u_{or} Gas velocity through the orifice, $[m/s]$

U_{Tb} Trailing bubble velocity, $[m/s]$

U_{void} Void propagation velocity, $[m/s]$

V_b Visible bubble flow $[m^3/s]$

V_o Bubble volume $[m^3]$

$\overrightarrow{V_{i,j,k}}$ Dense phase velocity in a point i, j for image k, $[cm/s]$

$\overrightarrow{\overline{V}}$ Time averaged dense phase velocity,$[cm/s]$

w Fluidized bed width, $[cm]$

w_b Weight for α_b, $[-]$

w_j Weight for α_j, $[-]$

t Fluidized bed thickness, $[cm]$

Greek letters

α_{Da} Stirring effect of the distributor $[-]$

α_j Stirring effect of the jet $[-]$

α_b Stirring effect of the bubble formation $[-]$

ρ_e Emulsion density $[kg/m^3]$

ρ_g Gas density $[kg/m^3]$

ρ_L Liquid density $[kg/m^3]$

ρ_p Particle density $[kg/m^3]$

ψ Ratio between the observed bubble flow and the excess flow $[-]$

ϕ $\frac{\alpha_{Da}}{f_a}$ $[-]$

υ_b Bubble size $[m^3]$

Bibliography

Bokkers G.A., Laverman J.A., van Sint Annaland M., Kuipers J.A.M. Modelling of large-sclae dense gas-solid bubbling fluidised beds using a novel discrete bubble model. *Chemical Engineering Science* 61 (2006) 5590-5602.

Briongos J.V., Guardiola J., Free top fluidized bed surface fluctuations as a source of hydrodynamic data, *Powder Technol.* 134 (2003) 133-144.

Briongos, J.V., Aragón, J.M. Palancar, M.C. Phase space structure and multiresolution analysis of gas solid fluidized beds hydrodynamics: Part II: Dynamic analysis. *Chem. Eng. Sci.* 62 (2007) 2865-2879.

Briongos J.V., Sanchez-Delgado S., Acosta A. and Santana D. "A novel approach for modelling bubbling gas-solid fluidized bed: the activation region mechanism. Submitted for publication in a AICHE Journal, 2009

Broomhead, D.S. y King, G. P.. Qualitative dynamics from experimental data, *Physica D*, 20 (1986) 217-236

Brown R.C., Brue E., Resolving dynamical features of fluidized beds from pressure fluctuations, *Powder Technol.* 119 (2001) 68-80.

Caram H.S., Hsu K.-K. (1986). Bubble formation and gas leakage in fluidized beds. *Chemical Engineering Science* 41 (1986) 1445-1453.

Clift R., Grace J.R. Coalescence of Bubbles in fluidized beds. *AIChE Symp. Ser.* 116 vol. 67 (1971) 23-33.

Davidson J.F. and Harrison D., Fluidised particles. Cambridge University Press. 1963

Davidson J.F, Clift R., Harrison D. (1985). Fluidization (2nd Ed.). Academic Press Inc. (London). ISBN: 0-12-205552-7

Daw C.S. and Halow J.S. Modelling deterministic chaos in gas fluidized beds. *AIChE Symp. Ser.* 289 vol. 88 (1992) 61-69.

Fan, L.-S., Tsuchiya, K. *Bubble Wake Dynamics in Liquids and LiquidSolid Suspensions*. Butterworth-Heinemann, Stoneham, MA. (1990)

Geldart D., Types of gas fluidization. *Powder Technol.*, 7(1973) 285-292

Grace J.R., Harrison D. The behavior of freely bubbling fluidised beds. *Chemical Engineering Science* 24 (1969) 497-508

Grassberger P., Procaccia I., Characterization of strange attractors, *Phys. Rev. Let.* 50 (1983) 346-349.

Hoffmann A.C., Janssen L.P.B.M., Prins J., Particle segregation in fluidized binary mixtures. *Chemical Engineering Science* 48 (1993) 1583-1592

Jonhsson F., Andersson and Leckner B., Expansion of a freely bubbling fluidized bed. *Powder Technology* 68, 117-123.

Johnsson F, Zjierveld R.C., Schouten J.C., Van den Bleek C.M., Leckner B., Characterization of fluidization regimes by time-series analysis of pressure fluctuations, *Int. J. of Multiphase Flow* 26 (2000) 663-715.

Karamavru A.I., Clarck N.N., Local Differential Pressure Analysis in A Slugging Bed Using Deterministic Chaos Theory, *Chem. Eng. Sci.* 52 (1997) 357.

Kendoush A.A.. The virtual mass of a spherical-cap bubble. *Physics of fluids* 15 (2003) 2782-2785.

Kunii D. and Levenspiel O., Fluidization engineering. Butterworth-Heinemann. ISBN: 0-409-90233-0, 1991

Leung L.S. (1971). Design gas distributor and prediction of bubble size in large Gas−Solids Fluidized beds. emphPowder Technology 6 (1971) 189-193.

Lockett M.J., Davidson J. F., Harrison D. On the two-phase theory of fluidization. *Chemical Engineering Science* 22 (1967) 1059-1066.

Müller C.R., Holland D.J., Davidson J.F., Dennis J.S., Gladden L.F., Hayhurst A.N., Mantle M.D. and Sederman A.J., Geometrical and hydrodynamical study of a gas jets in packed and fluidized beds using magnetic resonance. *The Canadian Journal of Chemical Engineering.* 2009, 87, 517-525

Pannala S., Daw C.S., Halow J.S. Dynamic interacting bubble simulation (DIBS): an agent-based bubble model for reacting fluidized beds.*Chaos* 14 (2004) 487-498.

Rees A.C., Davidson J.F., Dennis J.S., Fennell P.S., Gladden L.F., Hayhurst A.N., Mantle M.D., Müller C.R., Sederman A.J. The nature of the flow just above the perforated plate distributor of a gas-fluidised bed, as imaged using magnetic resonance. *Chemical Engineering Science* 61 (2006) 6002 - 6015

Ruzicka M., Drahos J., Zahradnik J., Thomas N. H. Natural modes of multi-orifice bubbling from a common plenum. *Chemical Engineering Science* 54 (1999) 5223-5229

Sánchez-Delgado S., Almendros-Ibáñez J.A., Soria-Verdugo A., Santana D., Ruiz-Rivas U., in J. Werther, W. Nowak, K.E. Wirth, E.U. Hartge, (Eds.). TuTech Innovation GmbH, Hamburg, 2008, p. 1007

Sasic S., Johnsson F. and Leckner B. Interaction between a fluidized bed and its air-supply system: Some observations 2004. *Industrial and Engineering Chemistry Research* 43 (18), pp. 5730-5737

Sasic S., Leckner B. and Johnsson F. Fluctuations and waves in fluidized bed systems: The influence of the air-supply system 2005 *Powder Technology* 153 (3), pp. 176-195

Schouten, J.C., Takens, F. y Van den Bleek, C. M. Maximun likelihood estimation of the entropy of an atractor, *Phys. Rev. E*, 49 (1994) 126-129.

Shanon C.E., Weaver W. *The Mathematical Theory of Communication*, The University of Illinois press: Urbana, (1949).

Vakhshouri K. and Grace J.R. Modeling of bubble formation at a submerge orifice in gas-fluidized bed. *Chemical Engineering Research and Design*. 87 (2009) 843851

Ruud van Ommen J., Robert-Jan de Korte and Cor M. van den Bleek. Rapid detection of defluidization using the standard deviation of pressure fluctuations. *Chemical Engineering and Processing* 43 (2004) 1329-1335

Villa J.,Ruud van Ommen J. and Cor M. van den Bleek. Early Detection of Foam Formation in Bubble Columns by Attractor Comparison. *AIChE Journal*, 49-9 (2003) 2442-2444

Werther J. and Hartge E.U. Gas Distributor and Plenum Design in Fluidized Beds, in W.C. Yang (ed.)*Handbook of fluidization and fluid-particle systems*, Marcel Dekker Inc., New York, pp. 113-128 (2003)

Xiao S., Tan R.B.H. Bubble formation at multiple orifices-bubble synchronicity and frequency. *Chemical Engineering Science* 60 (2003) 179-186

Yang G.Q., Bing Du and Fan L.S. Bubble formation and dynamics in gasliquidsolid fluidizationA review. *Chemical Engineering Science* 62 (2007) 227

Chapter 6

Conclusions

This PhD thesis presents different results about the fluid-dynamics of a two-dimensional fluidized bed through non-intrusive experimental techniques such as Particle Image Velocimetry (PIV), Digital Image Analisis (DIA) and pressure probes.

The non-intrusive nature, avoiding the interaction of the measurement system and the fluidized bed during the experiments, combined with the low computational cost in comparison with the Computational Fluid Dynamic approaches (CFD), makes the combination of both PIV and DIA a powerful tool to characterize the fluidized bed dynamics.

The application and combination of PIV and DIA in a 2D fluidized bed allowed the characterization of the time-averaged global behaviour of the fluidized bed: the use of DIA reports information about bubble size, bubble position and bubble velocity, whereas the PIV technique provides information about the dense phase velocity. With this information the time averaged bubble concentration, the time averaged particle velocity fields and the averaged particle circulation times were reported for different operation conditions.

The fluidized bed was designed to allow for the variation of its thickness, and this in term made it possible to calculate a new correlation to obtain the minimum fluidization velocity in 2D fluidized beds for different particle sizes, bed thickness and heights of the fluidized bed. The correlation only depends on the non-dimensional variable t/d_p being t the variable thickness and d_p the particle size. The results obtained with this correlation are in a good agreement with the results of other works.

Thanks to the two-dimensional character of the fluidized bed, a bubble can be followed during the rising movement from the bottom to the top of the bed. The post-processing of the information recorded by the high speed camera allowed the analysis of the mean and the instantaneous fluctuations of the velocity of the dense phase around the bubble, measuring the region of influence of the bubble in the dense phase. It was

possible to measure an upward movement of the dense phase in the nose and in the wake of the bubble (drift) and a downward movement of the dense phase on the sides of the bubble, the size of these regions being related with the bubble size. This work also presents results on the volumetric dissipation of kinetic energy, where we conclude that the energy dissipation in the dense phase is proportional to the square of the bubble velocity.

It has been proved how two uniform multi-orifice distributors having the same pressure drop but a different grid configuration, lead to the same dynamical bubble pattern and time-averaged dense phase velocity fields when the beds are operated in the same fluidization conditions. This effect is observed in the whole bed except in a region close to the distributor "the activation region". This is a region free of bubbles where the jets interaction takes place, this interaction becomes a bubble in the top of the activation region. This mechanism of bubble generation is supported by a previous phenomenological model. As a result of the comparison between the experimental and the simulated data, it is concluded that the activation region mechanism proposed, explain the observed bubble generation phenomena at multiple orifice-generation.

Bibliography

Almendros-Ibáñez J.A., Sobrino C., de Vega M. and Santana D., A new model for ejected particle velocity from erupting bubbles in 2-D fluidized beds. *Chemical Engineering Science*,2006. vol. 61, pp. 5981-5990

Almendros-Ibáñez J.A., Sánchez-Delgado S., Sobrino C., and Santana D., Experimental observations on the different mechanisms for solid ejection in gas-fluidized beds.*Chemical Engineering and Processing.* 2009, 48, 734-744

Almendros-Ibáñez J.A., Pallarès D., Johnsson F., Santana D., Novel approach to characterize fluidized bed dynamics combining Particle Image Velocimetry and Finite Element Method, *Ind. & Eng. Chem. Res.*, 48(2009), 5010-5023

Bokkers G.A., Laverman J.A., van Sint Annaland M., Kuipers J.A.M. Modelling of large-sclae dense gas-solid bubbling fluidised beds using a novel discrete bubble model. *Chemical Engineering Science* 61 (2006) 5590-5602.

Briongos J.V., Guardiola J., Free top fluidized bed surface fluctuations as a source of hydrodynamic data, *Powder Technol.* 134 (2003) 133-144.

Briongos J.V., Guardiola J., New methodology for scaling hydrodynamic data from a 2D-fluidized bed, *Chem. Eng. Sci.*, 60(2005), 5151 5163

Briongos, J.V., Aragón, J.M. Palancar, M.C. Phase space structure and multiresolution analysis of gas solid fluidized beds hydrodynamics: Part II: Dynamic analysis. *Chem. Eng. Sci.* 62 (2007) 2865-2879.

Briongos J.V., Sanchez-Delgado S., Acosta A. and Santana D. "A novel approach for modelling bubbling gas-solid fluidized bed: the activation region mechanism. Submitted for publication in a AICHE Journal, 2009

Broomhead, D.S. y King, G. P.. Qualitative dynamics from experimental data, *Physica D*, 20 (1986) 217-236

Brown R.C., Brue E., Resolving dynamical features of fluidized beds from pressure fluctuations, *Powder Technol.* 119 (2001) 68-80.

Busciglio A., Vella G., Micale G. and Rizzuti L., "Analysis of the bubbling behaviour of 2-D gas solid fluidized beds Part I: digital image analysis technique". *Chemical Engineering Journal.* 2007, 140, 398-413

Busciglio A., Vella G., Micale G. and Rizzuti L., Analysis of the bubbling behaviour of 2D gas solid fluidized beds. Part II. Comparison between experiments and numerical simulations via Digital Image Analysis Technique, *Chem. Eng. J.*, 148(2009), 145-163

Caicedo G.R., Juan J. Prieto Marqués, Mónica García Ruíz and Jesús Guardiola Soler. A study on the behaviour of bubbles of a 2D gas-solid fluidized bed using digital image analysis. *Chem. Eng. Process.*42 (2003) 9-14

Caram H.S., Hsu K.-K. (1986). Bubble formation and gas leakage in fluidized beds. *Chemical Engineering Science* 41 (1986) 1445-1453.

Cheremisinoff N.P., Review of experimental methods for studying the hydrodynamics of gas-solid fluidized beds, *Ind. Eng. Chem. Process Des. Dev.*, 25(1986) 329-351

Clift R., Grace J.R. Coalescence of Bubbles in fluidized beds. *AIChE Symp. Ser.* 116 vol. 67 (1971) 23-33.

Clift R., in D. Geldart (ed.), Gas Fluidization Technology. Wiley, Chichester, 1986, p. 53

Darton R.C., LaNauze R.D., Davidson J.F. and Harrison D., 1977. Bubble growth due to coalescence in fluidised beds. *Transactions of the Institute Chemical Engineering*, vol. 55, pp. 274-280

Davidson J.F. and Harrison D., 1963. *Fluidised particles.* Cambridge University Press

Davidson J.F, Clift R., Harrison D. (1985). Fluidization (2nd Ed.). Academic Press Inc. (London). ISBN: 0-12-205552-7

Daw C.S. and Halow J.S. Modelling deterministic chaos in gas fluidized beds. *AIChE Symp. Ser.* 289 vol. 88 (1992) 61-69.

Fan L.T., Song J.C. and Yutani N., Radial particle mixing in gas-solids fluidized beds. *Chem. Eng. Sci.* 41 (1986) 117

Fan, L.-S., Tsuchiya, K. *Bubble Wake Dynamics in Liquids and LiquidSolid Suspensions.* Butterworth-Heinemann, Stoneham, MA. (1990)

Geldart D., The size and frequency of bubbles in two- and three-dimensional gas-fluidised beds, *Powder Tech.*, 4(1970), 41-55

Geldart D., 1973. Types of gas fluidization, *Powder Technology*, vol. 7, pp. 285-292

Glicksman L.R. Scaling relationships for fluidized beds. *Chemical Engineering Science* 39 (1984) 1373-1379

Glicksman L.R. and McAndrews G., The effect of bed width on the hydrodynamics of large particle fluidized beds, *Powder Technol.*, 42(1985), 159-167

Glicksman L.R., Hyre M. and Woloshun K. Simplified scaling relationships for fluidized beds. *Powder Technology*, 77 (1993) 177-199

Goldsmith J.A. and Rowe P.N., The shape of the bubbles in a two-dimensional gas fluidised bed. *Chemical Engineering Science*, 1975, 30, 440-442.

Grace J.R., Harrison D. The behavior of freely bubbling fluidised beds. *Chemical Engineering Science* 24 (1969) 497-508

Grace J.C. Chem. Engng. Prog. Symp. Ser. 1971. 67, 116-159

Grace J.R. and Clift R., 1974. On the two-phase theory of fluidization. *Chemical Engineering Science*, vol. 29, pp. 327-334

Grace J.R. and Baeyens J., in Geldart D.(ed.), Gas Fluidization Technology. Wiley, Chichester, 1986, p. 415

Grasa G. and Abanades J.L., The use of two different models to describe the axial mixing of solids in fluidised beds. *Chemical Engineering Science*. 2002, 57, 2791-2798

Grassberger P., Procaccia I., Characterization of strange attractors, *Phys. Rev. Let.* 50 (1983) 346-349.

Guardiola J., Rojo V., Ramos G., Influence of particle size, fluidization velocity and relative humidity on fluidized bed electrostatic, *J. Electrost.*, 37(1996), 1-20

Hoffmann A.C., Janssen L.P.B.M., Prins J., Particle segregation in fluidized binary mixtures. *Chemical Engineering Science* 48 (1993) 1583-1592

Holland D.J., Müller C.R., Sederman A.J., Mantle M.D., Gladden L.F., Davidson J.F., Magnetic resonance imaging of fluidized beds: Recent advances, *Theor. Found. Chem. Eng.*, 42(2008) 469-478

Jackson R., in L.S. Fan and T.M. Knowlton (eds.), Fluidization IX: Proceedings of the Ninth Engineering Foundation Conference of Fluidization. New York, 1998, p. 1

Jackson R., *The Dynamics of Fluidized Particles*, Cambridge University Press, 2000

Johnson P.C., Nott P.R., Jackson R., 1990. Frictional-collisional equations of motion of particulated flowsand their aplications to chutes, *Journal of Fluid Mechanics*, vol. 210, pp. 501-536.

Jonhsson F., Andersson and Leckner B., Expansion of a freely bubbling fluidized bed. *Powder Technology* 68, 117-123.

Johnsson F., Zijerveldb R.C., Schoutenb J.C., van den Bleek C.M., Leckner B., Characterization of fluidization regimes by time-series analysis of pressure fluctuations, *International Journal of Multiphase Flow.* 2000,26, 663-715.

Karamavru A.I., Clarck N.N., Local Differential Pressure Analysis in A Slugging Bed Using Deterministic Chaos Theory, *Chem. Eng. Sci.* 52 (1997) 357.

Kathuria D.G. and Saxena S.C., A variable-thickness two-dimensional bed for investigating gas-solid fluidized bed hydrodynamics, *Powder Technol.*, 53(1987), 91-96

Kendoush A.A.. The virtual mass of a spherical-cap bubble. *Physics of fluids* 15 (2003) 2782-2785.

Khan A.R., Richardson J.F. ,1989. Fluid-particle interactions and flow characteristics of fluidized beds and sttling suspensions of spherical-particles, *Chemical Engineering Science*, vol. 78, pp. 111-130.

Kunii D. and Levenspiel O., 1969. *Fluidization Engineering.* John Wiley & Sons

Kunii D. and Levenspiel O., *Fluidization Engineering (2nd edition)*, Butterworth-Heinemann, 1991

Lacey P.M.C., Developments in the theory of particle mixing, *J. appl. Chem.*, 4, May, 1954, 257-268

Laverman J. A., Roghair I., Van Sint Annaland M. and Kuipers H. Investigation into the hydrodynamics of gas-solid fluidized beds using particle image velocimetry coupled with digital image analysis. *The Canadian journal of chemical engineering.* 2008, 86, 523-535

Leung L.S. (1971). Design gas distributor and prediction of bubble size in large Gas−Solids Fluidized beds. emphPowder Technology 6 (1971) 189-193.

Lim C.N , Gilbertson M.A. and Harrison A.J.L., Bubble distribution and behaviour in bubbling fluidised beds. *Chemical Engineering Science*, 2007, 62 56-59

Link J., Zeilstra C., Deen N., Kuipers H., Validation of a discrete particle model in a 2D spout-fluid bed using non-intrusive optical measuring techniques, *Can. J. Chem. Eng.*, 82(2004), 30-36

Liu Z., Zheng Y., Jia L. and Zhang Q., Study of bubble induced flow structure using PIV, *Chemical Engineering Science* 60 (2005) 3537-3552.

Liu X., Xu G., Gao S., Micro fluidized beds: Wall effect and operibility, *Chem. Eng. J.*, 137(2008), 302-307

Loezos P.N., Costamagna P., Sundaresan S., The role of contact stresses and wall friction on fluidization, *Chem. Eng. Sci.*, 57(2002), 5123-5141

Lockett M.J., Davidson J. F., Harrison D. On the two-phase theory of fluidization. *Chemical Engineering Science* 22 (1967) 1059-1066

Lu L-S. and Hsiau S-S Mixing in a vibrated granular bed: Diffusive and convective effects. *Powder Technology*. 184 (2008) 31-43

Massimilla L., Westwater J.W., Photographic study of solid-gas fluidization, *AIChE J.*,6(1960), 134-138

Mudde R.F., Schulte H.B.M., van den Akker H.E.A., Analysis of a bubbling 2-D gas-fluidized bed using image processing, *Powder Technol.*, 81(1994), 149-159

Müller C.R., Davidson J.F., Dennis J.S. and Hayhurst A.L., 2007. A study of the motion and eruption of a bubble at the surface of a two-dimensional fluidized bed using particle image velocimetry (PIV), *Industrial & Engineering Chemistry Research*, vol. 46, pp. 1642-1652

Müller C.R., Holland D.J., Sederman A.J., Mantle M.D., Gladden L.F., Davidson J.F., Magnetic Resonance Imaging of fluidized beds, *Powder Technol.*, 183(2008) 53-62

Müller C.R., Holland D.J., Davidson J.F., Dennis J.S., Gladden L.F., Hayhurst A.N., Mantle M.D. and Sederman A.J., Geometrical and hydrodynamical study of a gas jets in packed and fluidized beds using magnetic resonance. *The Canadian Journal of Chemical Engineering*. 2009, 87, 517-525

Otsu N., 1979. A threshold selection method from gray-level histograms, *IEEE Transactions on Systems Man and Cybernetics*, 9 (1979) 62-66

Pallarès D. and Johnsson F., A novel technique for particle tracking in cold 2-dimensional fluidized beds-simulating fuel dispersion. *Chemical Engineering Science* 2006, 61, 2710 - 2720

Pannala S., Daw C.S., Halow J.S. Dynamic interacting bubble simulation (DIBS): an agent-based bubble model for reacting fluidized beds.*Chaos* 14 (2004) 487-498.

Ramos Caicedo G., García Ruiz M., Prieto Marqués J.J., Guardiola Soler J., Minimum fluidization velocities for gas/solid 2D beds, *Chem Eng. Proc.*, 41(2002) 761-764

Rees A.C., Davidson J.F., Dennis J.S., Fennell P.S., Gladden L.F., Hayhurst A.N., Mantle M.D., Müller C.R., Sederman A.J. The nature of the flow just above the perforated plate distributor of a gas-fluidised bed, as imaged using magnetic resonance. *Chemical Engineering Science* 61 (2006) 6002 - 6015

Rhodes MJ., Wang XS., Nguyen M., Stewart P., Liffman K. Study of mixing in gas-fluidized beds using a DEM model *Chem. Eng. Sci* 56, 8, (2001) 2859-2866

Richardson J.F., Zaki W.N., 1954. Sedimentation and fluidisation, *Transaction of the Institution of Chemical Engineers*, vol. 32, pp. 35-53

Rodríguez-Rodríguez J., Martínez-Bazán C. and Montañes J.L.,A novel particle tracking and break-up detection algorithm: application to the turbulent break-up of bubbles. *Measurements Science and Technology*, 2003, 14, 1328-1340

Rojo V., Guardiola J., Vian A., A capacitor model to interpret the electric behaviour of fluidized beds. Influence of apparatus geometry, *Chem. Eng. Sci.*, 41(1986), 2171-2181

Ronsse F., Pieters JG., Dewettinck K. Numerical spray model of the fluidized bed coating process *Drying Technology*. 25, 9, 2007, 1491-1514

Rowe P.N., A note on the motion of a bubble rising through a fluidized bed. *Chemical Engineering Science*, 1 (1964) 75-77

Rowe P.N., Partridge B.A., An x-ray study of bubbles in fluidised beds, *Trans. Inst. Chem. Eng.*, 43(1965), 157-175

Rowe P.N., Everett D.J., Fluidised bed bubbles viewed by x-rays. Part II-The transition from two to three dimensions of undisturbed bubbles, *Trans. Instn. Chem. Engrs.*, 50(1972), 49-54

Rowe P.N., Estimation of solid circulation rate in bubbling fluidised bed. *Chemical Engineering Science* 28 (1973) 979-980

Ruzicka M., Drahos J., Zahradnik J., Thomas N. H. Natural modes of multi-orifice bubbling from a common plenum. *Chemical Engineering Science* 54 (1999) 5223-5229

Sánchez-Delgado S., Almendros-Ibáñez J.A., Soria-Verdugo A., Santana D., Ruiz-Rivas U., in J. Werther, W. Nowak, K.E. Wirth, E.U. Hartge, (Eds.). TuTech Innovation GmbH, Hamburg, 2008, p. 1007

Sánchez-Delgado S., Acosta-Iborra A., Santana D., Dense phase velocity fluctuation in a 2-D fluidized bed. Submmited for publication to *Powder Technol.*

Santana D., Nauri S., Acosta A., García N., Macías-Machín A., Initial particle velocity spatial distribution from 2-D erupting bubbles in fluidized beds. *Powder Tech.*, 150(2005), 1-8

Sarra A., Miller A.L., Shadle L.J., 2005. Experimentally measured shear stress in the standpipe of a circulating fluidized bed, *AIChE Journal*, vol. 51, pp.1131-1143

Sasic S., Johnsson F. and Leckner B. Interaction between a fluidized bed and its air-supply system: Some observations 2004. *Industrial and Engineering Chemistry Research* 43 (18), pp. 5730-5737

Sasic S., Johnsson F., Leckner B., Fluctuations and waves in fluidized bed systems: the influence of the air-supply system, *Powder Technology*, 2005, 153, 176-195.

Saxena S.C., Jadav S., A two-dimensional gas fluidized bed for hydrodynamic and elutriation studies, *Powder Technol.*, 36(1983), 61-70

Schouten, J.C., Takens, F. y Van den Bleek, C. M. Maximun likelihood estimation of the entropy of an atractor, *Phys. Rev. E*, 49 (1994) 126-129.

Shanon C.E., Weaver W. *The Mathematical Theory of Communication*, The University of Illinois press: Urbana, (1949).

Shen L., Zhang M. and Xu Y. Solid mixing in fluidized beds. *Powder Technology*. 1995, 84, 207-212

Shen L., Johnsson F. and Leckner B., 2004. Digital image analysis of hydrodynamics two-dimensional bubbling fluidized beds. *Chemical Engineering Science*, vol. 59, pp. 2607-2617

Simons S.J.R., Imaging techniques for fluidized bed systems: a review, *Chem. Eng. J. Biochem. Eng. J.*, 56(1995) 83-93

Sobrino C., Almedros-Ibáñez J.A., Santana D.and de Vega M., Fluidization of group B particles with a rotating distributor, *Powder Technol.*, 181(2008), 273280

Srivastava A. and Sundaresan S., Role of wall friction in fluidization and standpipe flow, *Powder Technol.*, 124(2002), 45-54

Sveen J.P., http://www.math.uio.no/∼jks/matpiv (Last modified in August, 2004. Accesed in 2008)

Trisakti B., Oshitani J., Tanaka Z., Circulating particle flow and air bubble behavior at various superficial gas velocities in two-dimensional gas-solid fluidized beds, *Adv. Powder Technol.*, 12(2001), 507-519

Tzeng J.W., Chen R.C. and Fan L.S., Visualization of flow characteristics in a 2-D bubble column and three phase fluidized bed, *AIChe Journal*, 1993, 39, 733-744

Vakhshouri K. and Grace J.R. Modeling of bubble formation at a submerge orifice in gas-fluidized bed. *Chemical Engineering Research and Design*. 87 (2009) 843851

van Demeter J.J., in A.A.H. Drinkerburg (ed.), Proceeding of the international symposium on fluidization, Netherlands, Amsterdam. 1967

van Ommen J.R., Robert-Jan de Korte and Cor M. van den Bleek. Rapid detection of defluidization using the standard deviation of pressure fluctuations. *Chemical Engineering and Processing* 43 (2004) 1329-1335

van Ommen J.R., Mudde R.F., Measuring the gas-solids distribution in fluidized feds A review, *Int. J. Chem. React. Eng.*, 6(2008) Review R3

Villa J.,Ruud van Ommen J. and Cor M. van den Bleek. Early Detection of Foam Formation in Bubble Columns by Attractor Comparison. *AIChE Journal*, 49-9 (2003) 2442-2444

Wei F.,Cheng Y.,Jin Y. and Yu Z. Axial and lateral dispersion of fine particles in a binary-solid riser. *The Canadian Journal of Chemical Engineering*, 1998, 76, 19-26

Wei X., Sheng H. and Tian W., "Characterizing particle dispersion by image analysis in ICFB", *International Journal of Heat and Mass Transfer*. 2006, 49, 3338-3342

Werther J. and Molerus J., The local structure of gas fluidized beds-II. The spacial distribution of bubbles. *International Journal of Multiphase Flow*, 1973, 1, 123-138.

Werther J., Measurement techniques in fluidized beds, *Powder Technol.*, 102(1999) 15-36

Werther J. and Hartge E.U. Gas Distributor and Plenum Design in Fluidized Beds, in W.C. Yang (ed.)*Handbook of fluidization and fluid-particle systems*, Marcel Dekker Inc., New York, pp. 113-128 (2003)

Werther J. and Reppenhagen J. Atrittion, in W.C. Yang (ed.)*Handbook of fluidization and fluid-particle systems*, Marcel Dekker Inc., New York, pp. 97-106 (2003)

Xianfeng Fan, David J. Parker, ZhufangYang, Jonathan P.K. Seville and Jan Baeyens, The effect of bed materials on the solid/bubble motion in a fluidised bed, *Chemical Engineering Science*, 2008, 63, 943-950

Xiao S., Tan R.B.H. Bubble formation at multiple orifices-bubble synchronicity and frequency. *Chemical Engineering Science* 60 (2003) 179-186

Yang G.Q., Bing Du and Fan L.S. Bubble formation and dynamics in gasliquidsolid fluidizationA review. *Chemical Engineering Science* 62 (2007) 227